UNIVERSIDAD
DE MÁLAGA

Exchange through the Strait of Gibraltar in relation to the climatic forcing over the Mediterranean Sea

Tesis doctoral

Francisco Javier Soto Navarro

Grupo de Oceanografía Física de la Universidad de Málaga

Málaga 2012

UNIVERSIDAD DE MÁLAGA

Programa de doctorado

Dinámica de los flujos biogeoquímicos y sus aplicaciones

Exchange through the Strait of Gibraltar in relation to the climatic forcing over the Mediterranean Sea

Memoria presentada por F. Javier Soto Navarro

para optar al grado de Doctor por la Universidad de Málaga

Fdo. Francisco Javier Soto Navarro

Director:

Francisco Criado Aldeanueva

Profesor titular del departamento de Física Aplicada II

Universidad de Málaga

UNIVERSIDAD
DE MÁLAGA

D. FRANCISCO CRIADO ALDEANUEVA, profesor titular del departamento de Física Aplicada II de la Universidad de Málaga,

HACE CONSTAR:

Que el trabajo recogido en la siguiente memoria, titulada "Exchange through the Strait of Gibraltar in relation to the climatic forcing over the Mediterranean Sea", presentada por D. F. Javier Soto Navarro, ha sido realizada bajo mi supervisión y tiene, a mi juicio, contenido científico suficiente, de lo que informo favorablemente en orden a su presentación y defensa para optar al grado de Doctor por la Universidad de Málaga.

Para que así conste a los efectos oportunos firmo la presente en Málaga a 11 de julio de 2012.

Fdo. Dr. Francisco Criado Aldeanueva

La presente Tesis Doctoral ha sido realizada gracias a la concesión de una beca de Formación de Personal Investigador de la Consejería de Innovación, Ciencia y Empresa de la Junta de Andalucía, en el marco del Proyecto de Excelencia P07-RNM-02938 "Índices para el diagnóstico de tendencias climáticas en el mar Mediterráneo". El trabajo se ha realizado en el Departamento de Física Aplicada II de la Universidad de Málaga y, parcialmente, en el Centre National de Recherches Météorologiques (CNRM-Météo France) de Toulouse (Francia).

Agradecimientos

En primer lugar agradezco a mi director de tesis, Francisco Criado Aldeanueva, su dedicación, confianza e inestimable ayuda. Soy consciente del esfuerzo y la ilusión que ha depositado en este trabajo. A nivel personal, le doy las gracias por su apoyo y por el afecto con el que me ha tratado siempre.

Agradezco también al resto de compañeros del Grupo de Oceanografía Física de la Universidad de Málaga la ayuda y los consejos recibidos, en especial a Jesús García Lafuente por el ejemplo de dedicación que ha supuesto para mí. Muchas gracias a Antonio por su gran labor en las campañas y el tratamiento de los datos de la estación de Espartel, en los que se basa gran parte de mi trabajo. A José Carlos le debo la mitad de uno de los capítulos y muchos buenos ratos de arreglar el mundo en lo que dura un café. Por supuesto, no me olvido del resto de compañeros del laboratorio, y sobre todo de Conchita con la que he compartido coche, docencia y estrés.

Je remercie les membres du Groupe de Météorologie Grande Echelle et Climat (GMGEC), METEO-FRANCE – CNRS, leur chaleureux accueil et l'intérêt au cours de mon séjour de trois mois à Toulouse. En spécial a Samuel, Florence et Jonathan pour leur aide dans mon travail et sympathie.

En el plano personal, es difícil mencionar a todos los que han contribuido al camino que me ha traído hasta aquí. Sin duda, mi gran apoyo ha sido siempre mi familia, que no necesita que les demuestre un cariño que sabe suyo. En cuanto a mis amigos, creo sinceramente que sois lo mejor que he conseguido en la vida, así que os agradezco de corazón que hayáis estado siempre ahí, algunos desde que tengo memoria, otros desde que aparecí por Málaga. Parte de esto es vuestro porque sin vosotros no habría risas, y sin risas nada merecería la pena.

Pero entonces bailaban por las calles como peonzas enloquecidas, y yo vacilaba tras ellos como he estado haciendo toda mi vida mientras sigo a la gente que me interesa, porque la única gente que me interesa es la que está loca, la gente que está loca por vivir, loca por hablar, loca por salvarse, con ganas de todo al mismo tiempo, la gente que nunca bosteza ni habla de lugares comunes, sino que arde, arde, arde como fabulosos cohetes amarillos explotando igual que arañas entre las estrellas y entonces se ve estallar una luz azul y todo el mundo suelta un «¡Ahhh!».

Jack Kerouac

On the Road, 1957

A mis padres, Antonio y Cristina

y a mis hermanos, Jorge y Antonio

RESUMEN

Resumen de la memoria:

Intercambio a través del estrecho de Gibraltar en relación con el forzamiento climático en el mar Mediterráneo

1. Introducción

El mar Mediterráneo es una cuenca de concentración en la que la evaporación excede a los aportes de agua por precipitación y descarga de ríos, lo que genera un déficit hídrico que es compensado con la entrada de un flujo neto a través del estrecho de Gibraltar, su única conexión con el océano abierto (Bethoux and Gentilli, 1999; Mariotti et al., 2002). El agua atlántica (AW) que constituye el flujo de entrada, cálida y relativamente dulce, se va salinizando por efecto de la evaporación al adentrarse en la cuenca siguiendo la circulación anticiclónica de ésta (Millot, 1999). En la zona más oriental, la cuenca Levantina, alcanza su máximo de salinidad y debido al enfriamiento invernal se hunde a capas intermedias (150-600 m) dando lugar al agua levantina intermedia (LIW). En otras zonas de la cuenca en las que el forzamiento invernal es especialmente severo se producen fenómenos de convección profunda. Concretamente, el agua profunda del Mediterráneo oriental (EMDW) se forma principalmente en el Adriático, mientras que el agua profunda del Mediterráneo occidental (WMDW) se produce en el área del Golfo de León. Estas aguas se sitúan por debajo del LIW, aproximadamente entre los 600 m y el fondo marino. Finalmente, un flujo de aguas mediterráneas (MW) frías y salinas, constituido mayoritariamente por LIW y en parte

por WMDW, salva el umbral del estrecho y escapa de la cuenca hacia el océano Atlántico.

La célula termohalina descrita genera un intercambio bicapa en el estrecho de Gibraltar cuyas características están muy ligadas al forzamiento climático de la cuenca. Sin embargo, la variabilidad de dicho intercambio depende a su vez de la geometría del estrecho (Bryden and Kinder, 1991b). El objetivo de esta tesis doctoral es hacer una descripción exhaustiva de estos forzamientos, y aplicar este estudio a la estimación y caracterización del flujo atlántico. Para completar el estudio, se analizarán las tendencias en la salinidad y la temperatura del flujo en relación con las de las aguas atlánticas adyacentes. Finalmente, se llevará a cabo un estudio de validación de varios modelos climáticos en el estrecho, tanto en términos de transporte de volumen como de propiedades termohalinas del flujo mediterráneo de salida.

2. Resumen por capítulos

Capítulo 2: Variabilidad estacional e interanual de los flujos de calor y agua dulce a través de la superficie en el mar Mediterráneo: balances e intercambio a través del estrecho de Gibraltar

En este capítulo se describen las distintas componentes de los flujos intercambiados entre la atmósfera y el mar a través de su superficie: los flujos de calor y de agua dulce. El flujo de calor está constituido por cuatro componentes, dos radiativas: la radiación de onda corta procedente del Sol y la de onda larga emitida por la Tierra, y dos turbulentas: el calor latente y el calor sensible. Del flujo de agua dulce se analizan sus principales componentes: la precipitación (P), la evaporación (E) y el déficit hídrico (E-P).

Para este estudio se han empleado datos de reanálisis del National Centers for Enviromental Prediction-National Center for Atmospheric Research (NCEP-NCAR) (Kalnay et al., 1996), consistentes en valores medios mensuales de las distintas variables con una resolución espacial de aproximadamente 1.9º x 1.9º para todo el

Mediterráneo, y que abarcan el periodo de enero de 1948 a febrero de 2009. Como complemento se han analizado también valores mensuales de precipitación de CMAP (CPC Merged Analysis of Precipitation), cuya resolución es de 2.5ºx2.5º así como imágenes mensuales de alta resolución (4 km x 4 km) de SST (Sea Surface Temperature) del AVHRR (Advanced Very High Resolution Radiometer), de la misión pathfinder v5 de la NASA, entre 1985 y 2007. Los datos se han tratado estadísticamente para elaborar mapas de distribución espacial de las distintas variables para cada una de las estaciones, ciclos estacionales climatológicos y series interanuales.

Principales resultados

El ciclo estacional del flujo de calor total es positivo (hacia el océano) entre marzo y septiembre, con su máximo en enero, y negativo el resto del año. Para la cuenca completa, en promedio anual, se ha obtenido un balance neto prácticamente neutro de 0.7 Wm^{-2}. El balance es positivo para la cuenca occidental (~12 Wm^{-2}) y negativo para la oriental (-6.4 Wm^{-2}), debido a las grandes pérdidas de calor latente de este área (hasta 100 Wm^{-2}). La evaporación neta (E-P) tiene un ciclo estacional con un rango de variabilidad de 600 $mm{\cdot}año^{-1}$, alcanza su máximo en agosto-septiembre y su mínimo en mayo. El valor promedio para todo el periodo y para la cuenca completa del déficit de agua dulce es de 680±70 $mm{\cdot}año^{-1}$, aunque estas pérdidas son casi un 70% mayores en la cuenca oriental. Se ha encontrado una tendencia positiva para E-P en el periodo analizado (1948-2009) de 1.6±0.9 $mm{\cdot}año^{-2}$, consecuencia de un descenso de la precipitación.

A partir los valores climatológicos de la descarga de ríos y del intercambio neto con el mar Negro, se ha obtenido un valor del flujo neto a través del estrecho de Gibraltar de G=0.035±0.005 Sv (1 Sv= 10^6 m^3s^{-1}). Combinando este valor con el flujo medio de salida G_{out}=0.78±0.05 Sv obtenido a partir del registro de velocidades del perfilador Doppler (ADCP) instalado en la estación de Espartel, resulta un flujo medio de entrada de ($G_{in} = G + G_{out}$) 0.82 ± 0.05 Sv. Este resultado es un valor intermedio entre los pocos calculados previamente por otros autores, que al estar basado en una combinación de medidas experimentales de probada precisión y de una climatología que

involucra a toda la cuenca, se considera bastante realista. En lugar de usar las ecuaciones de conservación de sal para la estimación del flujo de entrada, que introducen mucha incertidumbre en el cálculo, se ha empleado la estimación realizada para determinar el cociente entre las salinidades del flujo de entrada y de salida, S_{in}/S_{out} = 0.956, que puede emplearse para futuros cálculos de las componentes del intercambio cuando únicamente se disponga de uno de los flujos, ya sea mediante estimaciones climatológicas o medidas in situ.

Considerando el flujo de entrada obtenido, se calcula una advección de calor hacia el Mediterráneo a través del estrecho de $Q_a = 3.2 \pm 1.5$ Wm^{-2}, un valor menor que los históricamente documentados pero que es probablemente más realista ya que las discrepancias son fruto de sobreestimaciones previas del flujo de entrada. Este valor de la advección, junto con la estimación del valor intercambiado con la atmósfera, implicaría un incremento del contenido neto de calor en el Mediterráneo durante las últimas décadas.

Capítulo 3: Influencia del forzamiento atmosférico a gran escala en los balances de calor y agua dulce del Mediterráneo: índices climáticos

Esta sección estudia la relación entre los patrones atmosféricos de gran escala que actúan sobre la cuenca mediterránea y la variabilidad de los flujos de calor y agua dulce. En concreto, se realiza un análisis comparativo entre el índice más comúnmente utilizado en el área del Atlántico Norte, el NAO (North Atlantic Oscilation), cuya influencia sobre la climatología mediterránea ha sido ampliamente documentada (Hurrel, 1995; Mariotti et al., 2002; Hurrel et al., 2003 y referencias del mismo para una amplia revisión), con un índice de carácter regional, el índice MO (Mediterranean Oscilation) (Conte et al., 1989), que podría ser un indicador más eficaz de la variabilidad de la cuenca, especialmente para los flujos objeto de estudio (Supic et al., 2004; Gomis et al., 2006).

Existen diversos criterios para la definición de los citados índices. Algunos de ellos se basan en la diferencia de presión atmosférica entre estaciones cercanas a los

centros de acción de los respectivos patrones, con el inconveniente de estar sujetas a la variabilidad local. En este trabajo se ha optado por una definición basada en las componentes principales (PC) de las funciones empíricas ortogonales (EOF) de la presión atmosférica, calculadas para el área completa de influencia de cada patrón, lo que proporciona un índice más representativo de esta área en su conjunto. Para el índice NAO se han usado los valores mensuales suministrados por el NOAA (National Oceanic and Atmospheric Administration), que utiliza la componente principal rotada de la presión atmosférica a 500 mb entre 20ºN y 90ºN. Para el MO, el índice se ha calculado como la PC de la EOF de la presión atmosférica a nivel del mar en un área extendida del Mediterráneo (30ºW-40ºE de longitud, 30ºN-60ºN de latitud), a partir de valores mensuales de reanálisis de NCEP.

Las variables estudiadas son la precipitación, la evaporación, el déficit hídrico (E-P) y el flujo neto de calor. Todas ellas han sido obtenidas de la base de datos de reanálisis de NCEP. Posteriormente se han construido series interanuales e interdecadales, así como promedios estacionales de cada una de ellas, con las que se ha realizado un análisis de correlación con los distintos índices. La significancia estadística se ha evaluado transformando la matriz de correlación en una distribución *t* de Student con N-2 grados de libertad, siendo N el número de elementos de la serie analizada.

Principales resultados

Ambos índices exhiben una importante variabilidad interanual e interdecadal, con periodos comunes de fases tanto positivas como negativas. Aunque el descenso en la precipitación promedio de la cuenca entre mediados de los 60 y mediados de los 80 se corresponde claramente con un incremento en ambos índices, la variabilidad de E-P no muestra una correlación tan clara, debido a la diferente sensibilidad de E y P, que se traduce en correlaciones de signo opuesto en las cuencas occidental y oriental.

La efectividad de los índices NAO y MO es muy parecida para P y E-P, pero en el caso de los flujos de calor y la evaporación el índice MO parece ser un mejor indicador de la variabilidad interdecadal ya que desde mediados de los 70 a principios de los 90 ambos índices difieren significativamente. Debido a la persistencia y estabilidad del MO durante todo el año los valores anuales del índice son los que presentan en general una mejor correlación. En el caso del NAO, son los promedios invernales los que presentan la mejor correlación para todas las variables dada la mayor proximidad de su centro meridional al Mediterráneo en esta estación.

Puesto que la similitud de ambos índices se limita a los meses de otoño e invierno, es plausible considerar que el MO representa un patrón específico de circulación regional más que una extensión regional de la NAO, por lo que constituye un índice adecuado para la monitorización en el Mediterráneo de la variabilidad a largo término de los balances hídrico y, especialmente, de calor.

Capítulo 4: Estimación del flujo atlántico de entrada a través del estrecho de Gibraltar mediante datos climatológicos y experimentales

El objetivo de este capítulo es la caracterización del flujo atlántico que entra en la cuenca mediterránea a través del estrecho de Gibraltar. Para este propósito se emplea una metodología indirecta basada en la combinación de medidas experimentales del flujo de salida mediterráneo con una estimación del flujo neto a partir del balance hidrológico de la cuenca, descrito por la ecuación:

$$\frac{dV}{dt} = S_f \frac{d\xi_M}{dt} = P - E + R + B + Q_0 \qquad \text{(R.1)}$$

donde dV/dt, es la derivada temporal del volumen de la cuenca, S_f la superficie de la misma (~$2.5 \cdot 10^6$ km^2) y ξ_M la componente másica de la anomalía del nivel del mar. Los términos de la derecha son las distintas contribuciones del balance hidrológico: precipitación, P, evaporación, E, descarga de ríos, R, el intercambio con el mar Negro a través de los estrechos turcos, B, y el flujo neto a través del estrecho de Gibraltar, Q_0. Esta ecuación (R.1) permite el cálculo de Q_0 a partir del resto de términos del balance

hidrológico, y, considerando que el flujo neto es la diferencia de los flujos de entrada (Q_1) y salida (Q_2), $Q_0 = Q_1 - |Q_2|$, el flujo de entrada puede estimarse a partir del neto y el de salida.

La evaporación y la precipitación se han obtenido de la base de datos de reanálisis NCEP. Para la descarga de ríos y el intercambio con el mar Negro se han empleado valores de estudios previos, Struglia et al. (2004) para R y Kanarska and Maderich (2008) para B. La componente másica del nivel del mar se ha calculado a partir de las anomalías totales de la altura del nivel del mar de la base de datos AVISO. Éstas consisten en medidas de altimetría por satélite de diversas misiones distribuidas en una malla de 1/8º x 1/8º de resolución espacial y con una resolución temporal de una semana en el periodo 1992-2009. Para obtener la componente másica, a estas anomalías totales hay que restarles la componente estérica, que da cuenta de las variaciones de volumen experimentadas por la columna de agua debido a variaciones de salinidad y/o temperatura. Esta última se calcula mediante la ecuación:

$$\xi_S = -\frac{1}{\rho_0}\int_{-H}^{0} \left.\frac{\partial\rho(S,T,P)}{\partial T}\right|_{T,P=cte} \cdot T'(z)dz + \frac{1}{\rho_0}\int_{-H}^{0} \left.\frac{\partial\rho(S,T,P)}{\partial S}\right|_{S,P=cte} \cdot S'(z)dz \quad \text{(R.2)}$$

donde $T'(z)$ y $S'(z)$ son las anomalías de temperatura y salinidad referidas a sus valores medios climatológicos; ρ_0 es una densidad de referencia y H la profundidad del fondo. Las anomalías de salinidad y temperatura se han calculado a partir de perfiles del modelo de circulación ECCO, que tienen una resolución espacial de 1º x 1º, resolución temporal de 10 días y cubren el mismo periodo que los datos de AVISO.

Por último, el flujo mediterráneo de salida se ha calculado a partir de los datos experimentales medidos en la estación permanente de Espartel (ES, 35º51.70'N, 5º58.60'W), fondeada a 360 m de profundidad en el canal meridional del umbral de Espartel en el marco de los proyectos INGRES del grupo de Oceanografía Física de la Universidad de Málaga. La estación está equipada con un ADCP, colocado mirando hacia arriba a 20 m sobre el fondo que mide la velocidad cada 30 minutos en celdas de 8 m de espesor, hasta una profundidad por encima de la interfase entre las capas atlántica y mediterránea, que en Espartel es de unos 190 m (Sánchez-Román et al., 2009), lo que permite registrar la velocidad de la vena mediterránea de salida. Por debajo del ADCP, a

unos 10 m sobre el fondo, hay colocada una sonda de conductividad y temperatura (CT), que permite muestrear las características termohalinas del agua mediterránea. La línea se completa con un correntímetro puntual que permite medir la velocidad del flujo de salida en la zona de sombra del ADCP, es decir, entre la boya y el fondo. El flujo de salida se calcula integrando la velocidad multiplicada por la sección a lo largo de la columna de agua:

$$Q_2(t) = \int_b^{h(t)} \langle u(z,t) \rangle W(z) dz \qquad \text{(R.3)}$$

donde $u(z,t)$ es la componente de la velocidad a lo largo del eje del estrecho, $W(z)$ la sección transversal del canal y $h(t)$ la profundidad de la interfase entre las capas atlántica y mediterránea, calculada por interpolación como la superficie de velocidad cero.

Principales resultados

La señal estacional del flujo neto, Q_0, depende del ciclo de E-P, que tiene un rango de 582±21 mm·año^{-1} y alcanza su máximo en agosto, y de la señal de la componente másica del nivel del mar, con un ciclo de amplitud 4.2 ±1.2 cm y máximo en noviembre. La descarga de ríos y el intercambio neto con el mar Negro se han incluido en el balance hídrico aunque su contribución es menor del 20%. Se obtiene un valor medio del flujo neto de 0.038±0.007 Sv, y un ciclo estacional con una amplitud anual de 0.042±0.018 Sv y máximo en septiembre.

A partir de los más de cuatro años de medidas experimentales se ha obtenido un valor promedio del flujo Mediterráneo de salida de -0.78±0.05 Sv, con una amplitud del ciclo anual de 0.027±0.015 Sv y semianual de 0.017±0.009 Sv y máximos en abril y septiembre respectivamente. Al sumar la serie de flujo neto, resulta un flujo atlántico promedio de 0.81±0.06 Sv, amplitud anual de 0.034±0.011 Sv con máximo en agosto y semianual de 0.022±0.014 Sv con máximo en abril. La serie temporal, la más larga obtenida hasta el momento, presenta una alta variabilidad interanual, con una anomalía

especialmente alta en el flujo de salida del año 2008 que puede haber sesgado parcialmente el cálculo del ciclo estacional. Se requerirán series temporales de mayor longitud para confirmar los resultados obtenidos.

La evolución temporal tanto de los flujos intercambiados como de la superficie interfacial de separación entre las capas atlántica y mediterránea sugieren un régimen de intercambio submáximo en el estrecho, reflejado en la fluctuación desfasada de las dos componentes de los flujos de entrada y salida. El forzamiento principal del flujo de entrada es la señal barotrópica del flujo neto, Q_0, que sigue el ciclo de E-P dando lugar al máximo a finales de verano. Un segundo mecanismo de forzamiento baroclino es la variación estacional de la gravedad reducida, $g' = g\,(\rho_2 - \rho_1)\,/\rho_0$, debida a los cambios en la densidad de la capa superficial que produce el ciclo estacional de intercambio de calor, cuyo máximo en septiembre contribuye al máximo del flujo atlántico.

Capítulo 5: Tendencias termohalinas recientes en las aguas atlánticas que fluyen hacia el interior del Mediterráneo

La estrecha interrelación entre las diferentes masas de agua que participan en la circulación termohalina del Mediterráneo hace que ésta sea muy sensible a la variabilidad de sus propiedades. En este sentido, un reciente estudio basado en medidas experimentales en la plataforma continental marroquí (Millot, 2007) detectó una tendencia inusualmente elevada (0.05 año^{-1}) en la salinidad de las aguas atlánticas entre los años 2003 y 2007, muy superior a las estimaciones para la década de 1990 en las aguas atlánticas adyacentes al estrecho (Boyer et al., 2005; Poliakov et al., 2005). El objeto de este capítulo es estudiar la evolución de la salinidad y la temperatura en este área durante los últimos años para establecer el origen de las tendencias observadas en Gibraltar.

El flujo atlántico está formado en su mayor parte por aguas provenientes de la corriente de las Azores, la componente sudoriental del giro subtropical noratlántico, aunque también recibe aguas de las corrientes ibérica y canaria (Klein and Siedler,

1989; Machin et al. 2006). Está constituido por agua superficial atlántica (SAW) y agua central del atlántico nororiental (ENACW).

El estudio se ha llevado a cabo analizando perfiles Argo de salinidad y temperatura. Las boyas Argo son sistemas autónomos que realizan perfiles de salinidad y temperatura entre la superficie y los 2000 m de profundidad. Se ha seleccionado una zona de estudio que abarca entre los 28ºN y los 42ºN en latitud y entre los 5ºW y los 24ºW en longitud. Entre enero de 2002 y mayo de 2010 se dispone de un total de 5997, de los que tras la aplicación de diversos controles de calidad para garantizar la precisión de los datos se seleccionaron 5077. En primer lugar se separaron los perfiles en tres zonas, una zona septentrional (entre los 37ºN y los 42ºN, zona 1), en la que está incluida la corriente ibérica y la ruta de las aguas mediterráneas (MW) que abandonan Gibraltar; una zona central (entre los 32ºN y los 37ºN, zona 2), que cubre la corriente de las Azores y una zona meridional (entre 28ºN y 32ºN, zona 3) influenciada por la corriente canaria. Una vez separados los perfiles se interpolaron en 22 niveles de profundidad, se promediaron mensualmente y se integraron verticalmente en cuatro capas: entre 0 y 100 m (capa del SAW), entre 100 y 600 m (capa del ENACW), entre 600 y 1200 m (capa del MW) y el perfil completo (0-2000 m). Las tendencias de salinidad y temperatura se estimaron mediante el ajuste por mínimos cuadrados de las series de tiempo obtenidas por este procedimiento.

Los cambios en las propiedades de una masa de agua que se encuentra a una determinada profundidad pueden ser debidos a dos causas diferentes: por un lado, un cambio en las propiedades intrínsecas de esa masa de agua debido a mezclas o advección horizontal y, por otro lado, a movimientos verticales de la columna de agua que provocan que masas de agua de diferentes densidades cambien su posición en la columna de agua sin variar sus propiedades. Puede separarse la contribución de cada uno de estos mecanismos para una determinada profundidad aplicando la ecuación de descomposición de Bindoff and McDougall (1994):

$$\left.\frac{d\xi}{dt}\right|_p = \left.\frac{d\xi}{dt}\right|_n - \left.\frac{dp}{dt}\right|_n \left(\frac{\partial \xi}{\partial p}\right) \qquad \text{(R.4)}$$

La parte izquierda de la ecuación representa la evolución temporal sobre superficies isobáricas de una magnitud escalar (salinidad o temperatura en este caso). El primer término de la derecha da cuenta de los cambios sobre superficies de igual densidad debidos tanto a mezcla como a advección y el segundo de los cambios a una determinada presión por desplazamientos verticales de las isopicnas.

Principales resultados

Se ha demostrado que las tendencias de salinidad (y en menor medida de temperatura) documentadas en el flujo atlántico de entrada a través del estrecho de Gibraltar se corresponden con una similar salinificación (calentamiento) en los primeros 600 m de las aguas atlánticas adyacentes al estrecho. La mayor tendencia en la salinidad se da en la capa superficial del área de la corriente de las Azores (0.04 año^{-1}), aunque también se han encontrado valores positivos al norte y al sur de esta área. Valores menores, también positivos, se encuentran en la capa correspondiente a la termoclina permanente (sobre 0.01 año^{-1}), que en cualquier caso exceden las estimaciones previas. Pero la mayor novedad de estos resultados es que, en contraste con otros estudios realizados en periodos anteriores, las tendencias calculadas son ahora consecuencia de cambios intrínsecos de las masas de agua, en lugar de ser el efecto de desplazamientos verticales de las isopicnas. Estos cambios en las propiedades de las masas de agua están probablemente ligados a un reciente incremento de la evaporación neta que afecta a la salinidad de las aguas superficiales y de la termoclina mediante procesos de advección y subducción.

Capítulo 6: Validación del transporte de volumen y las propiedades termohalinas del intercambio en el estrecho de Gibraltar en modelos regionales de circulación en el Mediterráneo

La importancia del estrecho de Gibraltar en la circulación general del Mediterráneo lo convierte en un punto clave en el desarrollo de modelos numéricos de circulación de la cuenca. La complejidad de los procesos que controlan tanto el transporte de volumen como las características termohalinas de los flujos intercambiados hace que no esté aún clara la capacidad de modelos de escala climática de reproducir o parametrizar correctamente los mismos. El objetivo de este capítulo es la validacón, mediante los datos experimentales de la estación de Espartel, de varios modelos regionales de circulación del Mediterráneo, tanto en términos de transporte de volumen como de propiedades del flujo de salida.

La validación se lleva a cabo para varias simulaciones numéricas realizadas con los modelos NEMOMED8, NEMOMED12 y NEMOMED36, desarrollados por el Grupo de Modelización de Gran Escala y Clima (GMGEC), del Centro Nacional de Investigaciones Meteorológicas (CNRM, Meteo-France) en Toulouse (Francia). Todos están basados en el modelo de circulación oceánica NEMO, implementado en el Mediterráneo y están concebidos para la simulación a escala climática. La mayoría de las simulaciones analizadas cubre el periodo 2002-2008, que coincide con las series de tiempo utilizadas para su validación (las medidas de la estación de Espartel). También se ha estudiado la variabilidad interanual y las tendencias de una simulación de largo periodo, de 1961 a 2010, para el NEMOMED8.

La diferencia fundamental entre los tres modelos es la resolución: 1/8ºx1/8º para NEMOMED8, 1/12ºx1/2º para NEMOMED12 y 1/36ºx1/36º para NEMOMED36. También difieren en las características de sus mallas, en el forzamiento que utilizan y algunas parametrizaciones. Además, se ha hecho un análisis de sensibilidad a las condiciones impuestas en la zona atlántica del dominio para NEMOMED8, con tres simulaciones que utilizan diferentes climatologías en esta área.

Principales resultados

NEMOMED8 muestra mejores resultados para el transporte de volumen, con valores medios muy próximos a los experimentales para todas las simulaciones y ciclos estacionales comprendidos en el rango de los observados. Las simulaciones que incluyen un término de relajación de la altura del nivel del mar en la zona atlántica del dominio muestran mejores resultados en la representación de los ciclos estacionales del flujo neto y de entrada. Por otro lado, el uso de diferentes climatologías en el forzamiento de esta zona no tiene ningún efecto relevante en la variabilidad del transporte. NEMOMED12 y NEMOMED36 subestiman los flujos de entrada y salida, aunque los ciclos estacionales son similares a los obtenidos por NEMOMED8. La diferencia de resultados entre los tres modelos probablemente se deba a su diferente geometría en el estrecho, particularmente a los valores de la sección transversal donde se calcula el transporte, aunque otros factores como sus distintos forzamientos también pueden contribuir.

Las aguas del flujo mediterráneo de salida observadas en NEMOMED8 son más cálidas y ligeramente más salinas que las medidas experimentales debido a tres causas principales: la primera es un agua levantina intermedia (LIW) excesivamente cálida, una desviación que no se da en la simulación acoplada con el modelo atmosférico ALADIN. La segunda es el bajo porcentaje de WMDW presente en el flujo debido a que esta masa de agua se encuentra a profundidades demasiado grandes en el mar de Alborán como para ser incorporada al flujo. Finalmente, el alto porcentaje de agua central Noratlántica (NACW), que es casi el doble del observado, lo que tiene un fuerte impacto en las propiedades del flujo debido a la gran diferencia entre las aguas atlánticas y mediterráneas. En el caso de NEMOMED12 y NEMOMED36 tanto las propiedades termohalinas del flujo mediterráneo como su composición se ajustan bastante bien a las observaciones, lo que podría ser consecuencia de una mayor capacidad para resolver los procesos que influyen en el intercambio.

El análisis de la variabilidad interanual de los flujos intercambiados en la simulación de largo término NM8-Long (1961-2010) muestra un buen acuerdo entre ésta y las observaciones y estimaciones indirectas de Soto-Navarro et al. (2010) en su

periodo común. Sin embargo, los valores de salinidad y temperatura en ES son mayores que los observados y presentan tendencias positivas que probablemente son consecuencia de las encontradas en las capas intermedia y profunda del Mediterráneo así como en la superficial de la zona atlántica.

Índice

Listado de acrónimos

AAIW:	Antarctic Intermediate Water
ADCP:	Acoustic Doppler Current Profiler
ADW:	Adriatic Deep Water
ALADIN:	Aire Limitée Adaptation Dynamique INitialisation
ARCM:	Atmospheric Regional Circulation Model
ARPEGE:	Action de Recherche Petite Echelle Grande Echelle
ARPERA:	Dynamical downscaling of ERA
AVHRR:	Advanced Very High Resolution Radiometer
AVISO:	Archiving, Validation and Interpretation of Satellite Oceanographic data
AW:	Atlantic Water
CEFREM:	CEntre de Formation et de Recherche sur les Environnements Méditerranéens
CLIO:	Coupled Large-scale Ice Ocean
CLIPPER:	High resolution modelling of the North Atlantic (project)

CMAP:	CPC Merged Analysis of Precipitation
COADS:	Comprehensive Ocean-Atmosphere Data Set
CS:	Camarinal Sill
CT:	Conductivity-Temperature
CTD:	Conductivity-Temperature-Depth
ECCO:	Estimating the Circulation and Climate of the Ocean
ECMWF:	European Center for Medium range Weather Forecast
EEN:	Energy and ENstrophy conservative
EMDW:	Eastern Mediterranean Deep Water
EMT:	Eastern Mediterranean Transient
ENACW:	Eastern North Atlantic Central Water
EOF:	Empirical Orthogonal Function
ERA:	ECMWF Re-Analysis
ES:	Espartel Sill
ETOPO:	Global Relief Model from the National Geophysical Data Center
GLORYS:	GLobal Ocean ReanalYses and Simulations
GTS:	Global Telecomunications System
HIPOCAS:	HIndcast of dynamic Processes of the Ocean and Coastal AreaS of Europe

INGRES:	Intercambios en el estrecho de Gibraltar y Su RESpuesta a forzamientos meteorológicos y climáticos
JPL:	Jet Propulsion Laboratory
LDW:	Levantine Deep Water
LIW:	Levantine Intermediate Water
LSW:	Labrador Sea Water
MAW:	Modified Atlantic Water
MB:	Majuan Bank
MEDAR-MEDATLAS:	MEditerranean Data Archeology and Rescue
MEDIMAP:	MEDIterranean morpho-bathymetry MAP
MO:	Mediterranean Oscillation
MW:	Mediterranean Water
NACW:	North Atlantic Central Water
NADW:	North Atlantic Deep Water
NAO:	North Atlantic Oscillation
NASA:	National Aeronautics and Space Administration
NCAR:	National Center for Atmospheric Research
NCEP:	National Centers for Enviromental Prediction
NEMOMED:	Nucleus for European Modelling of the Ocean (MEDiterranean Sea)

NM8/12/36:	NEMOMED8/12/36
NOAA:	National Oceanic and Atmospheric Administration
OASIS:	Ocean Atmosphere Sea Ice Soil
OPA:	Ocean PArallelise
PC:	Principal Component
SAW:	Surface Atlantic Water
RCM:	Regional Circulation Model
SN10:	Soto-Navarro et al., 2010
SSH:	Sea Surface High
SSS:	Sea Surface Salinity
SST:	Sea Surface Temperature
TRIP:	Total Runoff Integration Pathways
TVD:	Total Variance Dissipation
TN:	Tarifa Narrow
WIW:	Winter Intermediate Water
WAG:	Western Alboran Gyre
WMDW:	Western Mediterranean Deep Water

Objetivos

El objetivo principal de esta tesis doctoral es el estudio de la relación entre el forzamiento climático en el mar Mediterráneo y el intercambio en el estrecho de Gibraltar. Concretamente, se pretende realizar una descripción exhaustiva de los principales forzamientos climáticos de la cuenca, y aplicar este estudio a la estimación y caracterización del flujo atlántico que entra en la misma a través del estrecho. Como complemento a esta estimación, se analizarán las tendencias en la salinidad y la temperatura del flujo en relación con las de las aguas atlánticas adyacentes. Finalmente, se llevará a cabo un estudio de validación de varios modelos climáticos en el estrecho, tanto en términos de transporte de volumen como de propiedades termohalinas del flujo mediterráneo de salida.

Para desarrollar estos objetivos generales se plantean los siguientes objetivos más específicos:

- Estudiar la variabilidad estacional e interanual de los flujos de calor entre el mar y la atmósfera, así como de las distintas componentes del ciclo hidrológico, que constituyen los principales forzamientos de la circulación en la cuenca mediterránea.
- Analizar la sensibilidad de las variables estudiadas a distintos índices climáticos representativos del forzamiento atmosférico a gran escala. En concreto, examinar las diferencias entre índices basados en patrones atmosféricos de carácter general, como la Oscilación del Atlántico Norte (NAO), y local, como la Oscilación Mediterránea (MO).
- Aplicar el estudio del ciclo hidrológico, en combinación con el análisis de la variabilidad del nivel del mar y con datos experimentales medidos en el estrecho de Gibraltar para estimar el flujo atlántico que entra al Mediterráneo y caracterizar su ciclo estacional.

- Investigar, empleando los perfiles de la red Argo, las tendencias en la salinidad y temperatura en las aguas atlánticas adyacentes al estrecho de Gibraltar para tratar de esclarecer el origen de las tendencias observadas en el estrecho.

- Realizar un estudio de validación de los modelos de circulación del Mediterráneo NEMOMED8, NEMOMED12 y NEMOMED36 en el estrecho de Gibraltar, apoyado en las medidas experimentales de la estación de Espartel, que abarque el análisis tanto del intercambio en términos de transporte de volumen como de las propiedades termohalinas y la composición del flujo mediterráneo de salida.

CAPÍTULO 1

Introducción

1.1 Marco geográfico

El mar Mediterráneo (fig. 1.1) es una cuenca semicerrada con una extensión de aproximadamente 3700 km de este a oeste y de unos 1600 km de norte a sur, situada entre los 30ºN y los 45ºN en latitud y los 6ºW y los 36ºE en longitud. Tiene una superficie total aproximada de 2.5 millones de km^2 y está dividido por el Estrecho de Sicilia en dos subcuencas principales: la Oriental, con una superficie de unos 1.65 millones de km^2, que comprende las subcuencas Adriática, Egea, Jónica y Levantina, y la Occidental, de ~0.85 millones de km^2, con las subcuencas del Tirreno, Liguro-Provenzal, Argelina, Balear y de Alborán. Su longitud costera total es de 46000 km, de los cuales el 40% pertenece a islas, siendo las de mayor superficie Sicilia y Cerdeña.

Figura 1.1 Mapa del mar Mediterráneo y sus subcuencas más importantes.

La profundidad media de toda la cuenca es de 1500 m, la máxima es de 5567 m (Calypso Deep) al oeste Creta, en la cuenca Oriental, y en la cuenca Occidental la mayor profundidad se encuentra en el Mar Tirreno (3800 m). Al este, se comunica con el Mar Negro a través de los estrechos turcos (Dardanellos y Bósforo), y al oeste con el océano Atlántico a través del Estrecho de Gibraltar. Su plataforma continental es fundamentalmente una estrecha franja costera (20 km), con excepción del mar Adriático, el golfo de Gabés en la costa este de Túnez, y el Golfo de León, cuya extensa plataforma semicircular llega a los 100 km de anchura.

1.2 Marco oceanográfico

Desde hace varios siglos, es sabido que el Mediterráneo es una cuenca de concentración (Marsigli, 1681; Waitz, 1755; Nielsen, 1912), en la que el exceso de evaporación sobre los aportes de agua dulce de la precipitación y la descarga de los ríos es compensado por un flujo neto de agua atlántica a través del estrecho de Gibraltar (Garret et al., 1993; Bethoux and Gentilli, 1999; Boukthir and Barnier, 2000; Mariotti et al., 2002). Este aporte neto es el resultado de un intercambio bicapa en el que el flujo de entrada en la capa superior está constituido por agua atlántica relativamente dulce y

cálida (15ºC, 36.2), y el de salida, en la capa inferior, por aguas mediterráneas más salinas y frías (13.2ºC, 38.4; Bryden et al. 1994; García-Lafuente at al., 2002a, 2007).

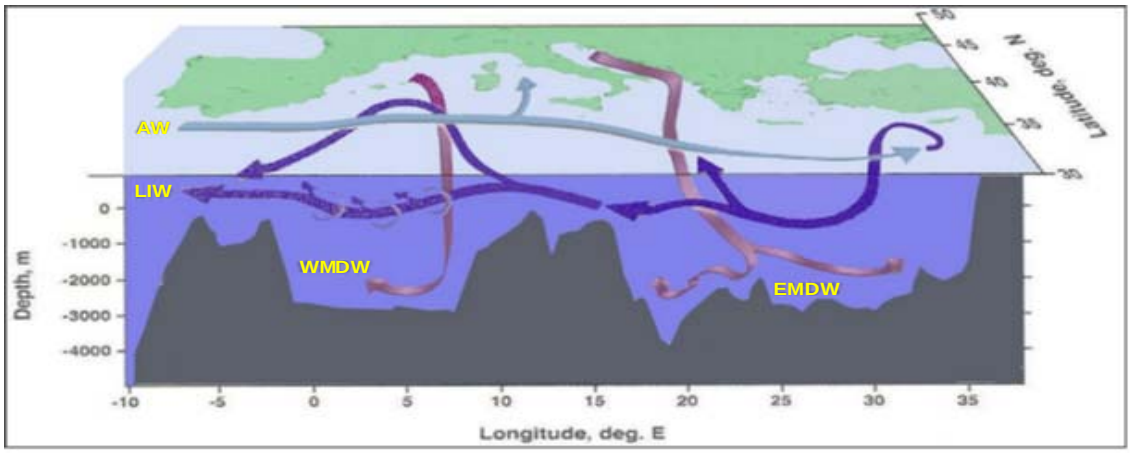

Figura 1.2 Esquema de la circulación termohalina general en el Mediterráneo. Las siglas identifican las distintas masas de agua: agua atlántica (AW), agua levantina intermedia (LIW), agua profunda del Mediterráneo oriental (EMDW) y agua profunda del Mediterráneo occidental (WMDW).

El proceso de transformación de las aguas atlánticas en mediterráneas se lleva a cabo mediante una célula termohalina que involucra toda la cuenca (fig. 1.2). Esquemáticamente, el agua atlántica se vuelve progresivamente más salina conforme se desplaza hacia el Este; en la zona más oriental, la cuenca Levantina (fig. 1.1), se enfría durante el invierno, aumenta su densidad y se hunde hasta profundidades intermedias (entre 150 y 600 m), dando lugar al agua levantina intermedia (LIW, por sus siglas en inglés). Ésta constituye el núcleo principal de aguas mediterráneas que abandonan el estrecho, ya que se sitúa en la capa cuya profundidad coincide con la del umbral de salida (~290 m).

Además de la formación de aguas intermedias, en determinados puntos de la cuenca donde el forzamiento atmosférico es especialmente severo, tiene lugar la formación de aguas profundas. Concretamente, en el Adriático (Schlitzer et al., 1991; Malanotte-Rizzoli et al., 1997) y, excepcionalmente, en el Egeo (Roether et al., 1996), se forma el agua profunda del Mediterráneo oriental (EMDW). En la cuenca occidental este proceso ocurre en el Golfo de León (Stommel, 1972; Mertens and Schott, 1998), dando lugar al agua profunda del Mediterráneo occidental (WMDW). El estrecho de

Sicilia (~320 m de profundidad) constituye una barrera para el EMDW e impide que estas aguas lleguen a la cuenca occidental y formen parte del flujo de salida. No ocurre lo mismo con el WMDW, que fluye en la capa profunda hasta Gibraltar y constituye parcialmente la vena mediterránea que abandona el estrecho (Stommel, 1972; Kinder and Bryden, 1990; García-Lafuente et al., 2007).

Al poseer una circulación termohalina propia, en la que además se dan procesos de formación de agua profunda, el mar Mediterráneo puede considerarse como un océano en miniatura (Bethoux, 1979; Bethoux et al., 1998,1999). Esta circulación está forzada por la interacción entre la atmósfera y el mar, principalmente por los intercambios de calor y agua dulce entre ambos sistemas. Dado el delicado equilibrio existente entre las diferentes masas de agua y su estrecha relación con el forzamiento atmosférico, el Mediterráneo es especialmente sensible a los efectos del cambio climático, y puede ser considerado como un "laboratorio a pequeña escala" en el que estudiar sus consecuencias.

1.3 Flujos de calor y balance hidrológico

La circulación del Mediterráneo está en gran medida condicionada por los flujos de calor y agua dulce entre el mar y la atmósfera. El primero está constituido por cuatro componentes, dos radiativas (la radiación de onda corta procedente del Sol y la de onda larga radiada por la Tierra) y dos turbulentas (el calor latente y el calor sensible). El flujo de agua dulce lo constituyen principalmente la evaporación (E) y la precipitación (P). El resto de términos del balance hidrológico: la descarga de ríos (R) y el intercambio con el mar Negro (B), ejercen una menor influencia. Los mares semicerrados, como el Mediterráneo, son adecuados para la caracterización de los flujos hídricos y de calor puesto que permiten establecer un balance cerrado. En este análisis juega un papel esencial la determinación del intercambio a través del estrecho de Gibraltar.

Macdonald et al. (1994), mediante observaciones in-situ en el estrecho de Gibraltar, calculan un flujo de calor medio de 5.2±1.3 Wm^{-2}. Los resultados de otros

estudios basados en estimaciones del transporte medio en Gibraltar varían entre 8.5 Wm^{-2} (Bethoux, 1979) y 5 Wm^{-2} (Bunker et al., 1982). La afinidad de estos resultados contrasta con la gran variabilidad de los obtenidos por la mayoría de los estudios que analizan el intercambio entre el mar y la atmósfera a través de la superficie de éste. Los promedios sobre toda la cuenca calculados a partir de datos climatológicos estiman una ganancia neta que oscila entre 20 y 30 Wm^{-2} (Bunker et al., 1982; Garrett et al., 1993; Schiano et al., 1993; Gilman and Garrett, 1994). El origen de esta discrepancia estriba en los métodos utilizados para la estimación de las diferentes componentes del flujo. Por un lado, se sobreestima la radiación de onda corta, debido a una parametrización inadecuada en las ecuaciones empíricas de la atenuación por aerosoles (Tragou and Lascaratos, 2003) y, por otro, se subestiman las pérdidas por radiación de onda larga (Bignami et al., 1995). Otra fuente de variabilidad son los diferentes periodos analizados así como la caracterización de los campos de viento (Ruti et al., 2008). Estudios más recientes basados en simulaciones numéricas calculan una pérdida sobre toda la cuenca de 1 Wm^{-2} (Ruiz et al., 2008).

Respecto al balance hidrológico, existe un gran número de estudios que abordan su caracterización (Bethoux, 1979; Peixoto et al., 1982; Bryden and Kinder, 1991b; Harzallah et al., 1993; Gilman and Garrett, 1994; Castellari et al., 1998; Angelucci et al., 1998; Béthoux and Gentili, 1999; Josey et al., 1999; Boukthir and Barnier, 2000; Mariotti et al., 2002). Sin embargo, el problema aún está lejos de resolverse ya que los resultados dependen fuertemente de las distintas bases de datos utilizadas así como de la metodología empleada en cada uno de ellos. La dificultad para obtener medidas de precipitación sobre el mar es la mayor fuente de incertidumbre, aunque no es la única. Como ejemplo para ilustrar la variabilidad en los resultados, las estimaciones de evaporación neta (E-P) varían entre 421 $mm \cdot año^{-1}$ (Gilmant and Garret, 1994) y 1230 $mm \cdot año^{-1}$ (Bethoux and Gentilli, 1999), una diferencia de casi un 400%. En general, la evaporación excede a la suma de los aportes fluviales y la precipitación en toda la cuenca; la única región donde las aportaciones de agua dulce superan las pérdidas por evaporación es el norte del Adriático (Raicich, 1996).

Los estudios sobre la descarga de los ríos estiman un aporte anual medio para todo el Mediterráneo en el rango 8.1-16 $\cdot 10^3\ m^3 s^{-1}$ (Tixeront, 1970; Ovchinnikov, 1974; Margat, 1992; Boukthir and Barnier, 2000; Struglia et al., 2004). Los valores más bajos

se corresponden con los estudios más recientes, lo que posiblemente se deba a la proliferación de embalses en los últimos años así como al incremento del regadío en las cuencas de captación fluviales. Otra posible causa es la variabilidad de los patrones atmosféricos, concretamente un alto índice de la oscilación del atlántico norte (NAO), que ha podido reducir la precipitación en el área mediterránea en los últimos años (Mariotti et al., 2002). El ciclo estacional de R tiene una amplitud de unos $5 \cdot 10^3$ $m^3 s^{-1}$, con su máximo a principios de primavera (Struglia et al., 2004), un valor muy inferior al de (E-P) (aproximadamente un 20%; Boukthir and Barnier, 2000; Mariotti et al., 2002). No obstante, debido a las fases de ambos ciclos, sus valores son comparables en primavera, por lo que a escala regional la descarga de ríos puede tener una influencia importante en la modulación de procesos oceánicos (Rohling and Bryden, 1992; Zavatarelli et al., 1998; Bethoux and Gentilli, 1999; Boscolo and Bryden, 2001).

El intercambio entre el mar Negro y el Mediterráneo se produce a través de los estrechos turcos, Bósforo y Dardanelos, cuyo umbral tiene una profundidad de unos 36 m. Es un intercambio bicapa, en el que fluye agua relativamente dulce hacia el Egeo en la capa superior, de unos 10 m de profundidad, mientras agua mediterránea más salina se adentra hacia el mar Negro. Está controlado por la diferencia de nivel del mar entre ambas cuencas y resulta en un flujo neto hacia el Mediterráneo. Según los diversos estudios publicados, éste flujo varía entre 5.8 y $9.6 \cdot 10^3$ $m^3 s^{-1}$ (Tolmazin, 1985; Unluata et al., 1990; Besiktepe et al., 1994, Bethoux and Gentili, 1999; Kanarska and Maderich, 2008; Liu et al., 2009). A efectos del balance hidrológico, son valores comparables con el de los aportes fluviales. De hecho, debido a la baja salinidad de sus aguas (~ 18), el intercambio con el mar Negro suele considerarse como un aporte fluvial más, aunque sus efectos sobre la circulación termohalina del norte del Egeo son importantes (Stanev and Peneva, 2002).

1.4 Circulación termohalina del Mediterráneo

1.4.a Transformación del flujo atlántico

El flujo atlántico constituye el mayor aporte de agua relativamente dulce al Mediterráneo. Tras modificarse ligeramente por mezcla con el flujo de salida en el estrecho de Gibraltar, se adentra en el mar de Alborán como agua atlántica modificada (MAW), con una salinidad de ~36.5. Al desplazarse hacia el este siguiendo la circulación ciclónica de la cuenca va incrementando gradualmente su salinidad debido a la evaporación hasta los 37.0 - 37.5 en el estrecho de Sicilia (Astraldi et al. 2002), llegando a los 38.6 en las cercanías del canal de Creta (fig. 1.3). Sin embargo, no toda el MAW salva el estrecho de Sicilia y cruza hacia el Mediterráneo oriental. Parte de ella permanece en el Mediterráneo occidental, y pasa a formar parte de la circulación de esta subcuenca. La cantidad de MAW que pasa al Mediterráneo oriental se estima en 1-3 Sv (1 Sv = 10^6 m^3s^{-1}. Millot, 1999).

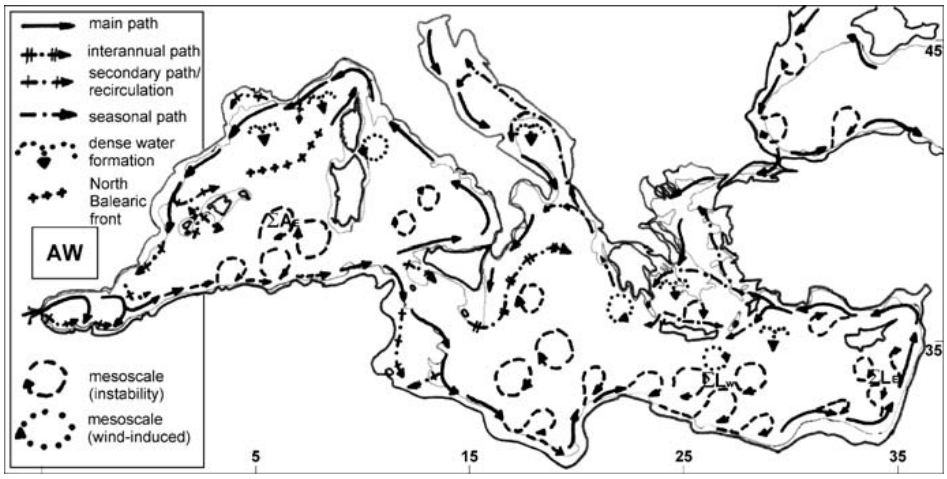

Figura 1.3 Circulación del MAW. Tomada de Millot and Taupier-Letage (2005).

En el mediterráneo occidental, el MAW que no atraviesa el estrecho de Sicilia se incorpora a la circulación ciclónica de esta cuenca, constituida por un giro en sentido antihoraio con algunas modificaciones causadas por la presencia de las islas de Córcega

y Cerdeña (fig. 1.3). Este giro transporta el MAW desde Gibraltar a lo largo de la costa norteafricana formando la inestable corriente argelina, de la que se desprenden estructuras mesoescalares (eddies) que transportan y mezclan MAW en el interior de la cuenca (Millot et al., 1997; Fuda et al., 2000). En el estrecho de Sicilia la corriente se separa en dos ramas, una pasa al mediterráneo oriental y la otra fluye hacia el norte por el Tirreno siguiendo la costa italiana. El flujo principal continúa a lo largo de las costas francesa y española, constituyendo la corriente norte, que se separa en dos ramas en la cuenca balear (Millot, 1999). Una de ellas se desplaza hacia el sureste de las islas Baleares mientras la otra continúa hacia el sur por la costa de la española y puede identificarse a profundidades de hasta 200 m en el mar de Alborán, transformada en "vieja" MAW, con salinidades en torno a 38.0-38.3 (Millot, 1999).

1.4.b Formación de aguas intermedias

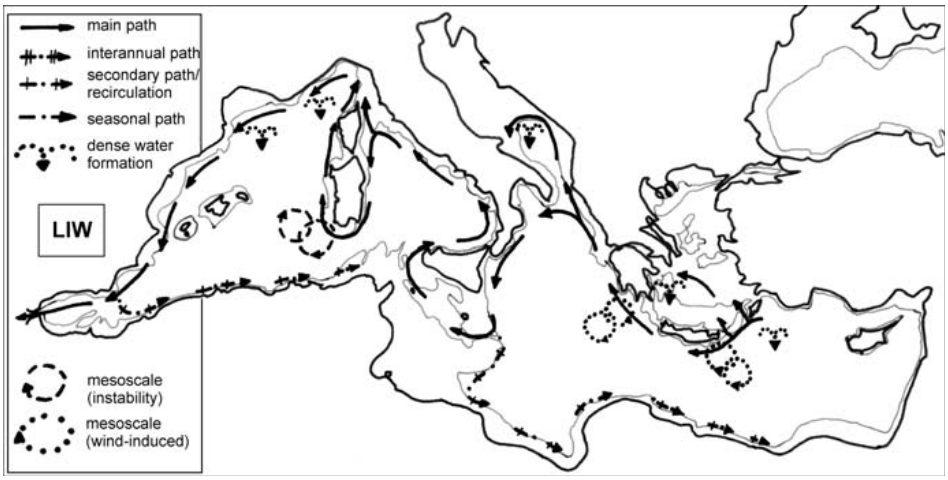

Figura 1.4 Circulación del LIW. Tomada de Millot and Taupier-Letage (2005).

El paulatino incremento en la salinidad del MAW hasta alcanzar la cuenca Levantina constituye el precondicionamiento necesario para que el efecto de la evaporación y el enfriamiento invernales aumenten su densidad provocando su hundimiento. Dependiendo de la profundidad que alcance, se formará agua levantina intermedia (LIW) o profunda (LDW). El agua levantina intermedia es la principal masa de agua del mar Mediterráneo y ocupa la capa entre los 200 y 500 m. Su núcleo es

generalmente identificado por un máximo en la salinidad de 38.95-39.05 cerca de las áreas de producción (Lascaratos, 1993) que se reduce a 38.75 en el estrecho de Sicilia (Bethoux and Gentilli, 1996, 1999; Astraldi et al., 1999, 2002) y a 38.4 en las proximidades del estrecho de Gibraltar (Tsimplis and Bryden, 2000). La producción anual de LIW varía según resultados numéricos entre 0.6 y 1.3 Sv, con un valor promedio usual de 1 Sv (Nittis and Lascaratos, 1998), consistente con estimaciones previas basadas en diferentes métodos (Ovchinnikov, 1984; Lascaratos, 1993; Tziperman and Speer, 1994).

La región típica de formación de LIW o LDW es el giro de Rodas (Ovchinnikov, 1984; Ovchinnikov and Plakhin, 1984; Malannote-Rizzoli and Hecht, 1988; Buongiorno-Nardelli and Salusti, 2000). El desarrollo de este giro ciclónico levanta las isopicnas facilitando la acción del forzamiento atmosférico en las capas sub-superficiales más densas (Lascaratos et al., 1993; Lascaratos and Nittis, 1998). Otras zonas en las que es probable que se produzca LIW son el Sur del Egeo y el sur de la cuenca Levantina (Wüst, 1961; Bruce and Charnock, 1965; Morcos, 1972; Ozturgut, 1976; Theocharis et al., 1988; Georgopoulus et al., 1989).

También existe formación de aguas intermedias en el Mediterráneo occidental, la denominada agua intermedia invernal (WIW, Millot 1999) que se forma en las costas septentrionales. Se caracteriza por un máximo de salinidad de 38.3 y fluye siguiendo la circulación ciclónica de la cuenca por debajo del MAW (Millot, 1999).

Tras su formación, el LIW se va desplazando hacia el oeste desde el sur del arco de Creta, ocupando las capas intermedias del mar Jónico (fig. 1.4). En el estrecho de Otranto se divide en dos ramas, una de las cuales penetra en el Adriático mientras la segunda sigue la costa sureste de Italia cruzando a la cuenca occidental (Millot, 1999). Existe cierta controversia respecto al camino seguido por el LIW a partir de este punto. Algunos estudios afirman que es similar al giro anticiclónico descrito por el MAW (Millot, 1987,1999). Por otro lado, diversos resultados numéricos sugieren la existencia de un camino directo a través de la cuenca hacia el estrecho de Gibraltar (Wu and Haines, 1996; Herbaut et al., 1997). Los resultados más recientes de Millot and Taupier-Letage (2005) refuerzan la hipótesis del giro antihorario, explicando la presencia de

LIW en el centro de la cuenca como consecuencia del transporte por eddies desprendidos de la corriente argelina.

1.4.c Formación de aguas profundas

La formación de aguas profundas en el Mediterráneo tiene lugar tanto en la cuenca occidental como en la oriental. En esta última, las aguas superficiales de la cuenca Levantina que no participan en la formación de LIW continúan circulando hacia el norte y el noroeste alcanzando las costas septentrionales del Egeo y el Adriático. Durante el invierno, bajo la acción de vientos fríos y secos de componente norte, se enfrían y salinizan aún más y, dependiendo de las pérdidas de calor que experimenten, pueden llegar a hundirse formando aguas profundas.

En el Adriático, este proceso se da tanto en el norte, cerca de la plataforma continental, como en el sur, en zonas de mar abierto, y está influenciado por la entrada de LIW a través del estrecho de Otranto (Ovchinnikov et al., 1987; Manca et al., 2002). El agua profunda producida en la plataforma se propaga hacia el sur mezclándose con la producida en mar abierto y dando lugar al agua profunda del Adriático (ADW), que puede sobrepasar el estrecho de Otranto y constituye la principal contribución al agua profunda del Mediterráneo oriental (EMDW). El flujo anual de ADW hacia el mar Jónico es del orden de 0.1-0.4 Sv, con fluctuaciones que llegan a 1 Sv (Manca et al., 2002), y se caracteriza por una densidad de ~ 29.4-29.9 kgm^{-3} (Franco et al., 1982; Malanotte-Rizzoli, 1991). La profundidad a la que se establecen estas aguas impide que superen el umbral del estrecho de Sicilia, quedando por tanto confinadas en la cuenca oriental.

A finales de los años 80 tuvo lugar una anómala producción masiva de agua profunda en el Egeo, que sobrepasó los estrechos del arco de Creta y sustituyó al ADW como principal constituyente del EMDW, extendiéndose por toda la cuenca oriental (Roether et al., 1996; Theocharis et al., 1999; Theocharis et al., 2002; Manca et al., 2003). Simultáneamente disminuyó la producción de agua profunda en el Adriático, lo que supuso un cambio drástico en la circulación termohalina del Mediterráneo oriental

(Manca, 2000; Del Rio et al., 2009). Este fenómeno, ampliamente estudiado y para el que se han propuesto diversas hipótesis como la redistribución interna de sal (Klein et al., 1999), los cambios en el forzamiento atmosférico local (Theocharis et al., 1999) o los cambios en algunos patrones de circulación (Malanotte- Rizzoli et al., 1999), se denomina Eastern Mediterranean Transient (EMT). A mediados de los años 90, se restableció la situación previa, pero el estudio del EMT y la determinación de sus casusas y consecuencias sigue siendo una cuestión abierta y de indudable interés para la comunidad científica del Mediterráneo.

En el Mediterráneo occidental, la formación de agua profunda tiene lugar en el Golfo de León (Stommel, 1972). Durante el invierno, los vientos fríos y secos predominantes del noroeste primero mezclan el MAW y WIW con las aguas subyacentes (LIW), más cálidas y salinas y, posteriormente`, las pérdidas de flotabilidad ligadas a las pérdidas de calor provocan su hundimiento, formando el agua profunda del Mediterráneo occidental (WMDW, Mertens and Schott, 1998). La producción de WMDW depende en gran medida del forzamiento atmosférico en el periodo inicial de precondicionamiento (desde finales de otoño hasta que se produce la convección), al que sigue una fuerte mezcla en células convectivas de aproximadamente 1 km de diámetro, que se extienden por una región de unos 100 km (Rhein, 1995; Marshal and Schott, 1999) cuando el proceso de formación se desarrolla completamente. Las aguas formadas, que no siempre alcanzan el fondo de la cuenca (Send et al., 1999), tienen una densidad característica de 29.1 kgm^{-3} (MEDOC group, 1970), y el volumen producido en cada evento varía mucho según el método usado para su estimación (0.4-3 Sv). El papel del WMDW en la circulación de la cuenca occidental es muy relevante: llena las capas profundas y su señal puede apreciarse en el flujo de salida a través del estrecho de Gibraltar (Stommel, 1972; Kinder and Bryden, 1990; García-Lafuente et al., 2007).

1.5 Influencia de los patrones atmosféricos de gran escala

Los patrones de variabilidad atmosférica a gran escala cuyos centros de acción se sitúan en las cercanías del Mediterráneo ejercen una potencial influencia en la

cuenca. Este el caso de la Oscilación del Atlántico Norte (NAO), uno de los más importantes indicadores de la variabilidad climática en el hemisferio norte (Walker and Bliss, 1932; van Loon and Rogers, 1978; Barnston and Livezey 1987; Hurrell et al., 2003). Consiste en un patrón bipolar de presión atmosférica a nivel del mar en la región del Atlántico Norte y Europa, con un centro de bajas presiones situado sobre Islandia y uno de altas presiones situado sobre las islas Azores. Su variabilidad está asociada con cambios en la intensidad de la corriente del Atlántico Norte, así como en las rutas de las tormentas y en el transporte de calor y humedad, que se reflejan en la temperatura y las precipitaciones sobre áreas muy extensas (Walker and Bliss 1932; van Loon and Rogers 1978; Rogers and van Loon 1979; Hurrell 1995; Serreze et al., 1997; Dai et al., 1997; Mariotti et al., 2002; Mariotti and Arkin, 2007).

Diversos estudios confirman la influencia de la NAO en la precipitación (Hurrell 1995; Mariotti et al., 2002), la descarga de ríos (Struglia et al., 2004) y la variabilidad del nivel del mar (Tsimplis and Josey, 2001) de la cuenca el Mediterránea. Se ha sugerido su posible influencia en el cambio repentino en las características del LIW observado en los años 1981 y 1982 (Brankart and Pinardi, 2001), así como en las propiedades del WMDW (Rixen et al., 2005). Aunque la vinculación de la NAO con un fenómeno de gran escala como el EMT no está del todo clara (Josey, 2003; Tsimplis et al., 2004; Rixen et al., 2005;), presenta una alta correlación con la temperatura de las aguas superficiales, lo que indica que pudo jugar un papel importante en su desarrollo (Demirov and Pinardi, 2002).

Algunos autores han sugerido la existencia de un patrón propio de oscilación en el Mediterráneo entre las cuencas oriental y occidental, la Oscilación Mediterránea (MO, Conte et al., 1989). Este índice de carácter local podría tener una influencia más específica sobres los procesos de la cuenca (Supic et al., 2004; Gomis et al., 2006), aunque hasta el momento ha sido poco estudiado.

1.6 Variabilidad del nivel del mar

La variabilidad total del nivel del mar en el Mediterráneo depende de dos contribuciones: la contribución estérica, debida a contracciones o dilataciones de la columna de agua a causa de variaciones en la salinidad o la temperatura, y la contribución másica, resultado de la adición o sustracción de agua debidas a la precipitación, evaporación, descarga de ríos, fusión de glaciares, etc. La primera está principalmente regulada por los flujos de calor entre el mar y la atmósfera, que regulan la variabilidad de la temperatura, mientras la segunda está ligada al ciclo hidrológico de la cuenca, al forzamiento atmosférico local (Tsimplis and Josey, 2001) y al gradiente de presión y régimen hidráulico en el estrecho de Gibraltar (Ross et al., 2000). Este último controla el acoplamiento entre los niveles del Atlántico y el Mediterráneo, es decir, la respuesta de la cuenca a las variaciones oceánicas.

Sólo existen unas pocas estaciones de medida con registros desde principios del siglo XX en la costa norte del Mediterráneo occidental (Marsella y Génova) y del Adriático (Trieste y Venecia). La tendencia del nivel del mar en tres de estas estaciones varía en el rango 1.1-1.3 mm·año^{-1} (Tsimplis and Spencer, 1997; Tsimplis and Baker, 2000), valores ligeramente menores que los estimados a nivel global de 1-2 mm·año^{-1} (Church et al., 2001). Las medidas en la cuarta estación, en Venecia, están afectadas por procesos geológicos locales de hundimiento del terreno causados por la extracción de aguas subterráneas, por lo que no pueden ser usadas para estimaciones de tendencias del nivel del mar (Woodworth, 2003).

La evolución del nivel del mar del Mediterráneo desde principios del siglo XX puede dividirse en tres periodos. Hasta los años 60, se observan tendencias similares a las medidas en el océano abierto (Tsimplis and Baker, 2000). Entre 1960 y 1990, el nivel del mar se mantuvo prácticamente sin cambios o, en todo caso, se observó una cierta disminución (Orlic and Pasaric, 2000; Tsimplis and Baker, 2000) debida principalmente a variaciones en la presión atmosférica durante los inviernos (Tsimplis and Josey, 2001; Woolf et al., 2003) así como a la disminución de la temperatura y cambios en la salinidad ligados a la NAO (Tsimplis and Rixen, 2002). Estos últimos estuvieron restringidos a las zonas septentrionales de la cuenca, en concreto, al

Adriático y el Egeo (Painter and Tsimplis, 2003), mientras que los gradientes de presión atmosférica afectan a todo el Mediterráneo (Tsimplis and Josey, 2001).

A partir de 1993 el análisis de los datos de altimetría por satélite del proyecto TOPEX/POSEIDON revela una estructura espacial muy compleja en la variabilidad del nivel del mar (Cazenave et al., 2002; Fenoglio-Marc, 2002; Criado-Aldeanueva et al., 2008; Del Rio-Vera et al., 2009). En los primeros años de este periodo se observó un rápido incremento en la cuenca oriental, ligado a cambios en la temperatura superficial del mar, con valores de hasta 7 mm·año^{-1} (Cazenave et al., 2002; Fenoglio-Marc, 2002). Posteriormente, se produjo una brusca reducción de las tendencias (~2 mm·año^{-1}), llegando éstas a ser negativas en zonas de la cuenca oriental, que también se vio reflejado en variaciones de la temperatura superficial del mar (Vigo et al., 2005; Criado-Aldeanueva et al., 2008; Del Rio-Vera et al., 2009). Este rápido incremento entre 1993 y 2001, y su posterior atenuación parecen estar relacionados con cambios de circulación asociados al EMT.

Durante el mismo periodo se observó una disminución en la diferencia entre los niveles del Atlántico y el Mediterráneo en el estrecho de Gibraltar, consecuencia de un cambio en el régimen hidráulico del estrecho (Ross et al., 2000) o en la diferencia de densidad entre las capas atlántica y mediterránea (Brandt et al., 2004). Esto hace pensar en una posible relación entre el nivel del mar en el Mediterráneo oriental y los saltos hidráulicos en el estrecho, probablemente a través de cambios en la salinidad del LIW (Tsimplis et al., 2005).

En general, la variación del nivel del mar a partir de la segunda mitad del siglo XX en el Mediterráneo difiere significativamente de la del océano Atlántico (Tsimplis and Baker, 2000; Woolf et al., 2003). La causa de esta diferencia puede estar tanto en la variabilidad atmosférica específica de la cuenca inducida por la NAO como en procesos estéricos a escala de cuenca o subcuenca. En cualquier caso, es poco probable que la situación se mantenga en el futuro considerando que la causa principal del incremento del nivel del mar en el Atlántico es el la adición de agua por la fusión de los casquetes polares (Miller and Douglas, 2004), lo que acabará afectando al gradiente de presión en Gibraltar y, por tanto, al nivel del mar en el Mediterráneo.

1.7 El estrecho de Gibraltar

1.7.1 Marco Geográfico

El Estrecho de Gibraltar es la única conexión del Mediterraneo con el oceáno Atlántico (fig. 1.5). Tiene una longitud de unos 60 km, con su eje principal inclinado unos 15 grados en sentido antihorario respecto a la dirección este-oeste, y 14 km de ancho en su zona más angosta, la sección de Tarifa. En la zona mediterránea la profundidad pasa de los 2000 m en el Mar de Alborán a los 800-900 m en la entrada oriental del estrecho (en la sección entre Tarifa y Ceuta) y disminuye bruscamente hasta los 290 m en el umbral de Camarinal (CS en la fig. 1.5). Hacia el oeste, la presencia de una cresta submarina, el Banco de Majuan (MB), divide el flujo de salida del Mediterráneo en dos canales, el septentrional, con una profundidad de unos 250 m y el meridional, de 360 m de profundidad. Este último desemboca en el umbral de Espartel (ES en la fig. 1.5), que es la principal puerta de salida del flujo mediterráneo

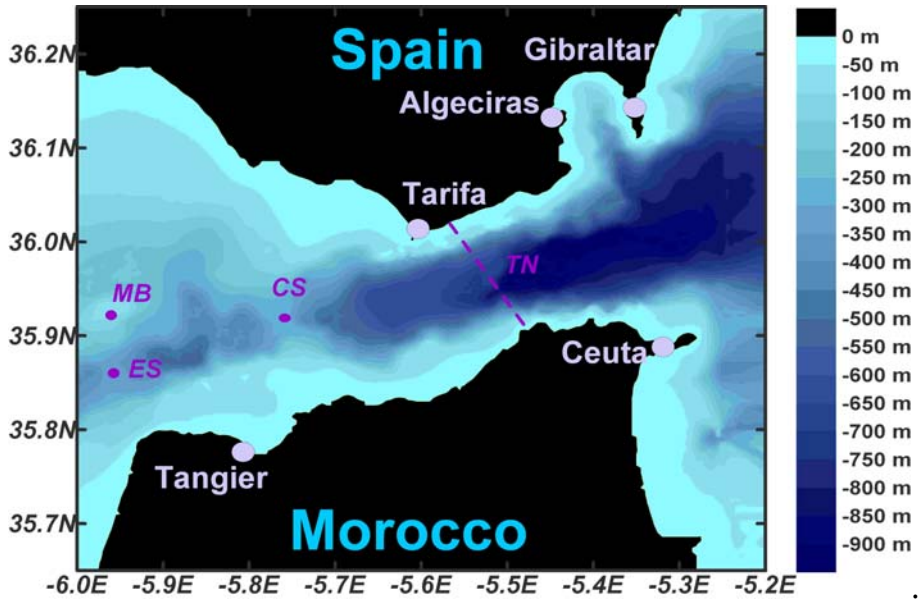

Figura 1.5 Mapa batimétrico del Estrecho de Gibraltar. Los puntos marcados son el umbral de Camarinal (CS), el Banco de Majuan (MB), que divide el canal de salida en dos, el umbral de Espartel (ES), punto principal de salida del flujo Mediterráneo y el estrechamiento de Tarifa (TN).

1.7.2 Intercambio en el estrecho de Gibraltar

El intercambio medio

La primera aproximación al estudio del intercambio en el estrecho de Gibraltar es la determinación del intercambio medio o intercambio secular, cuya dinámica se analiza en términos de un modelo de dos capas con temperatura y salinidad homogéneas: una corriente superficial de agua Atlántica relativamente cálida y poco salina entrando al Mediterráneo, y otra saliente en profundidad de agua Mediterránea más fría y bastante más salina (Lacombe and Richez, 1982; Bryden and Kinder, 1991b). El origen de esta circulación antiestuarina (Figura 1.6) es el exceso de evaporación sobre la cuenca Mediterránea, que da lugar a una pérdida de flotabilidad y a la formación de aguas profundas. De la diferencia de densidades entre las aguas de ambas cuencas (Mediterránea y Atlántica) se deriva un gradiente de presión que fuerza la salida de las aguas mediterráneas, mientras que el desnivel del mar en ambos lados del Estrecho (unos 16 cm, Garrett et al., 1989) crea un segundo gradiente que propicia la entrada del agua atlántica en el Mediterráneo. Si se utiliza la conservación simultánea de masa y sal del Mediterráneo, que conducen a las clásicas relaciones desarrolladas por Knudsen (1899), es posible realizar una estimación sencilla de los flujos intercambiados y de su diferencia. Sin embargo, la incertidumbre con la que se conocen las magnitudes involucradas, especialmente la evaporación neta de la cuenca (E-P), dificulta enormemente la verificación experimental de estas relaciones.

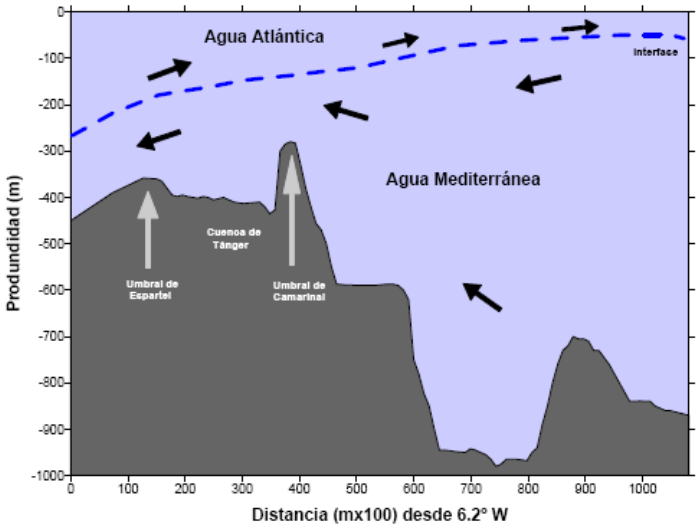

Figura 1.6 Batimetría a lo largo del eje principal del Estrecho donde se muestra la sección de mínima profundidad correspondiente al umbral de Camarinal (290 m) y el umbral secundario de Espartel (360 m). En medio se encuentra la cuenca de Tánger, con una profundidad media de 400 m. La línea discontinua azul muestra la profundidad media de la interfase de separación entre el agua atlántica y la mediterránea (Tomada de Sánchez-Román, 2008).

Por otro lado, el Estrecho de Gibraltar es un cuello de botella para el flujo entrante/saliente, puesto que la geometría limita la cantidad de agua que se puede intercambiar para una distribución dada de densidades. La consideración adicional de la ecuación de Bernoulli permite establecer esta cota para los flujos intercambiados (Armi and Farmer 1986; Farmer and Armi, 1987). El intercambio máximo se establece cuando existe un doble control hidráulico en las secciones de mínima profundidad (umbral de Camarinal, CS en fig. 1.5) y de mínima anchura (estrechamiento de Tarifa, TN en fig. 1.5), siendo el flujo entre ambas secciones subcrítico. En este contexto, un flujo se dice controlado si el número de Froude es igual a la unidad, y supercrítico (subcrítico) si es mayor (menor) que uno. Para un flujo bicapa el número de Froude G viene dado por:

$$G^2 = F_1^2 + F_2^2 = \frac{u_1^2}{g' h_1} + \frac{u_2^2}{g' h_2} \qquad (1.1)$$

donde u_i, h_i, ρ_i (i = 1, 2) son la velocidad, profundidad y densidad de las capas superior (i = 1) e inferior (i = 2) respectivamente. Por su parte, $g' = g(\rho_2 - \rho_1)/\rho_2$ es la gravedad

reducida. Bryden and Kinder (1991b) obtienen la siguiente expresión para los flujos máximos en función de la geometría y suponiendo que el flujo neto es pequeño en comparación con los flujos absolutos:

$$Q_1 \cong -Q_2 = P \cdot (g' b_c) \frac{W_c b_c}{2} \qquad (1.2)$$

siendo bc y Wc la profundidad y la anchura del estrecho en superficie en la posición del umbral de Camarinal, y *P* un número adimensional que depende de la fricción con el fondo y la geometría del canal. Para un canal triangular y parámetros basados en observaciones obtuvieron una transporte de $Q_1 = -Q_2 = 1.06$ Sv, lo que a raíz de estimaciones previas sugiere un intercambio al menos cercano al máximo posible. Puede pensarse que estos valores para el transporte son poco fiables debido a las diversas simplificaciones, de las que la más seria probablemente sea la consideración de una geometría tan poco realista, así como el simplificado sistema bicapa. No obstante, tanto medidas "in situ" como resultados de modelos numéricos tridimensionales proporcionan flujos realmente cercanos (Sannino et al. 2002, Sánchez Román et al., 2009).

Variabilidad temporal del intercambio

La variabilidad temporal de los flujos es muy importante, ya que en ocasiones las fluctuaciones llegan a superar el intercambio medio (~1 Sv) (Candela et al., 1990; Bryden et al., 1994; García-Lafuente et al., 2002a; García-Lafuente and Vargas, 2003), y pueden (potencialmente) llegar a invertir el sentido de la corriente en alguna de las dos capas, e incluso, en casos extremos, en ambas (Vargas et al., 2006; Sánchez-Román et al., 2009).

Las fluctuaciones respecto al flujo medio se dividen en tres categorías: fluctuaciones de marea, con periodos de 12 y 24 horas aproximadamente; fluctuaciones subinerciales (periodos de algunos días a varias semanas o pocos meses) y fluctuaciones de baja frecuencia, es decir, señales estacionales e interanuales (Lacombe and Richez, 1982; García-Lafuente and Vargas, 2003).

Las fluctuaciones de tipo mareal tienen su origen en la marea del Atlántico Norte y afectan tanto a la dirección e intensidad de las corrientes como a la superficie de separación de las capas de agua atlántica y mediterránea. Las observaciones realizadas durante el proyecto Gibraltar Experiment (Kinder and Bryden, 1987, 1988) indican que, en promedio, un 75 % y un 12 % de la energía cinética medida en el Estrecho se encuentran en las bandas semidiurna y diurna respectivamente (Candela et al., 1990). Las corrientes de marea son especialmente intensas en el Umbral de Camarinal (Bruno et al., 1999), donde son capaces de invertir el flujo de cada una de las capas con periodicidad semidiurna, de modo que en ciertos momentos de marea toda la columna de agua fluye en la misma dirección (Bryden et al., 1994; Vargas et al., 2006).

La variabilidad subinercial, con periodos comprendidos entre algunos días a varias semanas, puede dividirse en tres tipos: el primero, básicamente barotrópico, se origina por las variaciones de presión atmosférica, y de la tensión del viento asociada, sobre el Mediterráneo y la diferente respuesta del océano Atlántico a dichas variaciones (García-Lafuente, 1986; Garret et al., 1989; Candela et al., 1989; García-Lafuente et al, 2002b). El segundo tiene su origen en las variaciones quincenales y mensuales asociadas a los ciclos de marea viva-marea muerta, dando lugar a fluctuaciones de corriente de carácter fuertemente baroclino (Candela et al., 1989; Bryden et al., 1994; García-Lafuente et al., 2000; Tsimplis and Bryden, 2000). Otro tipo de interacción no lineal mediante el cual la banda de marea modula los flujos subinerciales, aunque no las corrientes propiamente dichas, se conoce como “flujos rectificados de marea”. Se trata de una contribución a los flujos intercambiados debida a una correlación positiva entre las corrientes y las variaciones de la profundidad de la interfaz en la banda de marea, siendo el reflejo del carácter baroclino de la marea en el Estrecho como consecuencia de su interacción con la topografía (Vargas, 2004).

Por último, las fluctuaciones de carácter estacional e interanual tienen su origen en la variabilidad climática del Mediterráneo. Las primeras responden principalmente al ciclo estacional del flujo de calor, cuyo efecto en el nivel del mar se traduce en variaciones en el desnivel entre el Atlántico y el Mediterráneo que llegan a los 6 cm (Bormans et al., 1986). Los procesos invernales de formación de WMDW en el Golfo de León también influencian la variabilidad estacional tanto del transporte como de las

propiedades del flujo mediterráneo (García-Lafuente et al., 2007). Estos procesos de formación de agua profunda a su vez reflejan la variabilidad en el forzamiento atmosférico sobre la cuenca, y también producen efectos a escala interanual en el intercambio. Otros factores responsables de las fluctuaciones a escala interanual son la presión atmosférica sobre el Mediterráneo Occidental y la circulación en el mar de Alborán (García-Lafuente et al., 2009).

CHAPTER 2

Seasonal and interannual variability of surface heat and freshwater fluxes in the Mediterranean Sea: budgets and exchange through the Strait of Gibraltar[1]

Abstract

Several NCEP climatological datasets have been combined to analyse the seasonal and interannual variations of the heat and water budgets in the Mediterranean Sea and compare the long term means with direct measurements in the Strait of Gibraltar. The seasonal cycle of the net heat is positive (toward the ocean) between March and September with maximum in June and negative the rest of the year with minimum in December. Although subject to inherent uncertainty, we obtain a practically neutral budget of 0.7 Wm^{-2} in a yearly basis. The net heat budget is positive for the western Mediterranean (~12 Wm^{-2}) and negative for the eastern Mediterranean (~ -6.4 Wm^{-2}) mainly due to the high latent heat losses of this basin. The E-P freshwater deficit has a seasonal cycle with a range of variation about 600 $mm \cdot y^{-1}$, maximum in August-September and minimum in May. The long-term mean of the basin-averaged deficit is 680±70 $mm \cdot y^{-1}$ but it is almost 70% greater in the eastern Mediterranean due to higher E and lower P in this basin. Combining the climatological values with in situ measurements in Espartel sill, a mean inflow through the Strait of Gibraltar of 0.82±0.05 Sv is obtained and a salinity ratio S_{in}/S_{out} = 0.956. A heat advection Q_a = 3.2±1.5 Wm^{-2} through the Strait of Gibraltar has been obtained that, combined with the long-term averaged surface heat flux, implies that the net heat content of the Mediterranean Sea would have increased in the last decades.

[1]Francisco Criado-Aldeanueva, Javier Soto-Navarro and Jesús García-Lafuente (2012). Seasonal and interanual variability of surface heat and freshwater fluxes in the Mediterranean Sea: budgets and exchange through the Strait of Gibraltar. *Int. J. Climatol.*, 32, 286-302, doi: 10.1002/joc.2268

2.1 Introduction

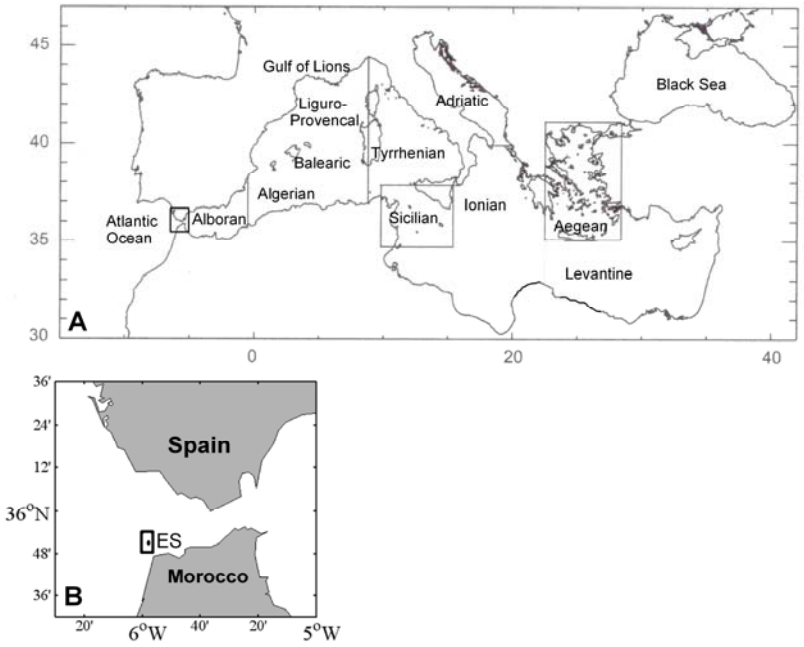

Figure 2.1 A) Map of Mediterranean Sea. The main basins and subbasins are indicated. B) Zoom of the Strait of Gibraltar region. The rectangle indicates the area selected as representative for Espartel (ES).

The Mediterranean Sea (Figure 2.1), a semi-enclosed basin that extends over 3000 km in longitude and over 1500 km in latitude with an area of $2.5 \cdot 10^{12}$ m^2, communicates with the Atlantic Ocean through the Strait of Gibraltar and with the Black Sea through the Turkish Bosphorus and Dardanelles Straits. The Sicily Channel separates the western and eastern Mediterranean basins. Evaporative losses (E) are not balanced by precipitation (P) and river runoff (R) and an Atlantic inflow through the Strait of Gibraltar is necessary to balance the freshwater and salt budgets. The Atlantic Water (AW) becomes saltier and denser while spreading into the western and eastern basins under the influence of intense air-sea interactions. Most of this flow returns to the Atlantic Ocean as Levantine Intermediate Water (LIW), formed during winter convection in the Levantine subbasin, while another part is transformed into Eastern Mediterranean Deep Water (EMDW) in the Adriatic and the Aegean subbasins and into Western Mediterranean Deep Water (WMDW) in the Gulf of Lions, the latter eventually being part of the Gibraltar outflow (Bryden and Stommel, 1982; Astraldi et

al., 2002; Millot et al., 2006; García-Lafuente et al., 2007, 2009). All processes of deep water formation involve LIW in less or greater extent, which makes all water masses be closely related and any significant modification of one of them may propagate its effect to the others. For this reason, the freshwater flux through the Mediterranean Sea surface plays an important role in the exchange between the Atlantic and the Mediterranean.

A great number of studies have dealt with the Mediterranean water budget (Bethoux, 1979; Peixoto et al., 1982; Bryden and Kinder, 1991b; Harzallah et al., 1993; Gilman and Garrett, 1994; Castellari et al., 1998; Angelucci et al., 1998; Béthoux and Gentili, 1999; Boukthir and Barnier, 2000; Mariotti et al., 2002) but, despite these efforts, the estimate of the freshwater flux at the surface has showed to depend on the datasets used and the methodology applied and remains largely uncertain, in particular its seasonal and interannual variability. For instance, estimates of E-P are found to range from 421 $mm \cdot y^{-1}$ (Gilman and Garrett, 1994) to 1230 $mm \cdot y^{-1}$ (Béthoux and Gentili, 1999), confirming the difficulty of obtaining a reliable estimate.

Air-sea heat fluxes are closely related to the water budget. The net heat budget consists of two radiation components (solar shortwave radiation absorbed by the sea and longwave radiation emitted by the sea) and two turbulent contributions (latent and sensible heat fluxes). In the long-term, vertical heat fluxes integrated over the basin must be balanced by heat transport through the Strait of Gibraltar. Macdonald et al. (1994), using in situ current and temperature observations estimated an annual average heat transport from the Atlantic to the Mediterranean of 5.2±1.3 Wm^{-2}. Other authors have also obtained the long-term heat flux through Gibraltar from estimates of the volume transport and the temperatures of the inflow and outflow. Results range from 8.5 Wm^{-2} (Béthoux, 1979) to 5 Wm^{-2} (Bunker et al., 1982). Since the uncertainty of these results is rather low, they can be used as a reference for the evaluation of the surface heat flux budget. Several studies (Bunker et al., 1982; Garrett et al., 1993; Schiano et al., 1993; Gilman and Garrett, 1994) have compared long term averages of vertical heat fluxes with the heat transport through the Strait of Gibraltar obtaining discrepancies of up to 30 Wm^{-2}. The reasons given for the disagreement are the different periods covered and the different bulk formula parameterisations or the wind forcing fields (Ruti et al., 2008). More recently, Ruiz et al. (2008) have examined 44 years

(1958-2001) of HIPOCAS model data to report a value of 1 Wm^{-2} for the vertical heat flux (heat loss from the ocean). They attribute the difference with respect to the heat gain through the Strait to an increase in the net heat content of the Mediterranean Sea during the last decades.

Semi-enclosed basins such as the Mediterranean are suitable for the characterisation of heat and water fluxes since they make a budget closure feasible. In this work we combine several datasets to analyse the seasonal and interannual variations of the components of heat and water budgets and compare the long term means with direct measurements in the Strait of Gibraltar. This double climatological and *in situ* approach makes it possible to provide an indirect determination of the inflow through the Strait of Gibraltar in a reliable way. The work is organised as follows: section 2.2 describes the data and methodology; in section 2.3 the main results are presented and discussed both for the heat and water fluxes. Budgets and the exchange through the Strait of Gibraltar are also addressed. Finally, section 2.4 summarises the conclusions.

2.2 Data

Monthly means from January 1948 to February 2009 of precipitation, evaporation and surface heat fluxes have been retrieved from the National Center for Enviromental Prediction-National Center of Atmospheric Research (NCEP-NCAR) reanalysis project (NCEP hereinafter, Kalnay et al., 1996), which is run at T62 spectral resolution (approximately a grid size of 1.9ºx1.9º) with 28 sigma levels. For comparison purposes, data from the Climate Prediction Centre Merged Analysis of Precipitation (CMAP, Xie and Arkin, 1996, 1997) have also been analysed. This dataset gives estimation of monthly mean precipitation at 2.5ºx2.5º resolution for the period 1979-2009. The standard version consists in a merged analysis mainly based on gauge stations over land and satellite estimates over the ocean. Auxiliary data of monthly mean sea level pressure, air temperature and wind fields at 2.5ºx2.5º for the period 1948-2009 have also been retrieved from NCEP database. Seasonal means have been computed by averaging JFM (winter), AMJ (spring), JAS (summer) and OND (autumn) monthly data.

Sea Surface Temperature (SST) data have been obtained from the Advanced Very High Resolution Radiometer (AVHRR) Pathfinder v5 mission of the NASA Jet Propulsion Laboratory (JPL). They consist in infrared high resolution radiometer images with 4km x 4km spatial resolution acquired onboard several satellite missions. Monthly means between 1985 and 2007 have been analysed.

In situ measurements of the outflow through the Strait of Gibraltar have been collected in the frame of the INGRES 1-2 projects. Data from a CT probe placed over Espartel sill, at 35º 51.70N, 5º 58.60W and 5 m above the seafloor between September 2004 and December 2009 have been used in this work to characterise its temperature. MEDATLAS database provided historical Conductivity-Temperature-Depth (CTD) profiles over Espartel in order to determine the inflow properties. The region within 35º 48.6'N – 35º 53.9'N / 05º 56.7'W – 06º 00.8'W (see Figure 2.1B) has been considered to be representative for the Espartel area. 48 CTD profiles spanning all seasons have been identified, most of them from the field work carried out during the Gibraltar Experiment (1986).

2.3 Results and discussion

2.3.1 Air and sea surface temperature fields

The spatial distribution of climatological sea level air temperature over the Mediterranean basin for 1948-2009 (Figure 2.2A) exhibits a north-south gradient with lower temperatures (below 10ºC) in the European coasts that progressively increase up to 22ºC in the African coasts. The eastern basin is warmer than the western one in all seasons, with maxima above 25ºC in the Levantine subbasin in summer. Minimum values between 5ºC-7ºC are found in the Adriatic, Aegean and Gulf of Lions in winter (not shown). The yearly time series of the basin-averaged air temperature (Figure 2.2B) has a mean value of 16.9ºC with minimum in 1956 (16.2ºC) and maximum in 1994 (17.7ºC). A positive trend of 0.012±0.003 $ºC \cdot y^{-1}$ is obtained but it nearly doubles if only the period from 1956 onwards is considered. Positive anomalies concentrate in the last decades and negative ones during the 60s and 70s. The Ionian subbasin is particularly

sensitive to this positive trend with values above 0.02 ºC·y^{-1} for the whole period (Figure 2.2C).

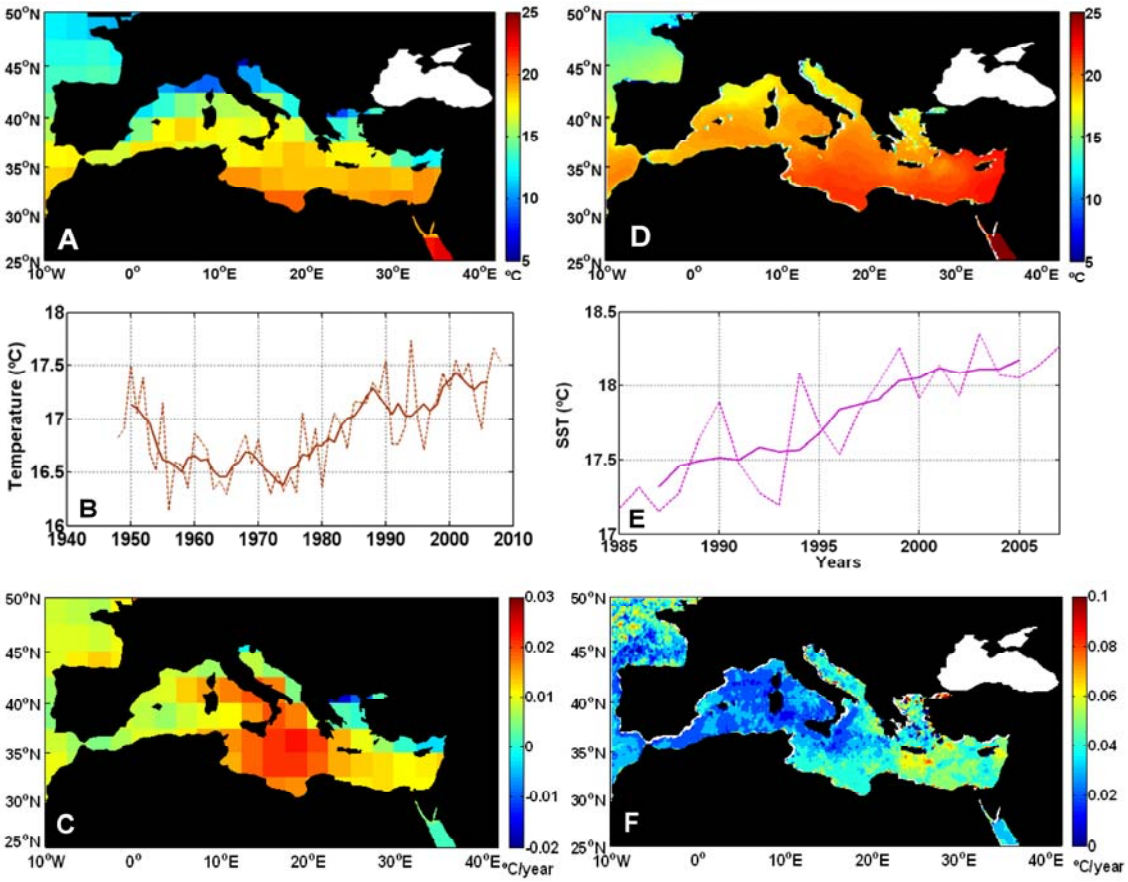

Figure 2.2 A) Spatial distribution of climatological sea level air temperature (ºC) in the Mediterranean Sea for 1948-2009. B) Yearly time series of the basin-averaged air temperature (ºC, dotted line). The 5-year running mean is also plotted (solid line). C) Spatial distribution of air temperature linear trend (ºC·y^{-1}) for 1948-2009. Panels D-F are the same but for SST during the period 1985-2007.

A similar pattern is observed for the climatological SST spatial distribution for 1985-2007 (Figure 2.2D) with temperatures increasing from north to south and from west to east. The Levantine subbasin and the south Ionian are warmer areas, with temperatures up to 28ºC in summer. In the western basin, warmer areas are located in the Algeric-Balearic region and the south-east Tyrrhenian. The Aegean, the northern Adriatic and the Gulf of Lions are again the coldest subbasins, with temperatures averaging 10ºC in winter. The yearly time series of the Mediterranean-averaged SST

(Figure 2.2E) has a mean value of 17.8ºC and a positive trend of 0.05 ± 0.01 ºC·y^{-1} for the period 1985-2007, slightly lower than the one obtained by Criado-Aldeanueva et al. (2008) for 1992-2005 and significantly lower than the 0.15 ºC·y^{-1} obtained by Marullo et al. (1999) for the period 1982-1990. The discrepancy may be due to the possibility mentioned by Moron (2003) that the trend had changed sign after reaching a SST relative maximum in year 2000, although the very hot years 2003 and 2008 shed doubts on the conclusion of Moron (2003). Mariotti et al (2008) and Mariotti (2010) analyze SST trends for various sub-periods between 1960 and 2005 and report decadal variations that follow those of the air temperature even though longer series are necessary to establish conclusions. SST trend (Figure 2.2F) is positive elsewhere with higher values in the eastern basin, especially south of Crete (up to 0.08±0.02 ºC·y^{-1} for the period analysed). Fenoglio-Marc (2002) and Cazenave et al. (2002) report negative trends in the western Ionian for the periods 1992-2000 and 1993-1998 respectively, which change sign when considering longer time series as in Criado-Aldeanueva et al. (2008). Superposed to these linear trends, both air temperature and SST show a very marked seasonal cycle (not shown), the former leading the latter by 15-20 days (maximum in mid-July).

2.3.2 Surface heat fluxes in the Mediterranean Sea

2.3.2.1 Spatial climatologies and seasonal cycle

Figure 2.3 displays the seasonal climatology of the different components of the net heat budget. Sensible heat flux, Q_h (panel A) concentrate higher losses during autumn and winter with maxima above 60 Wm^{-2} in the Aegean and Adriatic and slightly lower values in the Gulf of Lions and the Levantine subbasin (~50 Wm^{-2}). Elsewhere, the spatial distribution is rather uniform in these seasons with losses of some 20 Wm^{-2}. Heat gains up to 20 Wm^{-2} occur in spring and summer in the Aegean, the Levantine subbasin and some areas of the north-African coasts. Latent heat flux, Q_e (panel B) is larger in the eastern basin with losses up to 160 Wm^{-2} in the Levantine area in autumn and winter. In the western Mediterranean, the highest losses are located in the Gulf of Lions and the Balearic subbasin (~130 Wm^{-2}). Minimum fluxes take place in spring with a more uniform spatial distribution and lower values in the Adriatic and the

westernmost area (~20 Wm^{-2}). The solar shortwave net radiation, Q_s (panel C) depicts a north-south, west-east gradient in all seasons, with maxima in spring in the Levantine subbasin (more than 250 Wm^{-2}) and minima in autumn in the western European coasts (~50 Wm^{-2}). The longwave net radiation Q_b (panel D) is rather independent of seasonal variations. Higher losses of some 90 Wm^{-2} concentrate in summer in the Aegean Sea and Levantine subbasin whereas lower values correspond to the Balearic and Tyrrhenian subbasins in spring (~60 Wm^{-2}). The combination of these four contributions produces a marked seasonal-dependent net heat flux Q_n (not shown), with losses in autumn and winter and gains in spring and summer. Higher losses are observed in the Levantine subbasin, the Aegean, the northern Adriatic and the Gulf of Lions (>150 Wm^{-2}) in autumn, that favours the formation of intermediate and deep waters in these areas (Tziperman and Speer 1994; Candela 2001; Schroeder et al. 2009). Mean values for each contribution in the eastern and western basins are presented for all seasons in Table 2.1.

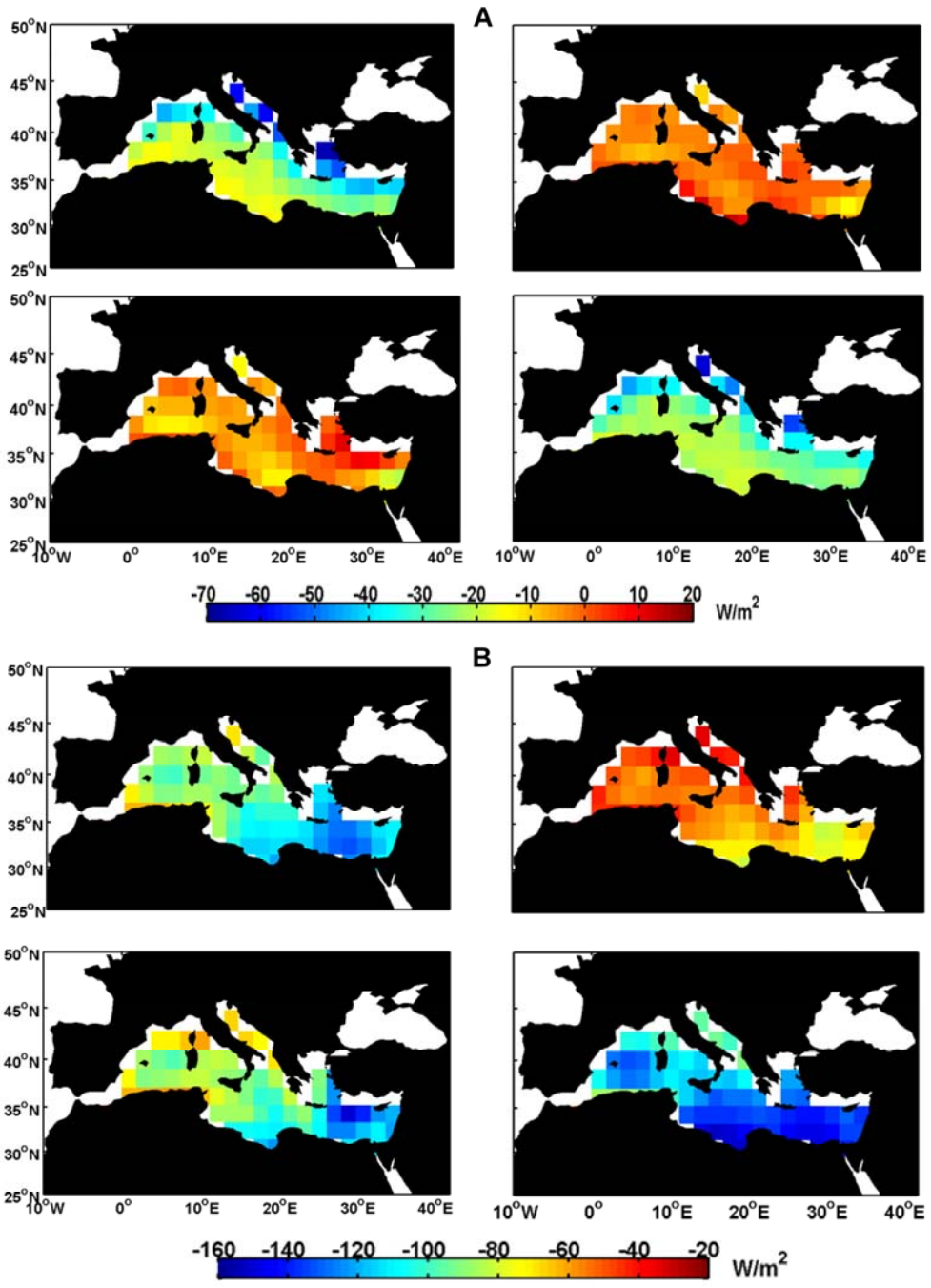

Figure 2.3 Continues in next page

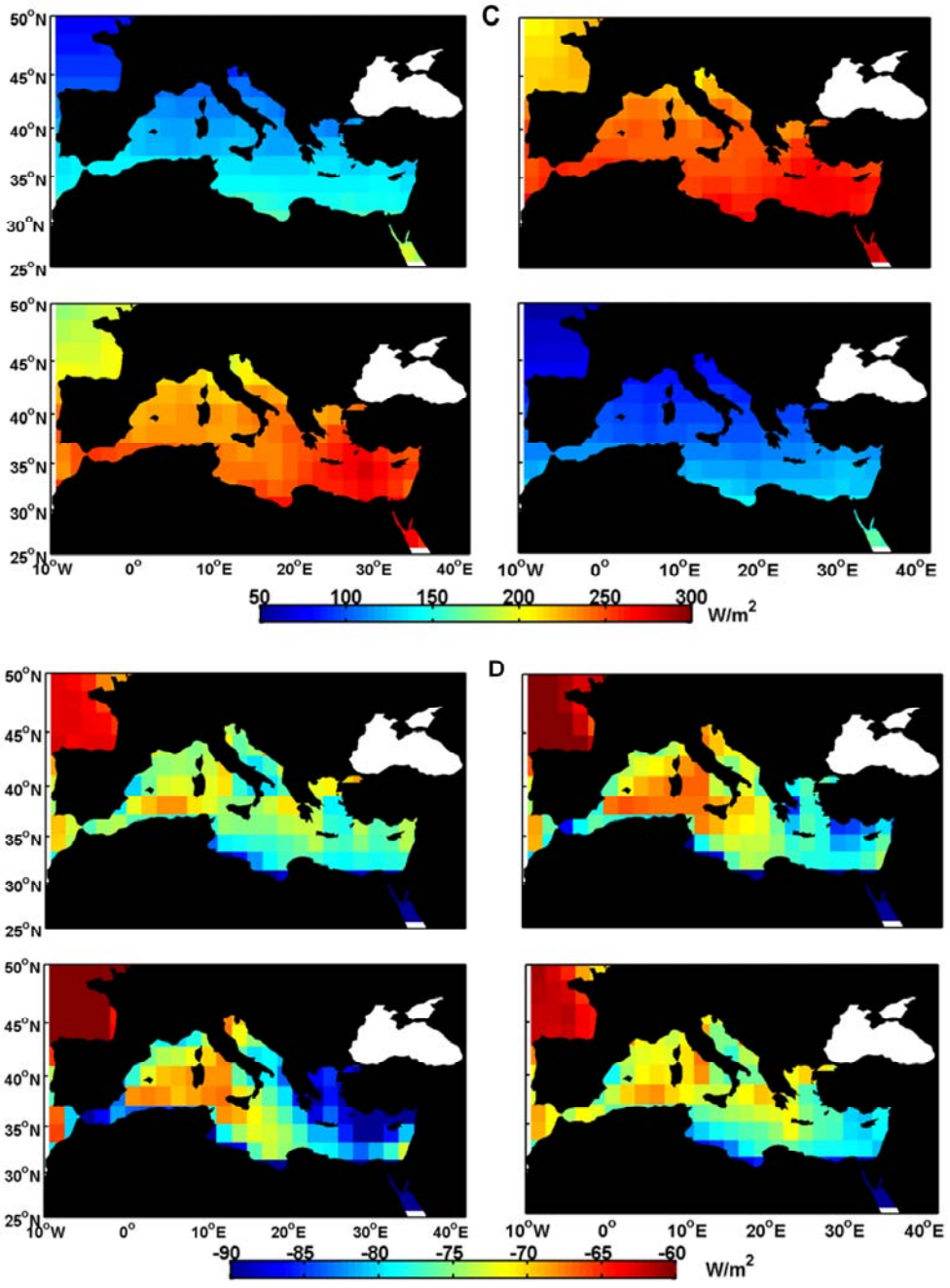

Figure 2.3 Seasonal climatology of the four components of the net heat budget in the Mediterranean for 1948-2009 (Wm^{-2}, positive toward ocean): sensible (panel A), latent (panel B), solar shortwave (panel C) and terrestrial longwave (panel D). In all panels: winter (top-left), spring (top-right), summer (bottom-left) and autumn (bottom-right).

	Mean			Winter			Spring			Summer			Autumn		
	Med	**Wm**	**Em**	**Med**	**Wm**	**Em**	**Med**	**Wm**	**Em**	**Med**	**Wm**	**Em**	**Med**	**Wm**	**Em**
Q_h	-15.1	-13.3	-16.2	-27.6	-22.3	-30.8	-1.5	-2.0	-1.2	-3.8	-3.7	-3.8	-27.6	-25.0	-29.1
Q_e	-93.5	-78.4	-103.4	-99.4	-82.3	-110.5	-57.9	-48.5	-64.0	-93.9	-75.9	-105.6	-123.1	-107.2	-133.5
Q_s	186.3	176.7	192.3	133.9	125.3	139.2	254.6	246.2	259.8	245.0	233.7	252.0	112.3	101.9	118.8
Q_b	-76.9	-73.1	-79.3	-76.9	-74.1	-78.6	-75.9	-71.5	-78.5	-78.8	-73.9	-81.8	-76.2	-72.9	-78.2
Q_n	0.73	11.7	-6.4	-70.0	-53.5	-80.7	120.0	120.0	120.0	69.6	80.1	61.1	-110.0	-100.0	-120.0

Table 2.1 Mediterranean (Med) long term mean heat fluxes contributions (Wm^{-2}). Values for the western (Wm) and eastern (Em) basins are shown for each season.

Authors	Q_h	Q_e	Q_s	Q_b	Q_n	Period
Bethoux (1979)	-13	-120	195	-68	-6	Not specified
Bunker et al. (1982) (1)	-13	-101	202	-68	20	1941-1972
Bunker et al. (1982) (2)	-11	-130	202	-68	-7	1941-1972
May (1986)	-11	-112	193	-68	2	1945-1984
Garrett et al. (1993)	-7	-99	202	-67	29	1946-1988
Gilman and Garrett (1994)	-7	-99	183	-77	0	1946-1988
Castellari et al. (1998)	-13	-122	202	-78	-11	1980-1988
Matsoukas et al. (2005)	-11	-90	186	-63	22	1984-2000
Ruiz et al. (2008)	-8	-88	168	-73	-1	1958-2001
This work	-15	-93	186	-77	1	1948-2009

Table 2.2 Mediterranean long term mean heat budget (Wm^{-2}) estimated by different authors. The periods to which the estimates refer are also indicated.

The Mediterranean-averaged climatological seasonal cycle for each component is presented in Figure 2.4. For the sensible heat flux Q_h, the values are negative all year round, with a range of variation of 34 Wm^{-2}, a maximum of -2 Wm^{-2} in June and a minimum of -36 Wm^{-2} in December. The latent heat flux Q_e, is minimum (-125 Wm^{-2}) in November and maximum (-50 Wm^{-2}) in May. The seasonal cycle of the shortwave radiation Q_s, positive all the year, has a range of variation of 196 Wm^{-2}, a maximum of 281 Wm^{-2} in June and a minimum of 85 Wm^{-2} in December. Finally, the net longwave radiation Q_b does not exhibit a clear seasonal cycle but a rather uniform value between -75 and -80 Wm^{-2}. These results are in reasonable good agreement with those obtained by Matsoukas et al (2005), who derive the radiative components by a radiation transfer model instead of bulk formulae. The seasonal cycle of the net heat shows positive values (heat gain by the ocean) between March and September with maximum in June (143 Wm^{-2}) and negative values during the rest of the year. It shows a minimum in December (-152 Wm^{-2}) and a range of variation of 295 Wm^{-2}, which is slightly less than the 330 Wm^{-2} obtained by Ruiz et al. (2008) and close to the lower limit of the interval reported by Garrett et al. (1993), 280 Wm^{-2}-360 Wm^{-2}. The obtained phase is in agreement with both works and slightly different from that obtained by Matsoukas et al (2005), who situate the maximum in May. Solar radiation and latent heat are the major contributions to the net heat flux.

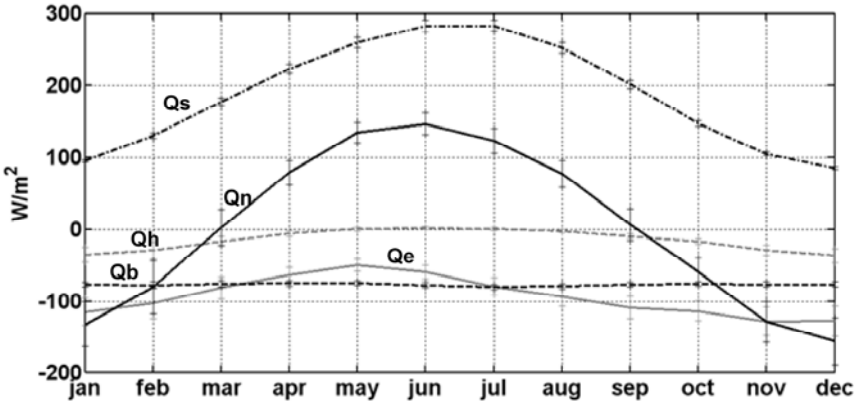

Figure 2.4 Mediterranean-averaged climatological seasonal cycle for sensible heat (Q_h, grey dashed line), latent heat (Q_e, grey solid line), shortwave (Q_s, black dashed-dotted line) and longwave (Q_b, black dashed line) contributions for the period 1948-2009. Net heat seasonal cycle is also presented (Q_n, black solid line). Bars are the standard deviation.

The heat flux Q_n is the time derivative of the heat content H, $Q_n = dH/dt$, responsible of the thermosteric anomaly. If we assume a harmonic function for the annual cycle of Q_n, then H will also have a harmonic shape but delayed $\pi/2$ (3 months) and therefore the thermosteric sea level cycle is expected to peak in September, in agreement with previous works (Fenoglio-Marc et al., 2006; García et al., 2006; Criado-Aldeanueva et al., 2008).

2.3.2.2 Basin-averaged annual means and long-term fluctuations

Figure 2.5A displays the yearly, Mediterranean-averaged, time series of the different contributions and the net heat flux. Solar shortwave radiation is the only positive contribution with a mean value of ~186±4 Wm^{-2}. The other contributions are negative with mean values about -93±6 Wm^{-2}, -77±2 Wm^{-2} and -15±3 Wm^{-2} for latent, longwave and sensible heat, respectively. As a result, we obtain a nearly neutral budget of 0.7 Wm^{-2}. The mean values have also been computed for each basin (Table 2.1): the net heat budget is positive (~12 Wm^{-2}) for the western Mediterranean and negative for the eastern Mediterranean (~ -6.4 Wm^{-2}) due to the high latent heat losses (up to 100 Wm^{-2}).

The long-term averages of each component are compared with previous estimates in Table 2.2 The value for shortwave radiation is the same as the one obtained by Matsoukas et al (2005) from a radiation transfer model, a value lower than most previous estimations except for those of Gilman and Garrett (1994) and Ruiz et al. (2008) who computed a contribution 10% lower from 1958-2001 HIPOCAS reanalysis data, probably due to a different parameterisation scheme. The latent heat flux is also lower than previous estimations and similar to that of Matsoukas et al. (2005) and Ruiz et al. (2008), which is thought to be rather accurate due to the higher spatial resolution of HIPOCAS dataset. The value for longwave radiation is the same as the one obtained by Gilman and Garrett (1994) and Castellari et al. (1998) and is close to that of Ruiz et al. (2008). The computed sensible heat flux is greater than all previous estimations, although it is not far from values reported by Bethoux (1979), Bunker et al. (1982) and Castellari et al. (1998). The net heat flux is in the range of previous studies, especially close to those of May (1986), Gilman and Garrett (1994) and Ruiz et al. (2008).

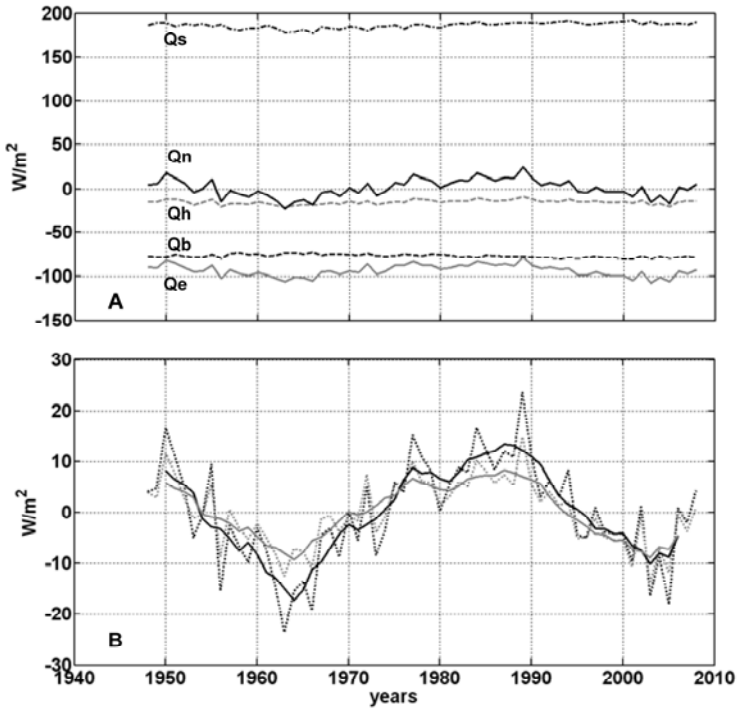

Figure 2.5 A) Yearly Mediterranean-averaged time series of sensible heat (Q_h, grey dashed line), latent heat (Q_e, grey solid line), shortwave (Q_s, black dashed-dotted line), longwave (Q_b, black dashed line) and net heat flux (Q_n, black solid line) for the period 1948-2009. B) Latent (grey) and net (black) heat anomalies (yearly means, dotted; 5-year running means, solid). A multi-decadal oscillation is clearly suggested.

Although there is no significant trend in the series, Figure 2.5B reveals three different periods in the heat flux anomalies: from early 50s to mid 60s, a negative trend of -1.6±0.6 $Wm^{-2}y^{-1}$ is observed. Trend changes to positive (1.1±0.3 $Wm^{-2}y^{-1}$) until late 80s when it changes sign again (-0.9±0.6 $Wm^{-2}y^{-1}$). Maximum heat gain of about 20 Wm^{-2} is observed in 1989 and maximum losses of the same order in 1963 and 2005. Since fluctuations in the net budget do not appear to be random, discrepancies with previous estimations could be related to the different periods analysed. It is interesting to remark that fluctuations in the net heat flux closely follow those of the latent heat (trends of -1.1±0.5 $Wm^{-2}y^{-1}$, 0.7±0.2 $Wm^{-2}y^{-1}$ and -0.7±0.4 $Wm^{-2}y^{-1}$ are observed for the same periods referred above), suggesting that this contribution is the main source of interannual variability. The visual inspection of Figure 2.5B also suggests a 40-year period multi-decadal oscillation of 11±2 Wm^{-2} and 7.5±1.4 Wm^{-2} amplitude for net and latent heat fluxes, respectively, probably related to long-term atmospheric forcing. However, long-term variability is the less reliable aspect of reanalyses datasets so some caution is necessary here. Although general good agreement is found with the results of Mariotti (2010) based on different datasets, this author reports an increase in the recent

period compared to the 1960s (i.e. a trend superposed to the decadal variability) that sheds doubts on the 40-year oscillation. Longer time series will be of great help to clarify this issue.

2.3.3 Surface freshwater fluxes in the Mediterranean Sea

2.3.3.1. Spatial climatologies and seasonal cycle

Figure 2.6 displays the spatial distributions of the climatological seasonal mean precipitation (P), evaporation (E) and deficit (E-P). For precipitation (panel A), NCEP data (with higher resolution than CMAP data) are presented. Autumn is the wettest season with a mean value of 853 $mm \cdot y^{-1}$. Higher precipitations are located in the northern Ionian, the Algerian-Balearic subbasin and the easternmost Levantine subbasin. Summer is the driest season (245 $mm \cdot y^{-1}$), with drier areas along the African coasts. In spring and summer, higher precipitations concentrate in the northern Adriatic. CMAP data (not shown) provide similar results (slightly lower values in all seasons). These patterns are in good agreement with the description of Mariotti et al. (2002) but values are significantly higher than those of Boukthir and Barnier (2000) from ECMWF ERA-15 (1979-1993) dataset.

Based on List (1951), evaporation (panel B) has been computed from the latent heat losses, Q_e and SST according to:

$$E = \frac{Q_E}{\rho L} \tag{2.1}$$

where ρ is the sea water density and $L = [2.501 - 0.00237 \cdot SST(^{\circ}C)] \cdot 10^6 \, J \cdot kg^{-1}$ the latent heat of vaporization. As the relative importance of the SST term is negligible, evaporation matches the spatial patterns of latent heat flux. It is more intense in autumn due to the strong and dry winds, with a mean value of 1553 $mm \cdot y^{-1}$, maximum about 2000 $mm \cdot y^{-1}$ in the southern Ionian and Levantine subbasins and lower values in spring (745 $mm \cdot y^{-1}$). In all seasons, evaporation is ~30% higher in the eastern basin except in autumn (only 13% higher). In the western Mediterranean, the Balearic subbasin shows the highest values. These patterns are in good agreement with those of Mariotti et al. (2002) but evaporation is higher than the values reported by Boukthir and Barnier

(2000). Mariotti et al. (2002) compare both NCEP and ERA-15 datasets and conclude that the latter tends to underestimate both P and E with respect to NCEP.

E-P (panel C) is positive (freshwater deficit) for most of the Mediterranean during all seasons, especially in the eastern basin due to higher evaporation and lower precipitation. Some areas of the western basin change sign seasonally and, in the northern Adriatic, E-P is predominantly negative (freshwater input) due to the high precipitation (see panel A). Mean values are positive for all seasons and a maximum of 974 $mm \cdot y^{-1}$ is reached in summer in NCEP data (in autumn in NCEP (E)/CMAP (P) data, 922 $mm \cdot y^{-1}$). The minimum is observed in spring in both datasets (495 $mm \cdot y^{-1}$ and 418 $mm \cdot y^{-1}$ for NCEP and NCEP/CMAP, respectively). Higher deficits concentrate in the Levantine subbasin in summer (1800 $mm \cdot y^{-1}$) and higher inputs in the northern Adriatic during spring (-400 $mm \cdot y^{-1}$). In all season, E-P is lower in NCEP data due to higher precipitation of this dataset with respect to CMAP. Table 2.3 summarises the above results.

The Mediterranean-averaged climatological seasonal cycles of E, P and E-P (NCEP and CMAP) are presented in Figure 2.7. A range of variation of 838 $mm \cdot y^{-1}$ is obtained in the NCEP precipitation data, with a maximum (959 $mm \cdot y^{-1}$) in December and a minimum (121 $mm \cdot y^{-1}$) in July. CMAP data are slightly lower in the second half of the year and ~100 $mm \cdot y^{-1}$ higher in spring. Its minimum coincides with that of NCEP and its maximum is somewhat lower (854 $mm \cdot y^{-1}$ in December). The spatial distribution of annual amplitude, (max-min)/2, is rather variable (Figure 2.8A, NCEP data) with maxima between 650 $mm \cdot y^{-1}$ and 850 $mm \cdot y^{-1}$ in the northern Ionian, the Levantine subbasin and some points of the Algerian subbasin. The phase distribution (not shown) peaks in December in most of the Mediterranean except some reduced areas (mostly in the Levantine subbasin) where it does peak in January. CMAP data (Figure 2.8B) gives lower values almost everywhere except in the northern Levantine subbasin.

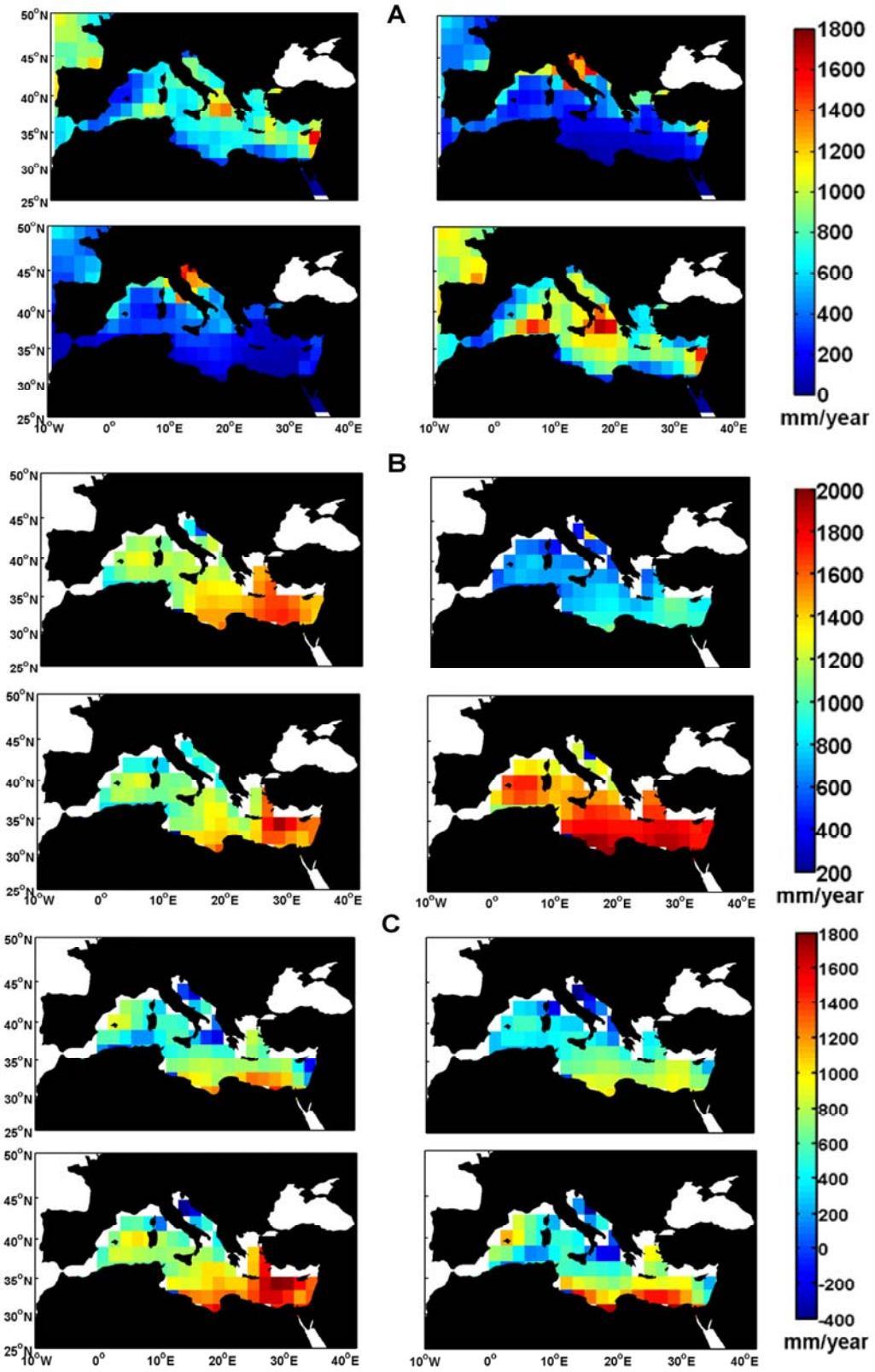

Figure 2.6 Seasonal climatology of P (mm·y^{-1}, panel A), E (mm·y^{-1}, panel B) and E-P (mm·y^{-1}, positive means freshwater deficit, panel C) in the Mediterranean for 1948-2009. In all panels: winter (top-left), spring (top-right), summer (bottom-left) and autumn (bottom-right).

	Mean			Winter			Spring			Summer			Autumn		
	Med	**Wm**	**Em**	**Med**	**Wm**	**Em**	**Med**	**Wm**	**Em**	**Med**	**Wm**	**Em**	**Med**	**Wm**	**Em**
E	1186	1011	1296	1256	1061	1378	745	625	820	1193	979	1330	1553	1382	1559
P(NCEP)	506	527	491	675	630	702	249	281	232	245	299	209	853	897	818
P(CMAP)	469	517	442	614	551	649	305	415	244	205	312	145	754	790	734
E-P (NCEP)	680	484	806	581	430	676	495	345	589	947	680	1121	700	485	841
E-P (NCEP/CMAP)	678	497	777	597	479	663	418	212	532	922	681	1055	780	623	867

Table 2.3 Mediterranean (Med) long term mean freshwater contributions ($mm \cdot y^{-1}$). Values for the western (Wm) and eastern (Em) basins are shown for each season. For E-P computation from CMAP P dataset, only the period 1979-2009 of NCEP E time series has been used.

Authors	E	P	E-P	Method
Tixeront (1970)	1200	350	850	Observations and assumptions
Jaeger (1976)	1210	550	660	Derived from observations
Gilman and Garrett (1994)	1121-1430	$550^{(1)}$-$700^{(2)}$	421-880	Derived from observations
Angelucci et al. (1998)	1100	450	650	Analyses, ECMWF/NCEP
Castellari et al. (1998)	1320-1570	$550^{(1)}$-$700^{(2)}$	620-1020	Derived from observations
Bethoux and Gentili (1999)	1360-1540	310	1050-1230	Derived from observations
Boukthir and Barnier (2000)	920	326	594	Reanalyses, ECMWF 1979-1993
Mariotti et al. (2002)	1171	504	667	Reanalyses, NCEP 1948-1998
Mariotti et al. (2002)	1113	433	680	Reanalyses, NCEP 1979-1993
Mariotti et al. (2002)	934	331	603	Reanalyses, ECMWF 1979-1993
Mariotti et al. (2002)	1176	477	699	UWM/COADS, CMAP 1979-1993
This work	1186	506/469	680/678	Reanalyses, NCEP 1948-2009/CMAP 1979-2009

Table 2.4 Climatological contributions to the Mediterranean water budget ($mm \cdot y^{-1}$) estimated by different authors. (1): Adopted from Jaeger (1976); (2): Adopted from Legates and Wilmott (1990).

The evaporation seasonal cycle (Figure 2.7) leads ~2 months that of precipitation and reaches its minimum in May (650 $mm \cdot y^{-1}$) and its maximum in November (1614 $mm \cdot y^{-1}$). The amplitude, (max-min)/2, is between 500 $mm \cdot y^{-1}$ and 650 $mm \cdot y^{-1}$ with lower values in the northern areas of the western basin (Figure 2.8C). The phase distribution (not shown) is also rather uniform with a maximum in November except for some isolated points where it moves to October or to December.

The E-P seasonal cycle (Figure 2.7) has a range of variation between 582 $mm \cdot y^{-1}$ (NCEP) and 644 $mm \cdot y^{-1}$ (NCEP/CMAP) with a maximum in August-September (~1000 $mm \cdot y^{-1}$) and a minimum in May, ~100 $mm \cdot y^{-1}$ lower in NCEP/CMAP data. The highest amplitudes, (max-min)/2, concentrate in the Levantine subbasin and lower values are observed in the central Mediterranean (Figure 2.8D) with a good agreement between NCEP and NCEP/CMAP distributions although the latter gives higher values (Figure 2.8E). Good agreement is also found in the phase pattern (only NCEP is shown, Figure 2.8F) that peaks between July and November with a rather irregular spatial distribution.

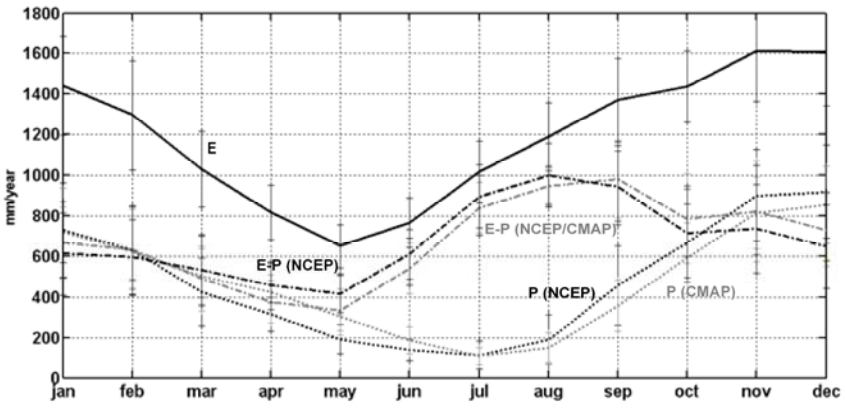

Figure 2.7 Mediterranean-averaged climatological seasonal cycle of E (black solid line), P (dotted lines, black for NCEP and grey for CMAP) and E-P (dashed-dotted lines, black for NCEP and grey for NCEP (E)/CMAP (P)) for the periods 1948-2009 (NCEP) and 1979-2009 (CMAP). Bars are the standard deviation. Labels indicating each cycle are also shown for clarity.

The seasonal cycles are in reasonably good agreement with the results of Mariotti et al. (2002). Lower amplitudes are reported by Boukthir and Barnier (2000) from ERA-15 and maximum evaporation is obtained in September instead of November. Mariotti (2010) has analysed how long-term changes in E and P affect the mean seasonal cycles. For E-P noticeable changes are observed when comparing with

the 1996-2005 period. For these years, the seasonal cycle clearly peaks in September and reaches a relative maximum in February that is not observed for previous time periods. The author attributes these changes to E increase for the September peak and to P decrease for the February peak.

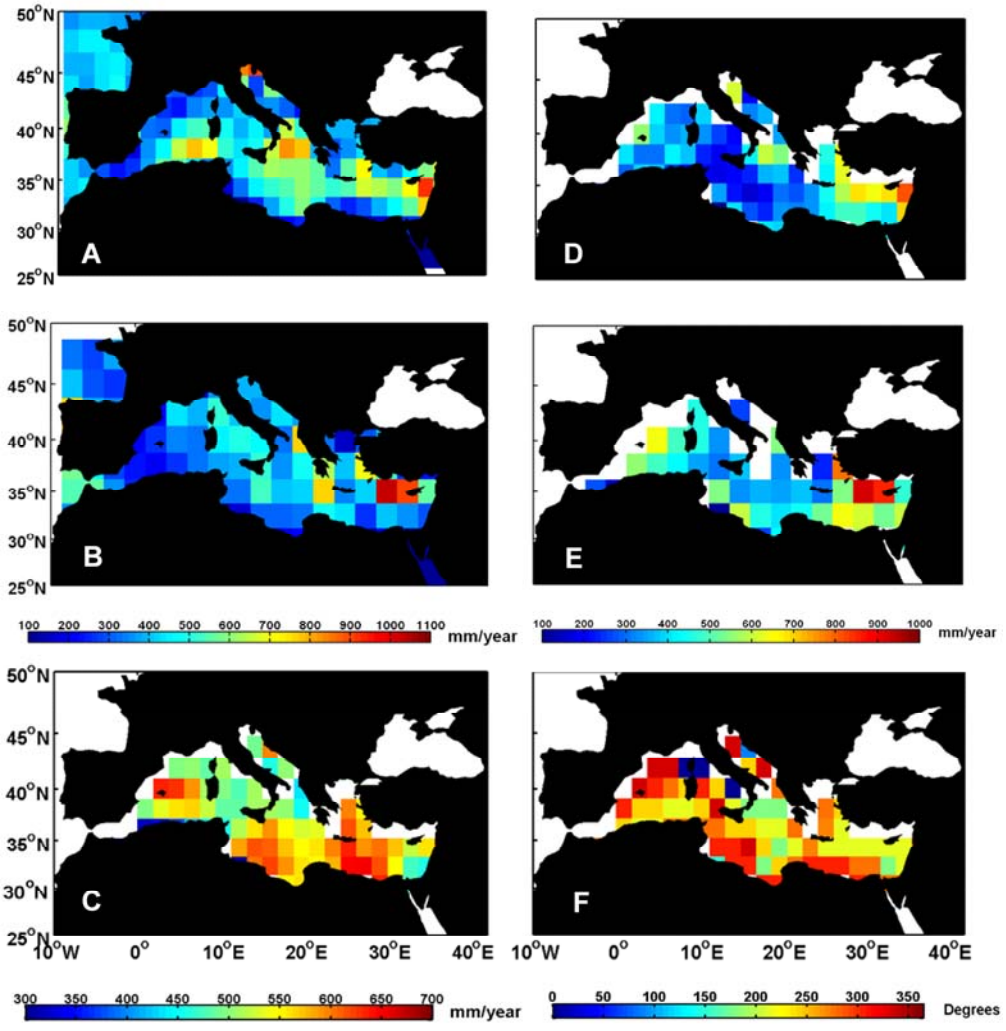

Figure 2.8 Spatial distribution of annual amplitude ($mm \cdot y^{-1}$) and phase (degrees) of the main surface freshwater fluxes contributions: A) P annual amplitude (NCEP); B) P annual amplitude (CMAP); C) E annual amplitude; D) E-P annual amplitude (NCEP); E) E-P annual amplitude (NCEP (E)/CMAP (P)) and F) E-P annual phase (NCEP).

2.3.3.2 Basin-averaged annual means and long-term oscillations

Figure 2.9A displays the Mediterranean-averaged time series of E, P and E-P. From NCEP data, the long-term mean precipitation is 506 ± 66 $mm \cdot y^{-1}$ with a maximum in 1966 (617 $mm \cdot y^{-1}$), a minimum in 1989 (355 $mm \cdot y^{-1}$) and a negative trend of -1.1 ±0.9 $mm \cdot y^{-2}$, similar to that reported by Mariotti (2010). At the decadal scale, however, three 20-year periods of different trend are revealed: 1948-69 (4±2 $mm \cdot y^{-2}$), 1969-89 (-8±4 $mm \cdot y^{-2}$) and 1989-2008 (9±4 $mm \cdot y^{-2}$). From CMAP data, a slightly lower average value is obtained (469 ± 66 $mm \cdot y^{-1}$). Although both datasets provide fairly similar series until late 90s, they considerably differ (about 100 $mm \cdot y^{-1}$) from 2002 to 2008. The 60-year mean evaporation is 1186 ± 81 $mm \cdot y^{-1}$ with a maximum of 1360 $mm \cdot y^{-1}$ in 2003 and a minimum of 1000 $mm \cdot y^{-1}$ in 1989. The time-evolution of positive and negative anomalies follow that of P and the same three 20-year periods apply for E as well with trends of 8±4 $mm \cdot y^{-2}$, -7±3 $mm \cdot y^{-2}$ and 9±5 $mm \cdot y^{-2}$, respectively that suggests the existence of a multi-decadal oscillation that could be related to long-term atmospheric forcing (Figure 2.9B). A least-squares fit provides amplitudes of 69±21 $mm \cdot y^{-1}$ and 95±18 $mm \cdot y^{-1}$ at 40 years period for P and E, respectively.

The long-term E-P mean deficit is 680 ± 70 (678 ± 75 from NCEP/CMAP) with a maximum of 817 $mm \cdot y^{-1}$ in 2001 and a minimum of 530 $mm \cdot y^{-1}$ in 1951. A positive trend (higher deficit) of 1.6±0.9 $mm \cdot y^{-2}$ is observed for the entire period in which the decrease in P accounts for ~70%. The multi-decadal E-P oscillation is not so clear (Figure 2.9B, bottom) and is more likely to correspond to multi-decadal variability and a positive trend as pointed by Mariotti (2010). The decadal variations in E reported here are consistent with those found by Mariotti (2010), although this author finds an increase in E in the recent period compared to the 1960s (i.e. a trend superposed to the decadal variability). In contrast, precipitation decrease based on NCEP found here is too large compared with estimates based on land-gauges around the Mediterranean reported in Mariotti (2010). This is also reflected in our conclusion that 70% of the recent increase in E-P derives from P, while Mariotti (2010) underlines the role of evaporation changes. As previously pointed out, long-term variability is the less reliable aspect of reanalyses datasets, so our results must be considered here with caution.

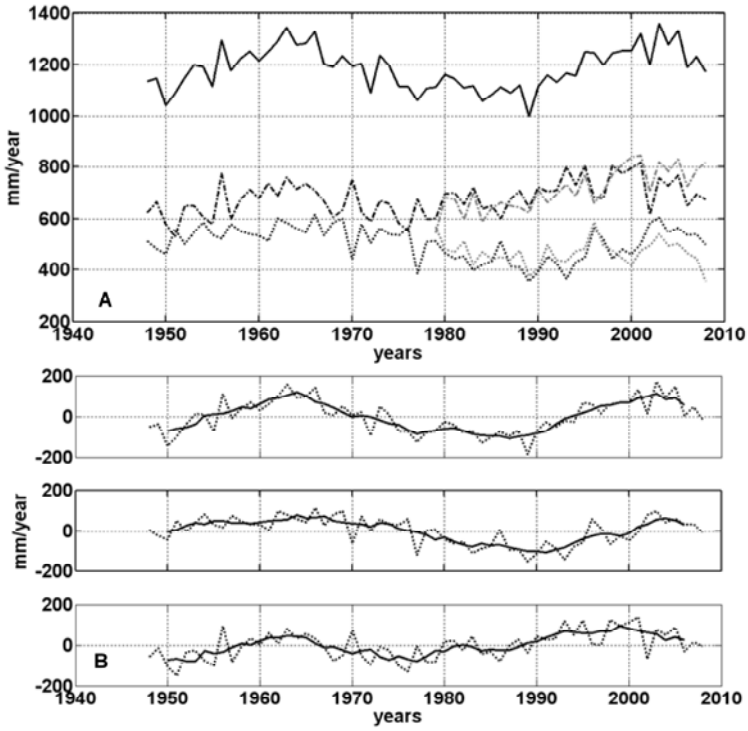

Figure 2.9 A) Yearly Mediterranean-averaged time series of E (black solid line), P (dotted lines, black for NCEP and grey for CMAP) and E-P (dashed-dotted lines, black for NCEP and grey for NCEP (E)/CMAP (P)). B) Anomalies (yearly means, dotted; 5-year running means, solid) are shown in this panel (E top, P middle, E-P bottom) to highlight the interannual variability. The multi-decadal oscillation is clearly suggested.

Mean values have also been computed for each basin and are displayed in Table 2.3 E-P is almost 70% higher in the eastern Mediterranean due to higher E and lower P in this basin. We now compare these results with previous estimations (Table 2.4). E ranges from 920 $mm \cdot y^{-1}$ to 1570 $mm \cdot y^{-1}$. The two lowest estimates (Mariotti et al., 2002 and Boukthir and Barnier, 2000) use the ERA-15 reanalyses whereas the highest of Castellari et al. (1998) and Bethoux and Gentili (1999) derive from observations. Our result is an intermediate value close to those of Mariotti et al. (2002) from NCEP dataset although for different time periods. P ranges 310 $mm \cdot y^{-1}$ to 700 $mm \cdot y^{-1}$. Again, the values from ERA-15 are among the lowest ones. Our result (from NCEP) is slightly higher than most of the previous perhaps due to the increase of P in the most recent years (see the positive trend in Figure 2.9B). Our result for E-P falls within the range of previous estimates (from 421 $mm \cdot y^{-1}$ to 1230 $mm \cdot y^{-1}$) and is especially close to those of Mariotti et al. (2002) from different datasets and periods analysed.

2.3.4 Budgets and exchange through the Strait of Gibraltar

Should the Mediterranean be in a steady state, the net water and heat transport through the straits (horizontal advection) must balance the vertical fluxes integrated over the basin. The first condition can be written as:

$$G = \int\int (E - P)\, dxdy - R - B \qquad (2.2)$$

where $G = G_{in} - G_{out}$ is the net flow through the Strait of Gibraltar (the difference between inflow G_{in} and outflow G_{out}) , R is the total river runoff and B the contribution of the Black Sea.

Several studies (Tixeront, 1970; Ovchinnikov, 1974; Margat, 1992; Boukthir and Barnier, 2000; Struglia et al., 2004) have dealt with the determination of climatological river discharge into the Mediterranean Sea using different methodologies and have obtained different results. Boukthir and Barnier (2000), analysing data from UNESCO (1996) for the period 1974-94 reported a climatological mean of $11 \cdot 10^3$ $m^3 \cdot s^{-1}$, 30% lower than the estimates of Tixeront (1970) based on rain maps and data from a few coastal stations, Ovchinnikov (1974), who gave $13.6 \cdot 10^3$ $m^3 \cdot s^{-1}$ or Margat (1992), who proposed $16 \cdot 10^3$ $m^3 \cdot s^{-1}$ from a global hydrological budget of the Mediterranean basin. Struglia et al. (2004), analysing data from Global Runoff Data Center (GRDC) and the Mediterranean Hydrological Cycle Observing System (Med-HYCOS), reported an annual mean climatological value of $8.1 \cdot 10^3$ $m^3 \cdot s^{-1}$ and mentioned $10.4 \cdot 10^3$ $m^3 \cdot s^{-1}$ as an upper bound to possible underestimates. This last value is close to that of Boukthir and Barnier (2000) and will be adopted for our calculations. In any case, a contribution of river discharge of $10.4 \cdot 10^3$ $m^3 \cdot s^{-1}$ (equivalent to 131 $mm \cdot y^{-1}$) is less than 20% of the more important E-P.

The Black Sea contribution has also been extensively studied (Tolmazin, 1985; Unluata et al., 1990; Besiktepe et al., 1994, Bethoux and Gentili, 1999; Karnaska and Maderich, 2008; Liu et al., 2009). Results range from $5.8 \cdot 10^3$ $m^3 \cdot s^{-1}$ of Bethoux and Gentili (1999) from the hydrological budget in the Aegean, to $9.6 \cdot 10^3$ $m^3 \cdot s^{-1}$ of Liu et al. (2009) from numerical simulation, which is close to those of Unluata et al. (1990)

and Besiktepe et al. (1994). Karnaska and Maderich (2008), from a 3D model obtain mean annual values of 38.8· 10^3 $m^3 \cdot s^{-1}$ for the upper layer (into the Mediterranean Sea) and 30.0· 10^3 $m^3 \cdot s^{-1}$ for the lower layer (into the Black Sea) and hence a mean net inflow of 8.8 · 10^3 $m^3 \cdot s^{-1}$. This intermediate value will be adopted for our calculations. Thus, the contribution of the Black Sea (equivalent to 111 $mm \cdot y^{-1}$) is similar to the river runoff.

With these values for R and B and the mean value of E-P = 680 $mm \cdot y^{-1}$ discussed above, equation (2.2) provides a net flow through the Strait of Gibraltar of 0.035 ± 0.005 Sv (Sverdrup, 1Sv = 10^6 $m^3 \cdot s^{-1}$), in good agreement with previous estimates (see Table 2.5). Our result is similar to those based on water budgets and slightly lower than that of Mariotti et al. (2002) from NCEP dataset because we have used more recent values of R and B, which are slightly higher.

Authors	G	Method
Lacombe and Tchernia (1972)	0.054	Current observations at Gibraltar
Bethoux (1979)	0.079	Ocean potential energy budget
Bryden and Kinder (1991a)	0.040-0.048	Current observations and salt budget
Bryden and Kinder (1991b)	0.040-0.050	Ocean model simulation
Bryden et al. (1994)	0.041	Current observation and salt budget
Garrett (1996)	0.041	Modelling at Gibraltar
Boukthir and Barnier (2000)	0.031	Water budget from ERA-15
Candela (2001)	0.04	Current observations at Gibraltar
Mariotti et al. (2002)	0.039	Water budget from several datasets
This work	0.035	Water budget from several datasets

Table 2.5 Annual mean of net water transport through the Strait of Gibraltar (Sv, 1Sv = 10^6 $m^3 \cdot s^{-1}$) as estimated by different authors.

Combining a 4 year-long time series of ADCP measurements over Espartel sill with results from a numerical model, Sánchez-Román et al. (2009) report a mean outflow of G_{out} = 0.78 ± 0.05 Sv, which implies a mean inflow ($G_{in} = G + G_{out}$) of 0.82 ± 0.05 Sv. The estimation of the inflow from direct observations has technical and operational limitations and only a few values (that range from 0.72 Sv to 1.2 Sv) have been reported in the literature (see Table 2.6). Indirect estimations are mainly based on the volume and salt conservation (the well-known Knudsen relationship) and depend on the inflow and outflow salinity (S_{in}, S_{out}, respectively) ratio:

$$G_{in} = \frac{1}{1 - S_{in}/S_{out}} G$$
$$G_{out} = \frac{1}{1 - S_{out}/S_{in}} G \qquad (2.3)$$

Using this approach with S_{in}/S_{out} = 0.96 (Lacombe and Tchernia, 1972), Harzallah et al. (1993) and Boukthir and Barnier (2000) obtained respectively 0.72 Sv and 0.77 Sv for the mean inflow. But equations (2.3) are very sensitive to small changes in the salinity ratio and S_{in}, S_{out} are not easy to determine, this causing large uncertainty. Our indirect approach avoids this problem and provides an intermediate value among those historically reported which is likely to be rather realistic since it combines reliable climatological and in situ datasets. Instead of using equation (2.3) for computing the inflow, we can use our values of G = 0.035 Sv and G_{in} = 0.82 Sv to determine a salinity ratio S_{in}/S_{out} = 0.956, slightly lower than the 0.96 adopted by Lacombe and Tchernia (1972), that can be used as a future reference when only a source of data (climatological or in situ) is available.

Authors	**G_{in}**	**Period of observations**
Lacombe and Richez (1982)	1.2	09/60 – 06/61
Bryden et al (1994)	0.72	1985 – 1986
Tsimplis and Bryden (2000)	0.78	01/97– 04/97
García Lafuente et al (2000)	0.92	10/95 – 04/96
Baschek et al (2001)	0.81	Various intervals between 10/94 and 04/97
Candela (2001)	1.01	1995-1996
García Lafuente et al (2002a)	0.96	Various intervals between 10/95 and 05/98
This work	0.82	09/04 – 12/08

Table 2.6 Mean inflow through the Strait of Gibraltar (Sv, 1Sv = 10^6 $m^3 \cdot s^{-1}$) as estimated by different authors

Unlike the water budget, the very reduced contribution of the Black Sea to the net heat budget can be neglected in all computations (Tolmazin, 1985). The Atlantic inflow through the Strait of Gibraltar is warmer than the Mediterranean outflow and it constitutes a positive heat advection Q_a given by:

$$Q_a = \rho C_p \left\{ V_i T_i - V_o T_o - \left(E T_e - P T_p - R T_r \right) \right\} \qquad (2.4)$$

where ρ is a reference water density, C_p the specific heat and T_i, T_o, T_e, T_p and T_r the mean temperature of inflow, outflow, evaporated water, precipitated water and river runoff. Assuming that T_e, T_p and T_r are not very different from T_o (which does not significantly alter the results, Garrett et al., 1993), Q_a can be expressed as:

$$Q_a = \rho C_p V_i \left(T_i - T_o \right) \qquad (2.5)$$

We now compute this heat advection from in situ measurements and historical MEDATLAS CTD profiles (see section 2.2 for details). A mean temperature of T_o=13.25 ± 0.07 ºC has been obtained for the outflow from the CT probe. A spatially (within 35º 48.6'N – 35º 53.9'N / 05º 56.7'W – 06º 00.8'W, see Figure 2.1B) and depth-averaged temperature above the mean depth of the interface (186 m, Sanchez-Roman et al., 2009) of T_i=15.6 ± 1.1 ºC has been obtained for the inflow which implies a temperature difference of 2.4ºC. With these values and our mean estimation of 0.82 Sv for the inflow, a result of Q_a = 3.2 ± 1.5 Wm^{-2} is obtained for the heat advection. Although the value of 186 m for the mean depth of the interface is a well-documented choice (Sánchez-Román et al., 2009), the result for the heat advection is fairly robust and only small variations (less than 10%) have been observed for a wide range (150-200 m) of the mean interface.

This value is lower than historical reports that range from 8.5 Wm^{-2} (Béthoux, 1979) to 5 Wm^{-2} (Bunker et al., 1982) but is thought to be realistic since it comes from reliable datasets. The discrepancies with other results are probably due to a previous overestimation of the inflow (usually set to values above 1 Sv) since the temperature difference is rather similar. When combined with the long-term averaged surface net heat flux, this implies that the net heat content of the Mediterranean Sea would have increased in the last decades. This is compatible with the increment of deep water temperature reported by different authors (Rohling and Bryden, 1992; Bethoux and Gentili, 1999; López-Jurado et al., 2005; Font et al., 2007) and also with a positive thermosteric sea level trend (Criado-Aldeanueva et al., 2008). In any case, considering the uncertainty inherent to the estimation of surface heat fluxes, this result must be considered with caution.

2.4 Summary and concluding remarks

We have used climatological datasets to analyse the seasonal and interannual variations of the components of heat and water budgets and compare the long term means with direct measurements in the Strait of Gibraltar.

The seasonal cycle of the net heat shows positive values (toward the ocean) between March and September with a maximum in June and negative values the rest of the year with a minimum in December. On a yearly basis, we obtain a nearly neutral budget of 0.7 Wm^{-2}. The net heat budget is positive (~12 Wm^{-2}) for the western Mediterranean and negative for the eastern Mediterranean (~ -6.4 Wm^{-2}) mainly due to the high latent heat losses of this basin (up to 100 Wm^{-2}). The E-P freshwater deficit has a seasonal cycle with a range of variation of about 600 $mm \cdot y^{-1}$, a maximum in August-September and a minimum in May. The long-term mean of the basin-averaged deficit is 680±70 $mm \cdot y^{-1}$ but it is almost 70% higher in the eastern Mediterranean due to higher E and lower P in this basin. A positive trend (higher deficit) of 1.6±0.9 $mm \cdot y^{-2}$ is observed for the entire period in which the decrease in P seems to be the most important factor, although Mariotti (2010) also underlines the role of evaporation changes.

Reanalyses are useful for a comprehensive description of climate and related water/energy cycles, especially for describing climatological characteristics. However there is no constrain on the closure of the water and energy budgets at the level of the Mediterranen Sea, so there are uncertainties associated to results based on these products. Long-term variability is the less reliable aspect of reanalyses datasets as variability on these timescales may be affected by artifices (e.g. deriving from non-stationary data inputs). For this reason, the suggested long-period oscillation (40-year period) for P, E and E-P (and also for the net and latent heat) that could be related to long-term atmospheric forcing must be considered with caution. Despite of these caveats, the good agreement with other previous results in the literature makes them reliable for the estimation of the heat and water exchange through the Strait of Gibraltar.

Assuming a climatological river discharge and Black Sea contributions of $10.4 \cdot 10^3$ $m^3 \cdot s^{-1}$ (Struglia et al., 2004) and $8.8 \cdot 10^3$ $m^3 \cdot s^{-1}$ (Kanarska and Maderich,

2008), respectively, a mean net flow through the Strait of Gibraltar of 0.035 ± 0.005 Sv is obtained. From a 4 year-long time series of ADCP measurements over Espartel sill and results from a numerical model, a mean outflow of G_{out} = 0.78 ± 0.05 Sv is obtained (Sanchez-Roman et al., 2009), which implies a mean inflow ($G_{in} = G + G_{out}$) of 0.82 ± 0.05 Sv. Our result is an intermediate value among the few (due to technical and operational limitations) historically reported and is likely to be rather realistic since it comes from a combined climatological and in situ reliable dataset. Instead of using the conservation of salt for computing the inflow, which is subject to large uncertainty, we determine a salinity ratio S_{in}/S_{out} = 0.956 that can be used as a future reference when only one data source (climatological or in situ) is available.

With the above value for the inflow, a heat advection of Q_a = 3.2 ± 1.5 Wm^{-2} through the Strait of Gibraltar is obtained. This value, although lower than historical, is thought to be realistic, the discrepancies with other estimates being attributable to a previous overestimation of the inflow. This heat advection, along with the long-term averaged surface net heat flux, implies that the net heat content of the Mediterranean Sea would have increased in the last decades. This result, although subject to the uncertainty of the surface heat fluxes estimation, is compatible with the findings of Rohling and Bryden (1992), Bethoux and Gentili (1999), López-Jurado et al. (2005) and Font et al. (2007) who report an increment of deep water temperature and also with the positive thermosteric sea level trend observed by Criado-Aldeanueva et al. (2008).

Acknowledgements

This work has been carried out in the frame of the P07-RNM-02938 Junta de Andalucia Spanish-funded project. JSN acknowledges a postgraduate fellowship from Conserjería de Innovación Ciencia y Empresa, Junta de Andalucía, Spain. Partial support from CTM2006– 02326 (M. of Science and Technology) and P08-RNM-03738 (Junta de Andalucía) Spanish-funded projects are also acknowledged. NCEP and CMAP data have been provided by the NOAA/OAR/ESRL PSD, Boulder, Colorado, USA, from their website at http://www.esrl.noaa.gov/psd/. The SST data were obtained from the Physical Oceanography Distributed Active Archive Centre (PO.DAAC) at the NASA Jet Propulsion Laboratory, Pasadena, CA. http://podaac.jpl.nasa.gov. Both of them are acknowledged for free dissemination.

CHAPTER 3

Large-scale atmospheric forcing influencing the long term variability of Mediterranean heat and water budgets: climatic indices

Abstract

Interannual to interdecadal precipitation (P), evaporation (E), water deficit (E-P) and total heat flux have been correlated with North Atlantic Oscillation (NAO) and Mediterranean Oscillation (MO) indices to explore the influence of large-scale atmospheric forcing in the Mediterranean water and heat budgets variability. Basin-averaged precipitation decrease from mid-60s to late-80s clearly corresponds to a switch from a low to a high state of both indices. E-P variability is not so well correlated with the atmospheric indices due to the different sensitiveness of E and P that leads to correlations of opposite sign in the eastern and western sub-basins. The effectiveness of NAO and MO indices is rather similar for P and E-P but the regional MO index has turned out to be a more successful indicator of interdecadal evaporation and net heat flux because from mid 70s to early 90s there is a considerable discrepancy with NAO index. Since the MO centre remains rather steady, it influences most of the Mediterranean all year round, then becoming more suitable for monitoring long term water and (especially) heat budgets variability.

3.1 Introduction

The Mediterranean Sea (Figure 3.1), a semi-enclosed basin that extends over 3000 km in longitude and over 1500 km in latitude with an area of $2.5 \cdot 10^{12}$ m^2, communicates with the Atlantic Ocean through the Strait of Gibraltar and with the Black Sea through the Turkish Bosphorus and Dardanelles Straits. Semi-enclosed basins such as the Mediterranean are suitable for the characterisation of heat and water fluxes since they make a budget closure feasible. Evaporative losses (E) are not balanced by precipitation (P) and river runoff (R) and an Atlantic inflow through the Strait of Gibraltar is necessary to balance the freshwater and salt budgets.

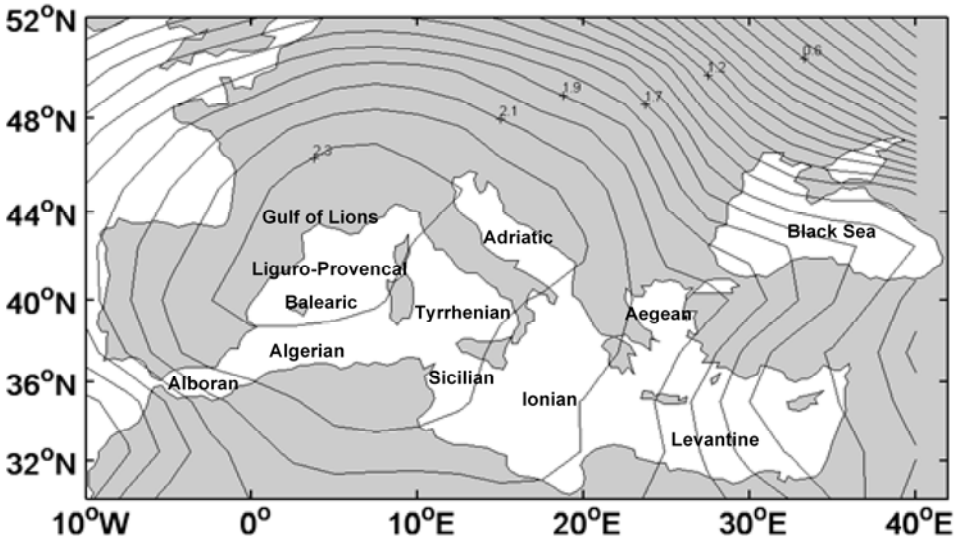

Figure 3.1 Map of the Mediterranean Sea. The main basins and sub-basins are indicated. The MO pattern (contours) has been computed as the first PC of normalised sea level pressure anomalies across the extended Mediterranean region (30ºW-40ºE, 30ºN-60ºN).

A great number of studies have dealt with the Mediterranean heat (Bethoux, 1979; Bunker et al., 1982; May, 1986; Garrett et al., 1993; Gilman and Garrett, 1994; Castellari et al., 1998; Matsoukas et al., 2005; Ruiz et al., 2008; Criado-Aldeanueva et al., 2012) and water (Bethoux, 1979; Peixoto et al., 1982; Bryden and Kinder, 1991b; Harzallah et al., 1993; Gilman and Garrett, 1994; Castellari et al., 1998; Angelucci et al., 1998; Béthoux and Gentili, 1999; Boukthir and Barnier, 2000; Mariotti et al., 2002; Mariotti, 2010; Criado-Aldeanueva et al., 2012) budgets but only in the recentmost ones, which use longer datasets, the attention focused on the interannual variability and

its forcing mechanisms. For instance, Criado-Aldeanueva et al. (2012) report three different periods in the precipitation and evaporation anomalies: from early 50s to late 60s, a positive trend is observed that changes to negative until late 80s when it changes sign again. This variability also reflects in the total heat flux exchanged between the ocean and atmosphere and suggests a 40-year period multi-decadal oscillation related to long-term atmospheric forcing that needs further investigation.

Indices of large-scale climate modes provide an integrated measure of weather linked more to the overall physical variability of the system than to any individual local variable. Among these indices, the North Atlantic Oscillation (NAO) is one of the most prominent modes of the northern hemisphere climate variability (Walker and Bliss, 1932; van Loon and Rogers, 1978; Barnston and Livezey 1987; see Hurrell et al., 2003 for a recent review). It consists of a dipole of the sea level pressure over the North Atlantic-European region with one centre reflecting the Iceland low and the other the Azores high. Both phases of the NAO (stronger and weaker dipole) are associated with basin-wide changes in the intensity and location of the North Atlantic jet stream and storm track and in large-scale modulations of the normal patterns of zonal and meridional heat and moisture transport, which in turn results in changes in temperature and precipitation patterns over extended areas, including the Mediterranean sea (Walker and Bliss 1932; van Loon and Rogers 1978; Rogers and van Loon 1979; Hurrell 1995; Serreze et al., 1997; Dai et al., 1997; Mariotti et al., 2002; Mariotti and Arkin, 2007).

Although NAO influences the climate conditions in the Mediterranean region, Conte et al (1989) suggested the possible existence of a Mediterranean Oscillation (MO) as a consequence of the dipole behaviour of the atmosphere in the area between the western and eastern Mediterranean. Differences in temperature, precipitation, circulation and other parameters between both basins were attributed to this MO and an index to measure the intensity of this dipole-like behaviour was proposed (Conte et al., 1989; Kutiel et al., 1996; Maheras et al., 1999; Supic et al., 2004; Suselj and Bergant, 2006). Some aspects of the Mediterranean climate variability have been reported to be better reflected by the MO index (Supic et al., 2004), including the flow exchange through Gibraltar (Gomis et al., 2006) but more research is required on this topic,

especially in what concerns to heat and water budgets variables, to which is devoted this work.

In this paper we correlate interannual to interdecadal precipitation, evaporation, water deficit (E-P) and total heat flux with atmospheric indices (NAO and MO) to explore the influence of large-scale atmospheric forcing in the Mediterranean water and heat budgets variability. The work is organised as follows: section 2 describes the data and methodology; section 3 presents and discuss the results both from a regional and global approach and finally section 4 summarises the conclusions.

3.2 Data and methodology

Since there is no unique way to describe the spatial structure of the NAO or MO, it follows that there is no universally accepted index to describe the temporal evolution of the phenomenon. Most recent NAO or MO indices are derived either from the simple difference in surface pressure anomalies between various locations (Rogers, 1984; Conte et al., 1989; Hurrell, 1995; Jones et al., 1997; Slonosky and Yiou, 2001; see Jones et al., 2003 for a comparison between several station-based indices) or from the Principal Components (PC) time series of the leading Empirical Orthogonal Function (EOF) of sea level pressure or some other climate variable (Suselj and Bergant, 2006; Gomis et al., 2006; Mariotti and Arkin, 2007; see Hurrell and Deser, 2010 for a review of diverse methods). A disadvantage of the station-based indices is that they are fixed in space and are significantly affected by small-scale and transient meteorological events that introduce noise (Trenberth, 1984; Hurrell and van Loon, 1997) whereas the PC time series approach is more optimal representation of the full spatial pattern (Hurrell and Deser, 2010) and will be used in this work unless differently stated.

The monthly NAO index from the National Oceanic and Atmospheric Administration (NOAA) Climate Prediction Center (CPC) has been retrieved. Its calculation is based on the Rotated Principal Component Analysis (Barnston and Livezey, 1987) applied to monthly mean standardized 500-mb height anomalies for 20ºN-90ºN (see http://www.cpc.ncep.noaa.gov/data/teledoc/teleindcalc.shtml for a detailed description). The MO pattern has been computed as the first PC mode of

normalised sea level pressure anomalies across the extended Mediterranean region (30ºW-40ºE in longitude, 30ºN-60ºN in latitude) which exhibits a single centre located over the central and western Mediterranean (Figure 3.1), fairly steady in all seasons. The MO index is then obtained as the corresponding time coefficients of the first PC mode. Since we define the positive phase when sea level pressure anomaly above the Mediterranean is positive, MO and NAO indices are positively correlated.

Monthly means from January 1948 to February 2009 of precipitation, evaporation and surface heat fluxes have been retrieved from the National Center for Enviromental Prediction-National Center of Atmospheric Research (NCEP-NCAR) reanalysis project (NCEP hereinafter, Kalnay et al., 1996), which is run at T62 spectral resolution (approximately a grid size of 1.9ºx1.9º) with 28 sigma levels. Auxiliary data of monthly mean sea level pressure and air temperature at 2.5ºx2.5º for the period 1948-2009 have also been retrieved from NCEP database. Despite the uncertainties derived from the use of reanalysis, Mariotti et al. (2002) showed that NCEP data exhibit good agreement when compared with observational datasets at interannual to inter-decadal time scales in the Mediterranean area. Moreover, the use of reanalysis allows the construction of homogeneous time series (both in time and space), this leading to a better representation of the basin-scale structures, which are the aim of this work. Seasonal means have been computed by averaging JFM (winter), AMJ (spring), JAS (summer) and OND (autumn) monthly data. The statistical significance of the correlation between the climatic variables and the atmospheric indices has been computed by transforming the correlation matrix in a *t*-student distribution with N-2 degrees of freedom, where N is the number of element of the analysed time series.

3.3 Results and discussion

3.3.1 Precipitation

Figure 3.2 displays the correlation between annual precipitation and winter NAO (panel A) and annual MO (panel B) indices for the period 1948-2008. The most effective (seasonal or annual) index will be selected for each variable hereinafter. A relatively high (anti)correlation (above 0.5) is observed in the Algeric-Balearic and Aegean and northern Levantine sub-basins (more evident for MO index). However, only in ~60% of the Mediterranean, precipitation and atmospheric indices are significantly correlated on annual basis with a mean absolute correlation, |corr|, about 0.4 (see table 3.1). The correlation increases in winter (or even the entire rainy period, October-March), especially for MO index, with wide regions close to -0.6 and a mean absolute value of 0.48 (not shown). Up to 80% of the basin (except the south-eastern sub-basin) is significantly correlated in this season, when P is generally linked to storm-track activity captured by atmospheric indices. In summer, most of precipitation across the Mediterranean region is of convective origin and is poorly correlated with the large-scale atmospheric variability.

Anti-correlation is expectable for P since the positive NAO phase (stronger dipole) strengthens and modifies the orientation of prevailing westerly winds and associated storm-track activity which cause increased precipitation over the northern Europe and dry anomalies in the Mediterranean region (Hurrell, 1995; Serreze et al., 1997; Dai et al., 1997). Roughly opposite conditions occur during the negative (weaker dipole) NAO phase. Since we have defined the negative phase of MO when sea level pressure anomaly above the Mediterranean is negative, it is linked to an intense cyclogenesis over the central/western Mediterranean that produces anomalously wet conditions over most of the Mediterranean and, hence, negative correlation with P.

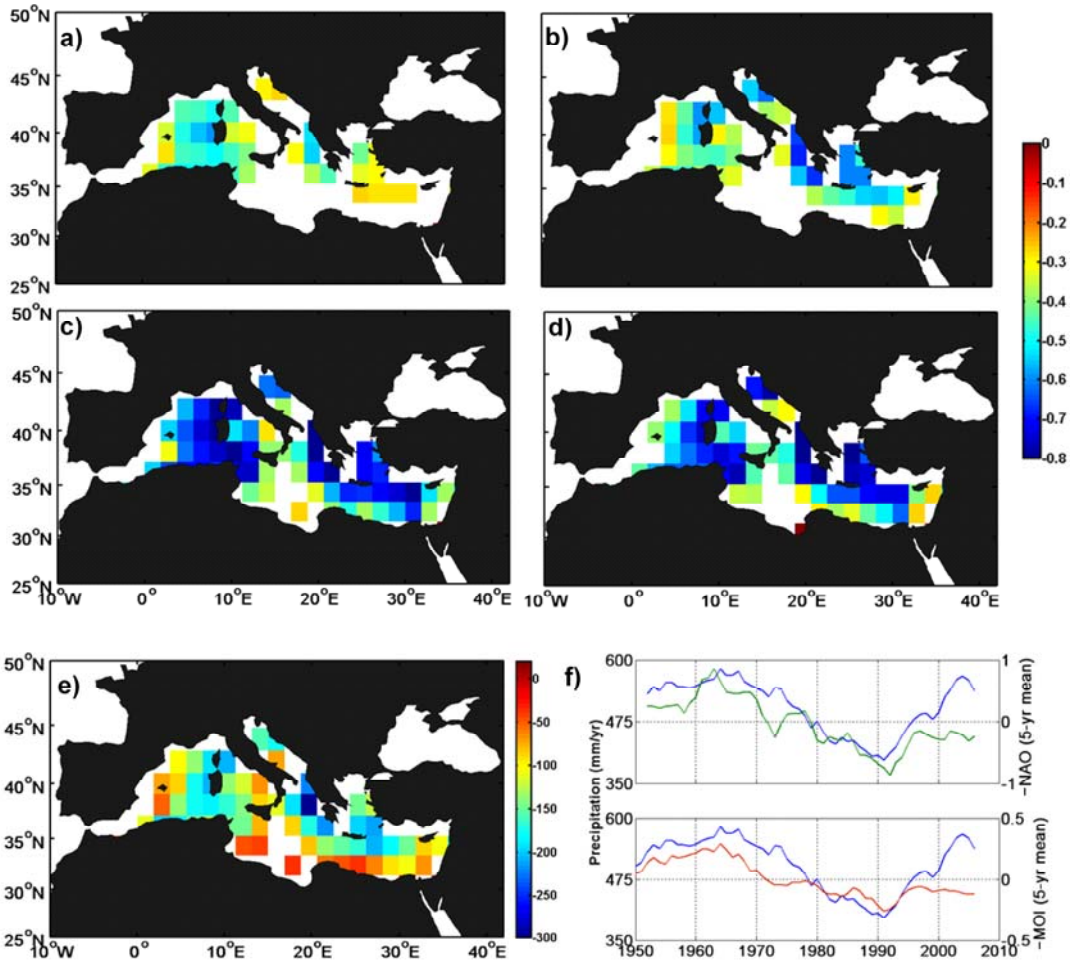

Figure 3.2 Correlation (95% significance) between precipitation (P) and large-atmospheric indices for the period 1948-2008. A) Annual P and winter NAO index; B) Annual P and MO index; C) 5-year running means of P and winter NAO index; D) 5-year running means of P and MO index. E) Regression of P with winter NAO index at decadal (5-year running means) timescales; F) Time series of 5-year running means of winter -NAO (upper, green) and annual -MO (lower, red) indices and Mediterranean-averaged P.

At decadal timescales (Figure 3.2C-D), the correlation considerably increases up to a mean absolute value close to 0.6 (table 3.1) with extended regions (especially the Algeric-Balearic and the Aegean and northern Levantine) highly correlated (~ -0.8) and a very similar performance of both NAO and MO indices. The precipitation anomalies resulting from the regression of precipitation with the NAO index (Figure 3.2E, results for MO index are rather similar, not shown) indicates that, following positive NAO index anomalies, the Mediterranean experiences a decrease in precipitation up to 150-200 mm/year in some regions, mostly restricted north of 35ºN, a result already mentioned by Mariotti et al. (2002).

Basin wide (Figure 3.2F), decadal to interdecadal variability of the Mediterranean precipitation appears to be even more closely related to NAO and MO indices with correlations of -0.8 and -0.78, respectively (table 3.1). In particular, the decrease from mid-60s to late-80s corresponds to a switch from a low to a high state of the indices (notice that –NAO and -MO indices have been plotted). These results are in good agreement with those of Mariotti et al. (2002), who obtained (only for NAO) a correlation of -0.51 and -0.84 for annual and decadal (5-year running means) variability, respectively.

	Annual means		**5-years means**		**5-years Med-averaged**	
	NAO index	**MO index**	**NAO index**	**MO index**	**NAO index**	**MO index**
P	0.40 (54%)	0.45 (56%)	0.58 (82%)	0.56 (80%)	w -0.8	a -0.77
E	0.37 (36%)	0.37 (**68%**)	0.53 (55%)	0.55 (**83%**)	w -0.48	s **-0.63**
E-P	0.38 (38%)	0.39 (38%)	0.50 (60%)	0.48 (59%)	w 0.25	a 0.22
Q	0.39 (55%)	0.37 (**74%**)	0.56 (83%)	0.59 (**93%**)	w -0.63	s **-0.70**

Table 3.1 Mean absolute correlation, |corr|, at 95% significance level between annual and decadal (5-years running means) NAO and MO indices and P, E, E-P and net heat flux (Q). The fraction of points significantly correlated is shown in brackets. The last two columns display the correlation between the indices and the Mediterranean-averaged variables at decadal (5-years running means) timescales (time series of panel F of Figures 3.2-5). The best correlated seasonal index is indicated (w: winter, s: summer, a: annual). Better results of MO index compared to NAO are highlighted in bold.

3.3.2 Evaporation

On annual basis, evaporation is poorly correlated with winter NAO (Figure 3.3A) and only the northern Levantine sub-basin seems to be sensitive to large-scale atmospheric forcing. More success is observed for the summer MO index (Figure 3.3B) that, although with a moderate correlation (between -0.3 and -0.5 in most regions and a mean absolute value of 0.37, see table 3.1) influences 70% of the Mediterranean.

Anti-correlation is again expected since, with negative indices, cold and dry air masses from the polar regions prevail, generating more severe weather conditions over the northern Mediterranean. With this state, an intensification of evaporative losses to the atmosphere is expected. Conversely, positive values of the indices are associated with a shift of the wind trajectories toward lower latitudes. Warmer and moister air

masses are then conveyed toward the Mediterranean leading to milder winters and a consequent decrease in the evaporative lost (Hurrell, 1995). But in autumn, when higher evaporation is observed (Mariotti et al., 2002; Criado-Aldeanueva et al., 2012), the southern centre of NAO is rather far from the Mediterranean and the regional MO index reflects more successfully local wind trajectories that condition evaporation. It is interesting to notice that summer MO index achieves the maximum correlation, which suggests some type of preconditioning during this season before the autumn peak.

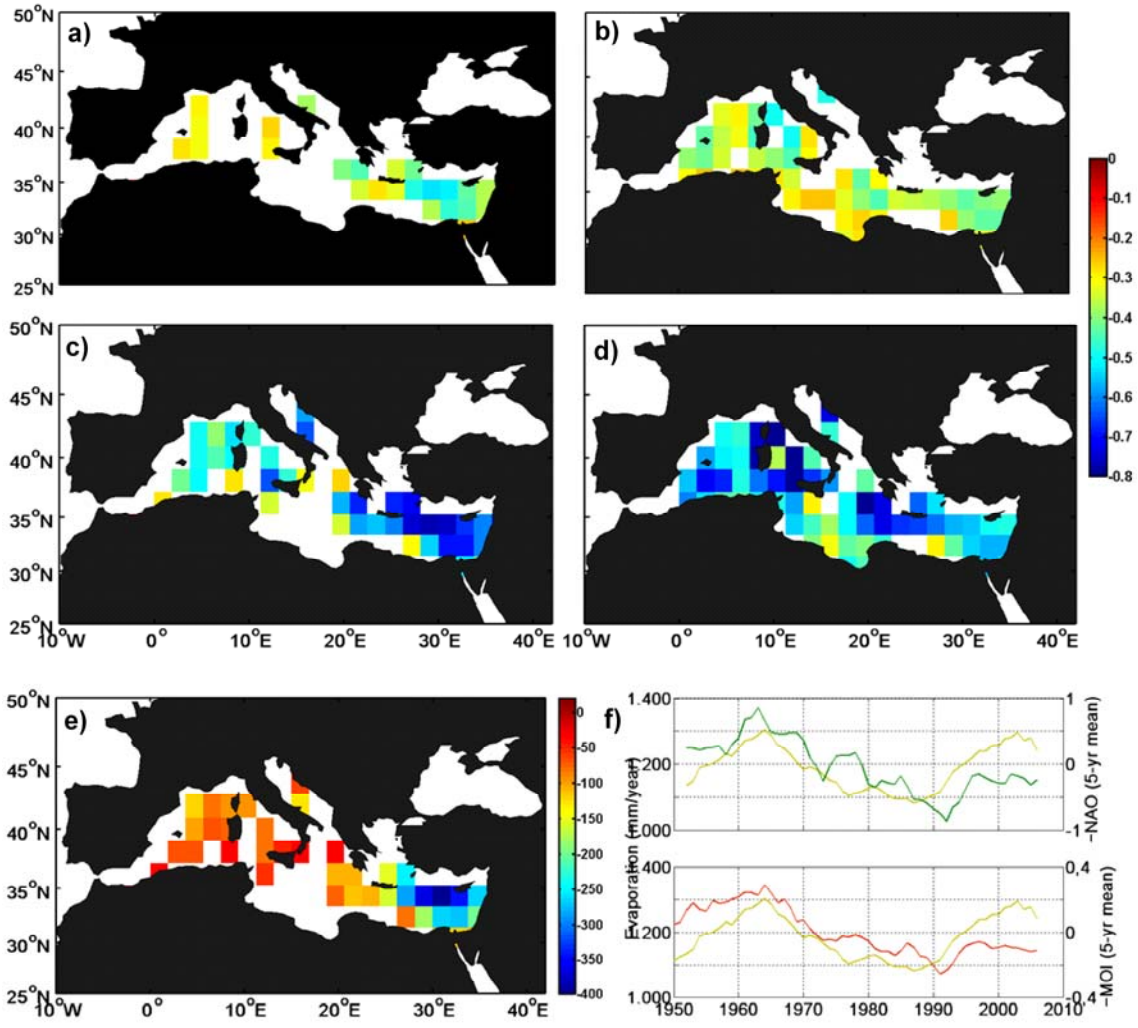

Figure 3.3 The same as Figure 2 for evaporation. The best correlated summer MO index has been selected for correlations with this variable.

At decadal timescales, the correlation increases up to a mean absolute value about 0.55 (table 3.1) with higher values (-0.7 to -0.8) in the Levantine (both indices) and Tyrrhenian (MO index) sub-basins (Figure 3.3C-D). But the difference between

NAO and MO influence remains evident (only 55% of the basin in sensitive to NAO and more than 80% to MO). The evaporation anomalies resulting from the regression with the indices (Figure 3.3E, only results for NAO index are shown) indicates that only the Levantine sub-basin, where higher evaporation is observed (Mariotti et al., 2002; Criado-Aldeanueva et al., 2012), experiences a considerable decrease in evaporation (250-350 mm/year) as a consequence of +1 NAO index anomalies.

Basin wide (Figure 3.3F), decadal to interdecadal variability of the Mediterranean evaporation is also better correlated to the regional MO index (see table 3.1). For instance, from mid 70s to early 90s, there is a considerable discrepancy between NAO index and E variability, which seems to be better captured by MO index.

3.3.3 E – P freshwater deficit

The annual freshwater deficit (E-P) is poorly correlated with atmospheric indices (Figure 3.4A-B). Only a reduced area near Corsica and Sardinia and the Adriatic (for the MO index) are positively correlated whereas the easternmost Levantine sub-basin is negatively correlated. Seasonal correlations are more successful: for instance, winter deficit is positively correlated with winter MO index with a mean value of 0.45 in most of the northern (above 35ºN) Mediterranean (not shown), but winter only accounts for 20% of annual deficit (Criado-Aldeanueva et al., 2012).

At decadal timescales, a clear bi-modal pattern is observed both for NAO and MO indices (Figure 3.4C-D): in the north-central Mediterranean, E-P is positively correlated (0.5-0.6) with the atmospheric forcing whereas in the Levantine sub-basin anti-correlation is observed (close to -0.6). In accordance, regression analysis of NAO (and, similarly MO, not shown) index with E-P also show an increment (decrement) in the freshwater deficit in the central (Levantine) sub-basins following +1 change (Figure 3.4E). This bi-modal behaviour can be explained based on the different sensitiveness of E and P to the atmospheric forcing in those regions. In the central basin, P is dominant (compare Figures 3.2E and 3.3E) and changes in E-P follow those of –P (hence, positive correlation is expected). In contrast, the Levantine sub-basin is highly sensitive to E (see Figure 3.3E) and changes in E-P follow those of E (hence, negative correlation).

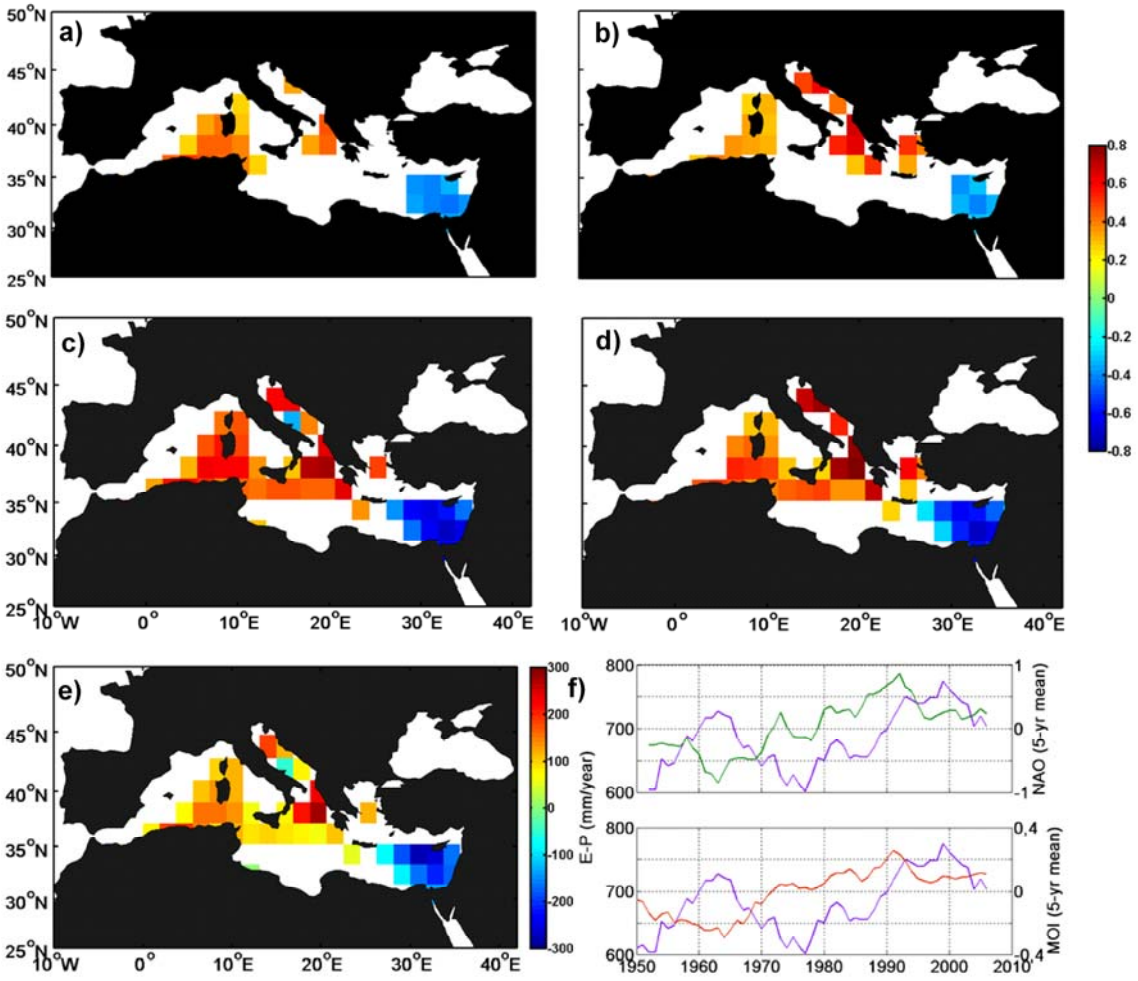

Figure 3.4 The same as Figure 2 for freshwater deficit E-P. Notice that positive NAO and MO indices have been plotted in panel F.

Mediterranean-averaged decadal to interdecadal E-P variability (Figure 3.4F) is not well correlated with the large atmospheric forcing (~0.25), probably due to this bi-modal pattern. The correlation doubles (0.5 and 0.48 for NAO and MO indices, respectively) if only the period from 1970 is considered (when a switch from a low to a high state of the indices seems to be followed by an increase in E-P), in agreement with the results of Mariotti et al. (2002), who report 0.18 from NCEP (1949-98) and 0.55 from ERA (1980-93) data. Longer time series are necessary for more precise correlation estimations.

3.3.4 Net heat flux

The net heat budget consists of two radiation components (solar shortwave radiation absorbed by the sea and longwave radiation emitted by the sea) and two turbulent contributions (latent and sensible heat fluxes). Annual net heat flux is moderately (mean absolute value close to 0.4) correlated with MO index (Figure 3.5B) in most parts of the Mediterranean (except the Alboran, Adriatic and north Aegean sub-basins). Similar results are found for NAO index but more extended areas (especially the southern Ionian) are not significantly correlated (Figure 3.5A). Decadal variations are more successfully correlated with both indices (|corr|~0.6, see table 3.1) with higher values close to -0.8 in the Levantine sub-basin (for NAO index, Figure 3.5C) and in the central Mediterranean (for MO index, Figure 3.5D).

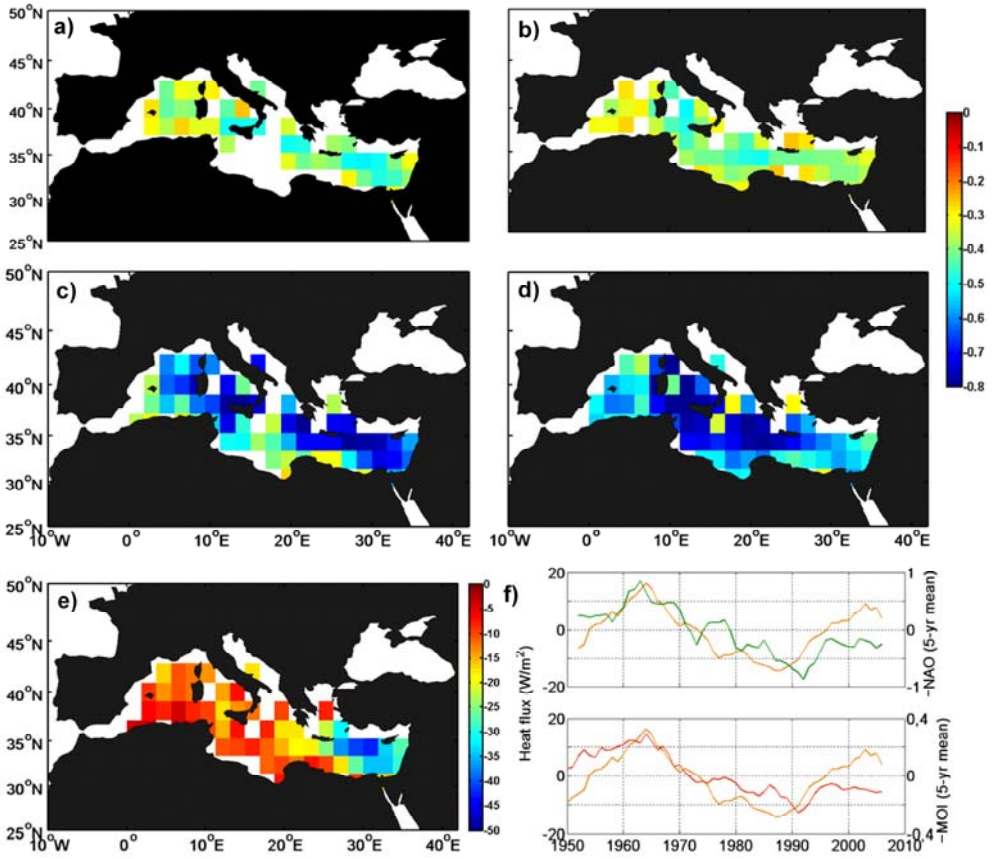

Figure 3.5 The same as Figure 2 for net heat flux Q. The best correlated summer MO index has been selected for correlations with this variable.

As shown by Criado-Aldeanueva et al. (2012), fluctuations in the net heat flux closely follow those of the latent heat, this contribution becoming the main source of interannual variability. Since latent heat losses are directly related to evaporation, similarity between Figure 3.3 and Figure 3.5 is expectable. However, better correlation is observed for net heat flux (see also table 3.1) due to the other heat contributions that correlate well with the atmospheric indices (especially the MO index, e.g. |corr| = 0.52 and 0.55 for long and shortwave radiation, respectively, in more than 80% of the basin at annual timescales). Notice that the sign of the correlation is negative because we have selected net heat flux positive toward the atmosphere (the same as evaporation). The net heat flux anomalies resulting from the regression with the indices (Figure 3.5E for NAO index and very similar for MO index, not shown) reveal that, similarly to evaporation, the Levantine sub-basin is the most sensitive to changes in the large-scale atmospheric forcing.

Basin wide (Figure 3.5F), decadal to interdecadal variability of the Mediterranean net heat flux is better correlated to the regional MO index (table 3.1). As previously said, from mid 70s to early 90s, there is a considerable discrepancy between NAO index and E (and hence, net heat) variability, which seems to be better captured by MO index.

3.4 Summary and concluding remarks

We have correlated interannual to interdecadal precipitation, evaporation, water deficit (E-P) and total heat flux with climatic NAO and MO indices to explore the influence of atmospheric forcing in the Mediterranean water and heat budgets variability. The indices exhibit considerable interannual and multi-decadal variability and prolonged periods of both positive and negative phases of the pattern are common. Although basin-averaged precipitation decrease from mid-60s to late-80s clearly corresponds to a switch from a low to a high state of both indices, E-P variability is not so well correlated with the large atmospheric forcing due to the different sensitiveness of E and P that leads to correlations of opposite sign in the eastern and western basins.

The effectiveness of NAO and MO indices is rather similar for P and E-P but the regional MO index has turned out to be a more successful indicator of interdecadal evaporation and net heat flux (see table 3.1, in bold) because from mid 70s to early 90s there is a considerable discrepancy with NAO index. Annual MO index seems to achieve the highest correlations except for E and net heat flux where summer influence suggests some type of preconditioning during this season. In contrast, winter NAO index always performs the best correlation with all variables.

A question then arises as whether MO pattern is just a regional representation of NAO or a regional circulation form. The annual time series of NAO and MO indices are highly correlated (~0.6), this indicating a close relationship between the indices due to the forcing of Atlantic low systems on Mediterranean cyclogenesis (Trigo et al., 2002). The MO can be seen as an oscillation of sea level pressure anomalies in the central and western Mediterranean, a significant source of cyclogenesis. Since the occurrence of these cyclones is partially linked with the activity of North Atlantic fronts governed by NAO, a high correlation is expectable.

The relationship can also be analysed from the comparison of their spatial patterns. In winter, the southern centre of the NAO is located closer to the Mediterranean and, for this reason, the best correlation for all variables is always observed for winter NAO index. But in summer and spring, the southern centre of the NAO moves westward (Hurrell, 1995) and lower correlation is observed. In contrast, the MO centre remains rather steady and it influences the Mediterranean all year round (hence annual indices are preferred). Due to the MO persistence in all seasons and close similarity to NAO only in winter and autumn, it is likely to represent (although influenced by NAO) rather than a regional representation of NAO, an own regional circulation form, more suitable for monitoring long term water and (especially) heat budgets variability.

Acknowledgements

This work has been carried out in the frame of the P07-RNM-02938 Junta de Andalucia Spanish-funded project. JSN acknowledges a postgraduate fellowship from Conserjería

de Innovación Ciencia y Empresa, Junta de Andalucía, Spain. Partial support from CTM2010-21229 (M. of Science and Technology) and P08-RNM-03738 (Junta de Andalucía) Spanish-funded projects are also acknowledged. NCEP data have been provided by the NOAA/OAR/ESRL PSD, Boulder, Colorado, USA, from their website at http://www.esrl.noaa.gov/psd/.

CHAPTER 4

Estimation of the Atlantic inflow through the Strait of Gibraltar from climatological and in situ data[1]

Abstract

Atmospheric data from reanalysis, satellite and experimental observations have been combined to calculate a four-year time series of the Atlantic inflow through the Strait of Gibraltar. The net flow through the strait, estimated from the Mediterranean water budget, and the Mediterranean outflow, estimated from currentmeter observations in Espartel sill (western Strait of Gibraltar) from October 2004 to January 2009, made it possible to estimate the Atlantic inflow as the sum of both of them. The obtained mean net flow is 0.038±0.007 Sv, with a seasonal cycle of 0.042±0.018 Sv annual amplitude and maximum in September. The Mediterranean outflow shows a seasonal signal with annual amplitude of 0.027±0.015 Sv peaking in April (in absolute value), and a mean value of -0.78±0.05 Sv. The resulting Atlantic inflow has a mean value of 0.81±0.06 Sv and a seasonal cycle with annual amplitude of 0.034±0.011 Sv, peaking in September, and high inter-annual variability. The inflow seasonal cycle is the result of a barotropic forcing associated with the cycle of the net flow, driven by the evaporative cycle, and a baroclinic forcing linked to the seasonal cycle of the reduced gravity that drives the exchange.

[1] Javier Soto-Navarro, Francisco Criado-Aldeanueva, Jesús García-Lafuente and Antonio Sánchez-Román (2010). Estimation of the Atlantic inflow through the Strait of Gibraltar from climatological and in situ data. *J. Geophys. Res.*, 115, C10023, doi. 10.1029/2010JC006302.

4.1 Introduction

The Strait of Gibraltar is a system of sills and narrows about 60 km long and 20 km wide, with a minimum width of less than 14 km in the Tarifa narrow section (TN) and a minimum depth of 290 m in the Camarinal sill (CS), located west of Tarifa (figure 4.1).

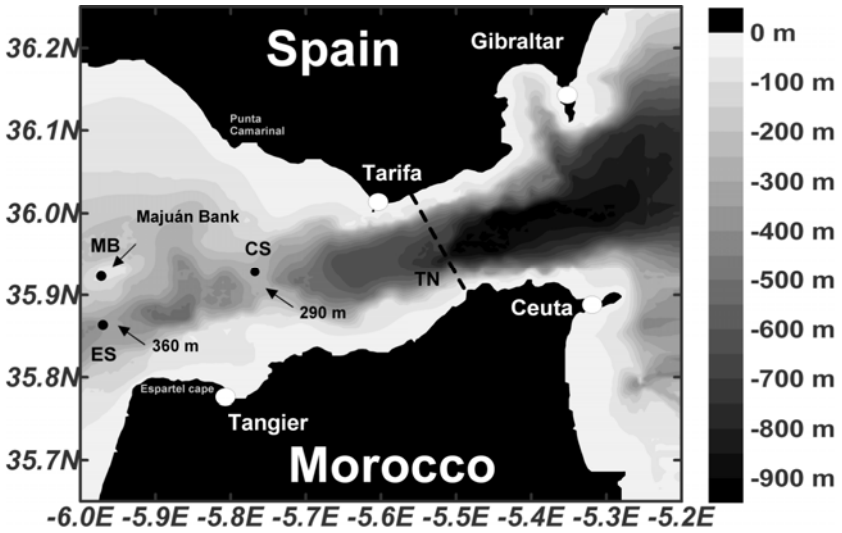

Figure 4.1 Bathymetric map of the Strait of Gibraltar showing the main topographic features. CS and ES indicate the location of the sills of Camarinal and Espartel, respectively. MB is the submarine ridge of Majuan bank and TN the Tarifa Narrows.

As the only connection between the world's oceans and the Mediterranean Sea, the Strait plays an important role in its water, salt and heat budgets (Bunker et al., 1982; Garret et al., 1993; Bethoux and Gentilli, 1999; Mariotti et al., 2002; Ruiz et al. 2008; Criado-Aldeanueva et al., 2012). The semi-enclosed nature of the Mediterranean basin and the fact that, on a yearly base, the spatially-averaged evaporation exceeds precipitation and river discharge makes the Mediterranean a concentration basin where the fresh water deficit is compensated by a net flow of Atlantic water entering through the Strait. This feature allows indirect net flow estimation based on the conservation equation

$$\frac{dV}{dt} = S_f \frac{d\xi_M}{dt} = P - E + R + B + Q_0 \qquad (4.1)$$

where dV/dt , is the volume temporal variation, S_f is the Mediterranean surface (~$2.5 \cdot 10^6$ km^2) and ξ_M the mass-induced sea level anomaly. The right-hand side terms are the different contributions to the budget: precipitation, *P*, evaporation, *E*, river discharge, *R*, the exchange with the Black Sea through the Turkish Straits, *B*, and the net flow through the Strait of Gibraltar, Q_0. The net flow constitutes a long term barotropic signal resulting from the difference between the Atlantic inflow, Q_1, and the Mediterranean outflow, Q_2, that do not cancel each other on monthly time scales. This seasonal input of mass-excess into the Mediterranean Sea is neither canceled out by the evaporative cycle at short time scales, giving rise to a seasonal cycle of mass content in the Mediterranean, which adds on the steric one due to temperature and salinity variations.

Many authors have estimated the net flow obtaining similar results (table 4.1). Boukthir and Barnier (2000) and Mariotti et al. (2002) using the mass conservation with different approaches calculate a long term mean of 0.031 and 0.039 Sv (1Sv=10^6 m^3/s) from data of the European Centre for Medium range Weather Forecast (ECMWF) and of the National Centre of Environmental Prediction (NCEP) respectively, although Boukthir and Barnier (2000) pointed out that evaporation is probably underestimated in the ECMWF data. For the seasonality of the net flow, García et al. (2006) reported an annual amplitude of 0.029 Sv peaking in January while Fenoglio-Marc et al. (2006) find an annual amplitude of 0.057 Sv peaking in September both using gravimetry observations (Gravity Recovery and Climate Experiment, GRACE-Mission). Direct estimations from current measurements vary between an annual amplitude of 0.04 Sv as found by Bryden et al. (1994) and Candela (2001), and 0.044 Sv peaking in September (semi-annual of 0.035 Sv peaking in July) as found by García-Lafuente et al (2002a).

Both the inflow and the outflow fluctuate at different timescales, the most noticeable being the semidiurnal, followed by the meteorological, seasonal and interannual variations (García-Lafuente et al. 2002b, 2007). Seasonal variability of the exchanged flows has been studied using different approaches (Bryden et al., 1994; Candela 2001; García-Lafuente et al., 2002a, 2007) obtaining results of about 0.10 Sv annual amplitude for the inflow, peaking in late summer, and from 0.03 Sv to 0.14 Sv

for the outflow peaking in late winter-early spring. Even though the more reliable source is in situ observations, these results must be considered cautiously due to the difficulties of computing the interface depth between the Mediterranean and Atlantic layers and from point-wise velocity observation.

From the hydraulic viewpoint, the exchange state depends on the existence of one or two hydraulic controls in the Strait (Farmer and Armi, 1986; Bormans et al., 1986; Bryden et al., 1994; García-Lafuente et al., 2002a). A first case is the maximal exchange regime, which occurs when the flow is controlled either at CS or at Espartel sill (ES in figure 4.1) and at TN (Farmer and Armi, 1986). In this situation, the region between the controls is isolated respect to the neighbour basins and thus, any variation in the inflow (outflow) is reflected in the outflow (inflow) so both flows are phase locked, which means that an increase (decrease) of one of them produce a decrease (increase) of the other one (García-Lafuente et al., 2002a). A second case is the submaximal exchange in which the TN control is lost and the flow is now affected by changes in the Mediterranean since it is now possible for a signal to travel through the strait into the Atlantic Ocean (Bormans et al., 1986; García-Lafuente et al, 2002a). This situation allows for independent variations of the flows.

This work focuses on the inflow seasonality, which has been less studied by other authors. A net-flow estimation based on the mass budget, combined with Acoustic Current Doppler Profiler (ADCP) observations at ES, from October 2004 to January 2009, have indirectly provided us a long time series of Atlantic inflow that allows a reliable estimation of its seasonal cycle. The paper is organized as follows: section 4.2 describes the data and methodology; in section 4.3 the main results are presented and discussed. Finally, section 4.4 summarises the conclusions.

4.2 Data and Methodology

Several datasets have been used to evaluate the different contributions to the Mediterranean budget in (Eq. 4.1). Evaporation and precipitation have been retrieved from NCEP (Kalnay et al. 1996), which is run at T62 spectral resolution (a grid size of approximately 1.9ºx1.9º) with 28 sigma levels. Monthly means from January 1948 to

January 2009 have been used to describe the seasonal cycle and daily means from October 2004 to January 2009 for the inflow computation.

The mass contribution of the sea level anomaly has been computed combining the AVISO (Archiving Validation and Interpretation of Satellite Oceanographic data) total sea level anomaly data with the estimation of the steric contribution from the Jet Propulsion Laboratory (JPL) ECCO (Estimating the Circulation and Climate of the Ocean) model salinity and temperature profiles.

The AVISO merged product is a combination of different satellite mission (T/P, ERS-1/2, GFO, ENVISAT and JASON 1) and consists in altimetry measurements with a spatial resolution in the Mediterranean region of 1/8ºx1/8º and a weekly time resolution covering the period 1992-2009. All standard geophysical and environmental corrections have been applied by AVISO processing algorithms (AVISO, 1996).

The ECCO model profiles have a spatial resolution of 1ºx1º, 46 depth levels with 10 m interval for the first 150 m and 10 days temporal resolution covering the same period than the AVISO data. The simulation uses NCEP/COADS (Comprehensive Ocean-Atmosphere Data Sets) as forcing. The steric contribution to the sea level anomaly has been calculated according to

$$\xi_S = -\frac{1}{\rho_0}\int_{-H}^{0}\left.\frac{\partial\rho(S,T,P)}{\partial T}\right|_{T,P=cte}\cdot T'(z)dz + \frac{1}{\rho_0}\int_{-H}^{0}\left.\frac{\partial\rho(S,T,P)}{\partial S}\right|_{S,P=cte}\cdot S'(z)dz \qquad (4.2)$$

where $T'(z)$ and $S'(z)$ are temperature and salinity anomalies referred to their climatological mean value; ρ_0 represents a reference density and H is the bottom depth.

The total sea level anomaly is the sum of the mass and steric contributions so that the mass contribution can be obtained as the difference between the total anomaly and the steric one, $\xi_M = \xi_T - \xi_S$. This assumption is arguable because both contributions are very difficult to separate out, but recent studies based on gravimetry techniques have shown a good agreement between direct estimation and the indirect approach (Fenoglio-Marc et al. 2006, García et al, 2006, Criado-Aldeanueva et al. 2008).

In situ velocity observations, used to estimate the outflow through the Strait of Gibraltar, were collected at a station located in the southern channel of ES (35º51.70'N, 5º58.60'W at 360 m depth in the framework of the Spanish-funded INGRES projects). This station is equipped with an up-looking ADCP settled 15 m above the seafloor, a point-wise current meter and an autonomous conductivity-temperature probe at 8 and 5 m above the seafloor respectively. It provides 3-D current velocity records every 30 minutes throughout the water column. It was first installed in September 2004 and is still acquiring information. Data from October 2004 to January 2009 have been used in this work.

To focus on seasonal variations, a 3rd order low-pass Butterworth filter with band pass and stop frequencies $f_1 = 2.496 \cdot 10^{-2}$ cpd and $f_2 = 4.992 \cdot 10^{-2}$ cpd has been applied to the time series used in the inflow estimation. Climatological and altimetry data were previously spatially averaged and all data were finally interpolated to 10-day time interval using cubic splines.

ADCP velocity data are the shortest time series and restricts the inflow estimation to the period October 2004-January 2009. However, the seasonal cycle analysis of the different components of the water budget has been performed with the full time series, by least-squares fitting them to the following function,

$$y(t) = y_0 + mt + A_a \cos(\omega_a - \varphi_a) + A_s \cos(\omega_s - \varphi_s) \qquad (4.3)$$

which includes annual, ω_a, and semi-annual, ω_s, frequencies.

4.3 Results and discussion

To estimate the Atlantic inflow we first need to characterise the several contributions of the Mediterranean water budget (Eq. 4.1). The main terms (E, P and $\frac{d\xi_M}{dt}$) are analysed from the different climatological datasets mentioned in section 4.2.

River runoff and Black Sea net flow data (*R* and *B* in Eq. 4.1) have been obtained from the literature.

Figure 4.2a displays the climatological monthly-averaged seasonal cycle of evaporation (E), precipitation (P) and E-P. Evaporation has a climatological mean of 1186±27 mm/year, with a seasonal cycle of 964±19 mm/year range (peak-to-peak), maximum in November and minimum in May. Precipitation seasonal cycle, with 506±24 mm/year mean, follows about two months the evaporative one with maximum in December, minimum in July and a range of 838±29 mm/year. Evaporation is more than twice precipitation during all the year, both producing a climatological mean of freshwater deficit (E-P) of 680±18 mm/year and a seasonal cycle of 582±21 mm/year range, maximum in August and minimum in May. Similar results have been reported by several authors analysing different datasets: Boukthir and Barnier (2000), Mariotti et al. (2002) and, more recently, Mariotti (2010) who analyse various experimental and reanalysis datasets, and Criado-Aldeanueva et al., 2012. There are not significant variations if the period from October 2004 to January 2009 (when outflow data are available) is considered for the cycle computation. The E-P range changes to 625±23 mm/year while the maximum and minimum remain in the same months. The most noticeable change is the appearance of a local maximum in November (figure 4.2b).

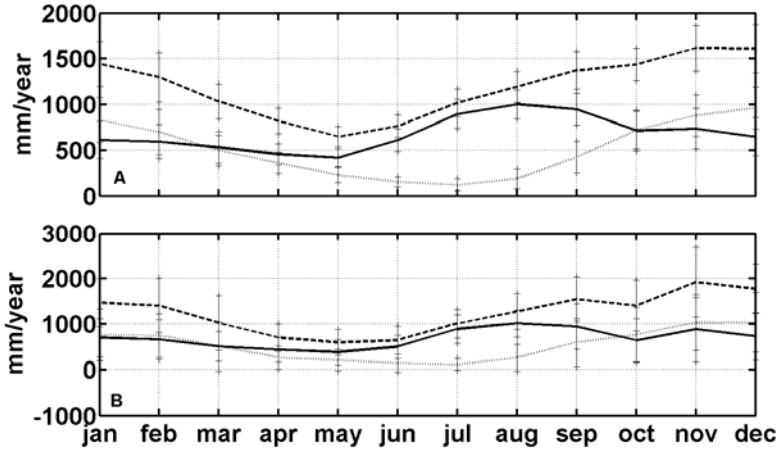

Figure 4.2 (A) Climatological monthly-averaged seasonal cycle of evaporation (E, dashed line), precipitation (P, dotted line) and E-P (solid line). The cycle is computed averaging the NCEP monthly means from 1948 to January 2009. Vertical bars are the standard deviation. (B) Same as (A) but computed from the daily values from October 2004 to January 2009, the period when the measures at ES are available.

The seasonal cycle of the total sea level anomaly, the steric and the mass contributions are shown in figure 4.3. The total anomaly has an annual amplitude of 7.0±2.1 cm peaking in October and the steric contribution, with an amplitude of 4.1±0.8 cm, reaches its maximum in September, about two months later than the sea surface temperature, in good agreement with previous results (Cazenave et al., 2002; Fenoglio-Marc, 2002; Criado-Aldeanueva et al., 2008), and three months later than the sea heat content (Ruiz et al., 2008; Criado-Aldeanueva et al., 2012). Subtracting both terms, a seasonal cycle of 4.1±1.2 cm amplitude and maximum in November is obtained for the mass contribution, almost the same as the 4.3 cm obtained using gravimetry by Fenoglio-Marc et al. (2006), and slightly lower than the 4.5 cm obtained, using the same technique, by García et al. (2006). Criado-Aldeanueva et al. (2008) made an exhaustive analysis of 14 years (1992-2005) of the same satellite data used here reporting similar results. If the period from October 2004 to January 2009 is considered the annual amplitude of the mass signal decrease to 3.0±1.1 cm due to the increase of the steric contribution amplitude to 4.6±0.9 and the decrease of the total anomaly amplitude to 6.8±1.8 cm (figure 4.3b).

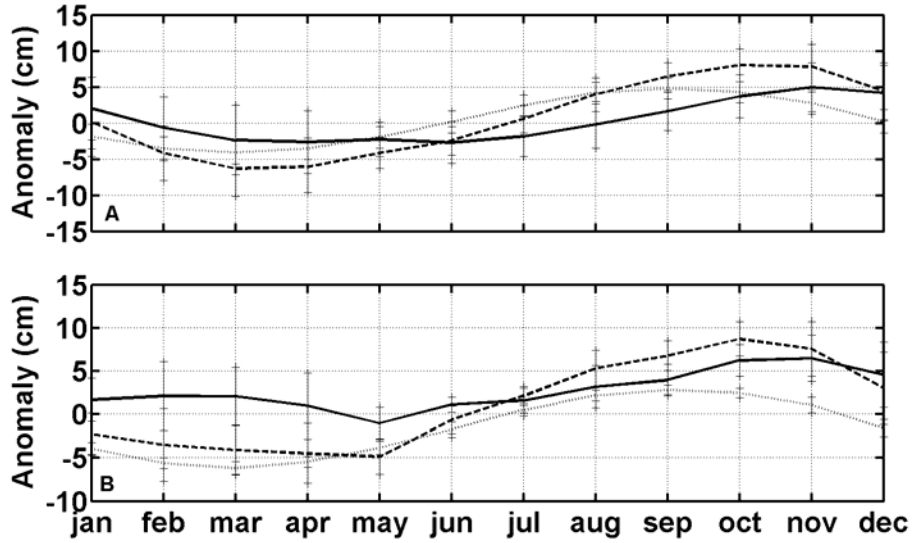

Figure 4.3 (A)Climatological monthly-averaged seasonal cycle of the total sea level anomaly (dashed line), the steric (dotted line) and the mass (solid line) contribution. Vertical bars are the standard deviation. (B) Same as (A) but computed from the daily values from October 2004 to January 2009, the period when the measures at ES are available..

Several studies have dealt with the determination of climatological river discharge into the Mediterranean Sea using diverse methodologies with different results. Boukthir and Barnier (2000) analysed data from UNESCO (1996) for the period 1974-94 and reported a climatological mean of $11 \cdot 10^3$ m^3/s with an annual cycle of $6.5 \cdot 10^3$ m^3/s range peaking in April, 30% lower than the estimates of Tixeront (1970, $16 \cdot 10^3$ m^3/s) based on rain maps and data from a few coastal stations, Ovchinnikov (1974, $13.6 \cdot 10^3$ m^3/s) or Margat (1992), who gives the same value than Tixeront (1970). Struglia et al. (2004) analyse data from Global Runoff Data Center (GRDC) and the Mediterranean Hydrological Cycle Observing System (med-HYCOS) and report an annual mean climatological value of $8.1 \cdot 10^3$ m^3/s ($10.4 \cdot 10^3$ m^3/s at most, setting an upper bound to possible underestimates), with a annual range of $5 \cdot 10^3$ m^3/s and maximum in March. This last value is close to that of Boukthir and Barnier (2000) and will be adopted for our calculations. In any case, the contribution of the river discharge is less than 20% of the most important E-P so the uncertainty of ~40% in R represent and incertitude of about 6% in the RHS of Eq. (4.1).

The Black Sea contribution has also been extensively studied, with results that range from $4.8 \cdot 10^3$ m^3/s of Bethoux and Gentilli (1999) from hydrological budget in the Aegean Sea to $9.6 \cdot 10^3$ m^3/s of Liu et al. (2009) from numerical simulation (a value close to those of Unluata et al., 1990 and Besiktepe et al., 1994). Kanarska and Maderich (2008) from a 3D model obtain mean annual values of $38.8 \cdot 10^3$ m^3/s for the upper layer (entering the Mediterranean) and $30.0 \cdot 10^3$ m^3/s for the lower layer (flowing out the Mediterranean) which means a mean net inflow of $8.8 \cdot 10^3$ m^3/s. These authors compute a seasonal cycle of $8 \cdot 10^3$ m^3/s peaking in late February, that will be adopted for our calculations. The contribution of the Black sea is also less than 20% of the E-P deficit, comparable to the river runoff.

The analysis of all components of the water budget leads to the estimation of the net flow through the Strait of Gibraltar. Figure 4.4a displays the different contributions of Eq. 4.1 (except *R* and *B*) and the resulting net flow (Q_0), which has a climatological mean of 0.038±0.007 Sv, an annual amplitude of 0.042±0.018 Sv peaking in September and semi-annual 0.011±0.009 Sv peaking in mid April. Results reported by different authors using the same or different methodologies are presented in table 4.1. Our

indirect estimation is quite similar to those reported by Bryden et al. (1994), Candela (2001) and García-Lafuente et al. (2002a), based on direct current measurements, and also to those based on water budgets of Boukthir and Barnier (2000) and Mariotti et al. (2002). The climatological monthly-averaged seasonal cycle of Q_0 (figure 4.4b) confirms this result and shows a net flow almost constant during winter and spring, with a local maximum in April, then increasing in May to reach its maximum in late summer. The Q_0 annual amplitude is the response to the seasonal cycles of E-P (figure 4.2) and dV/dt (figure 4.4b) while the semi-annual amplitude could be related to the wind stress cycle as pointed by García-Lafuente et al. (2002a).

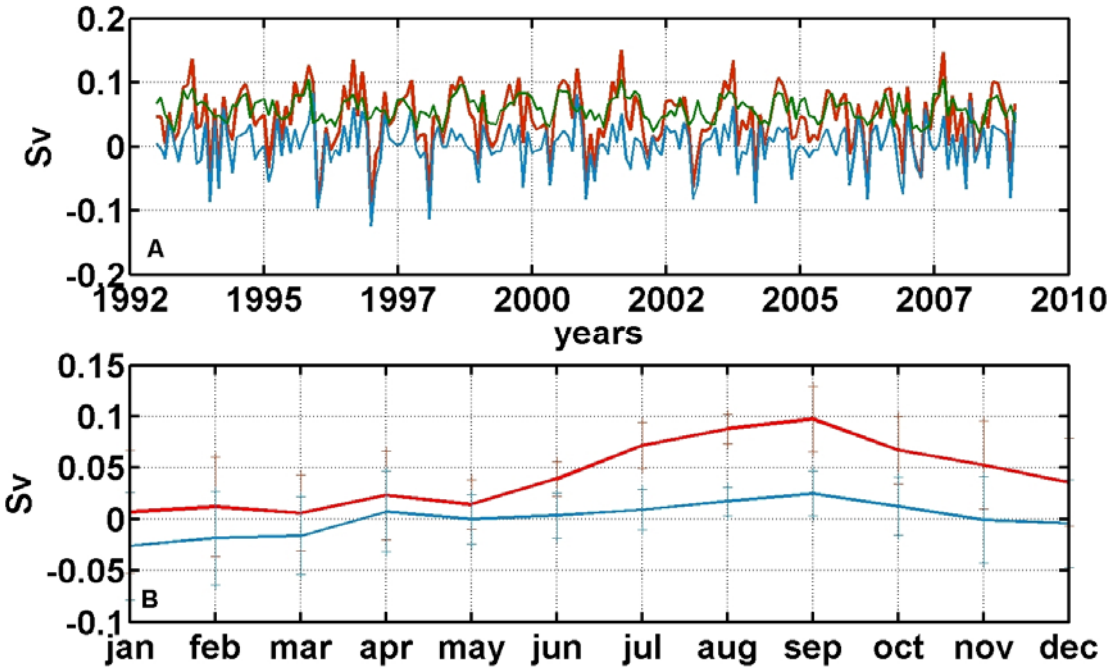

Figure 4.4 A) Time series of the net flow through the Strait of Gibraltar (red), E-P (green) and volume time-variation (dV/dt, blue) used in the computation (R and B are not shown). Panel B shows the climatological monthly-averaged seasonal cycle Q_0 and dV/dt (not canceled for the evaporative cycle on monthly basis). Vertical bars are the monthly standard deviation of each distribution.

Author	Methodology	Q_0 (Sv)
Bethoux (1979)	Energy budget	0.079
Bryden et al. (1994)	Current observations/Salinity budget	0.041
Boukthir y Barnier (2000)	Hydrologic budget	0.031
Candela (2001)	Current observations	0.040
Mariotti et al. (2002)	Hydrologic budget	0.039
García-Lafuente et al. (2002a)	Current observations	A_a = 0.044 Max. in September, A_s = 0.035 Max. in July
García et al. (2006)	Gravimetry/ Hydrologic budget	A_a = 0.029 Max. In January
Fenoglio-Marc et al (2006)	Gravimetry/ Hydrologic budget	A_a = 0.057 Max. in September
This Study	Hydrologic budget	A_a = 0.042 Max. in September A_s = 0.011Max. in April

Table 4.1 Estimations of the net flow through the Strait of Gibraltar from different authors (A_a and A_s denote annual and semi-annual amplitudes respectively).

The Mediterranean outflow has been computed from in situ ADCP velocity data collected in ES according to

$$Q_2(t) = \int_b^{h(t)} \langle u(z,t) \rangle W(z) dz \qquad (4.4)$$

where $\langle u(z,t) \rangle$ is the along-strait velocity, previously filtered to remove tidal and subinertial variability (periods lower than 21 days) and subsampled to 10 days temporal resolution; *W(z)* is the channel width at depth *z* and *h(t)* is the time-dependent depth of the surface of zero low-passed velocity (interface). More details about this procedure can be found in García-Lafuente et al. (2002a) and Sánchez-Román et al. (2009).

This transport computation presents two inconvenients: it has implicitly assumed that the single velocity profile at ES is representative of the entire channel section ignoring the cross-channel structure of the flow. Moreover, only the southern main channel of the Espartel section is considered (south of Majuan Bank, MB in figure 4.1), so Mediterranean water outflowing through the small, secondary northern channel is neglected. Sánchez-Román et al. (2009) used an improved version of the CEPOM numerical model developed by the Ocean Modelling Unit of ENEA to complement the observations and correct the flow estimations. Model outputs provide information to assess the accuracy of the outflow estimations from observations at a single station and shows that when the cross-strait structure of the velocity field is taken into account the

flow computed from a single station must be reduced around 22% due to lateral friction. The model also indicates that the fraction of the outflow through the northern channel of ES is around 18% of the total outflow. Both corrections have been incorporated to outflow estimations in (Eq. 4.4).

Figure 4.5 displays the time series of the outflow (A), the interface depth at ES (B) and the inflow (C).The resulting mean value for the Mediterranean outflow after all corrections is -0.78±0.05 Sv, similar to the -0.75 found by Sánchez-Román et al. (2009) from data between October 2004 and September 2007. The seasonal cycle of the outflow has annual amplitude of 0.027±0.015 Sv and semi-annual of 0.017±0.009 Sv, with maxima (in absolute values) in April and September respectively. The monthly-averaged seasonal cycle (figure 4.6a) shows a steep outflow increase from November to April probably linked to the replenishment of the deep western Alboran Sea with WMDW formed during winter convection in the Gulf of Lions (Garcia-Lafuente et al., 2007, 2009). From April onwards the outflow decreases until the minimum of November (-0.75±0.05 Sv).

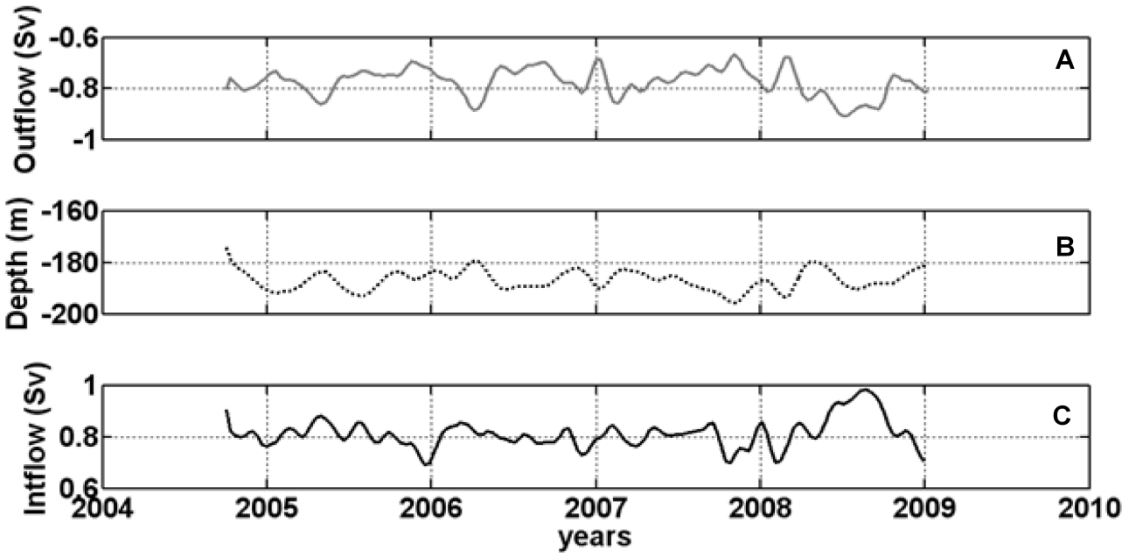

Figure 4.5 Time series of the low-passed outflow (A) and the interface depth (B) at ES for the period October 2004-January 2009. Panel (C) is the inflow computed as the difference between the net barotropic flow Q_0 and the outflow during the same period.

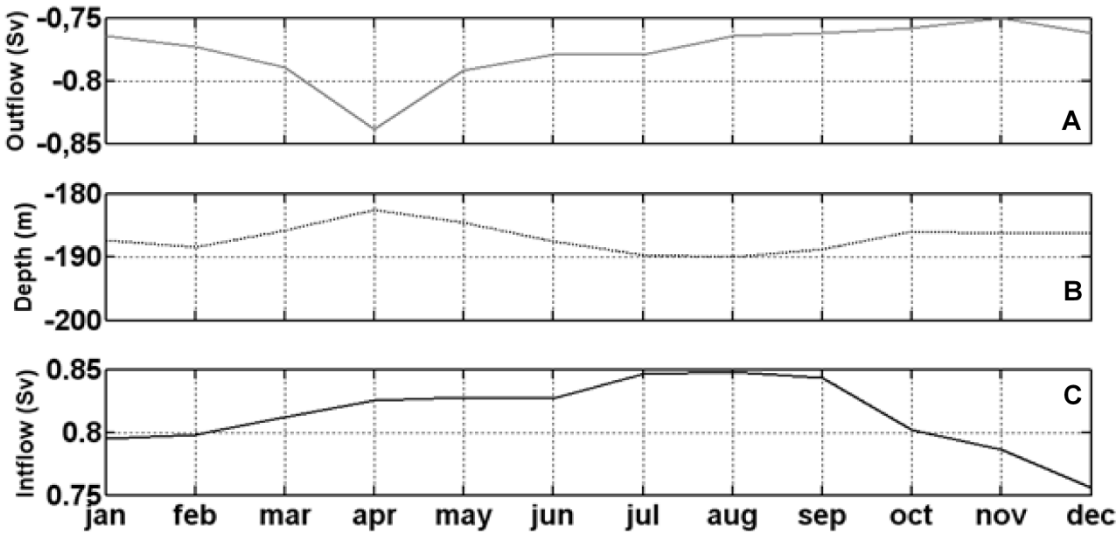

Figure 4.6 Climatological monthly averaged seasonal cycle of the outflow (A), the interface depth (B) and the inflow (C). The interface is deeper (shallower) when the inflow (outflow) is maximum (see text for details).

Bryden et al. (1994) and García-Lafuente et al. (2002a) obtained similar annual amplitudes but peaking in late winter from velocity data collected in 1985-86 and October 1995-May 1996 respectively. Candela (2001), using observations from November 1994 to September 1996, situates the maximum in early spring with an amplitude of 0.14 Sv, higher than our estimations. However, it must be taken into account that these time series are not long enough to neatly define the seasonality of the exchanged flows through the Strait. García-Lafuente et al. (2007) analysed two years of recent Q_2 measurements, collected in ES between October 2004 and October 2006, and situate the maximum in April, in good agreement with our findings, with annual amplitude of 0.05 Sv and semi-annual of 0.03 Sv.

The estimated inflow, computed as $Q_1 = Q_0 + |Q_2|$ (figure 4.5c), has a mean value of 0.81±0.06 Sv, with annual amplitude of 0.034±0.011 Sv and semi-annual of 0.022±0.014 Sv peaking in August and April respectively. The monthly-averaged seasonal cycle (figure 4.6c) also shows a maximum in late summer (August-September). The results are very influenced by the high anomaly of the year 2008, suggesting the necessity of longer time series to define the seasonality. Both the fitted signal and the monthly-averaged cycle are in good agreement with previous works (Bryden et al., 1994; Candela, 2001; García-Lafuente et al., 2002a); however, these authors found a higher value for the annual amplitude: 0.14 Sv in Bryden et al. (1994)

and 0.10 in García-Lafuente et al. (2002a). Similarly to the outflow our longer time series are thought to provide a more reliable seasonal cycle.

The maximum outflow found in April is not coupled with a minimum in the inflow and the outflow minimum is found in late autumn while the maximum inflow occurs in summer (figures 4.5 and 4.6). The fact that the inflow and outflow are not phase-locked suggests a situation of submaximal exchange with a unique hydraulic control either at CS or, more probably, at ES (García-Lafuente et al. 2002a).

The peak of the inflow in summer can be explained by two different mechanisms. The first one is barotropic in nature and follows the cycle of Q_0 which in turn is driven basically by the E-P cycle (figures 4.2 and 4.4b). A positive (towards the Mediterranean Sea) Q_0 is achieved by an increase of the inflow and a decrease of the outflow accompanied by a sinking of the interface. A second mechanism, baroclinic in nature, is the seasonal cycle of the density difference $\Delta\rho$ between the inflowing and outflowing waters. Inflow and outflow velocities are proportional to $(\Delta\rho)^{1/2}$ (actually, they are proportional to $g'^{1/2}$, g' being the reduced gravity defined $g'=g\Delta\rho/\rho_0$) so that when $\Delta\rho$ is at its maximum the velocities, and hence the flows, will also be. The outflow is not directly affected by air-sea exchanges, thus its density can be assumed to be constant. However, the inflow density is affected by the seasonal cycle of heat flux, also reflected in the steric anomaly that peaks in summer (Cazenave et al., 2002; Criado-Aldeanueva et al., 2008; Ruiz et al., 2008) and diminishes the upper layer density, increasing $\Delta\rho$ and inducing maximum inflow and outflow in this season. While both mechanisms act in the same direction to increase the inflow in summer, they do oppositely in the outflow, thus cancelling its expected summer maximum. The only well-defined signal in the outflow is the April maximum whose origin has been already commented.

4.4 Summary and conclusions

The seasonal variability of the Atlantic inflow through the Strait of Gibraltar has been characterized by a combination of indirect net flow estimation based on the Mediterranean water budget, described from reanalysis, satellite and model data, and direct outflow measurements at ES from October 2004 to January 2009, collected in the framework of the Spanish-funded INGRES projects.

The barotropic net flow signal, Q_0, depends on the E-P seasonal cycle, with 582±21 mm/year range and maximum in August, and on the mass-induced sea level signal, with a seasonal cycle of 4.1±1.2 cm amplitude peaking in November. The river discharge and the Mediterranean-Black Sea exchange have been included in the budget, although their contributions to the water budget are less than 20%. A mean value of 0.038±0.007 Sv and a seasonal cycle with annual amplitude of 0.042±0.018 Sv and maximum in September have been obtained for the net flow.

A mean value of -0.78±0.05 Sv with annual amplitude of 0.027±0.015 Sv and semi-annual of 0.017±0.009 Sv, peaking in April and September respectively, have been obtained for the Mediterranean outflow from more than four years of direct current measurements. As a result we have estimated a mean Atlantic inflow of 0.81±0.06 Sv with annual amplitude of 0.034±0.011 Sv peaking in August and semi-annual of 0.022±0.014 Sv peaking in April. The series is subject to noticeable inter-annual variability and the higher 2008 outflow anomaly may bias the resulting seasonal cycle. Longer time series that are presently being collected are necessary to improve the determination of the seasonal cycle.

The behaviour of the exchanged flows and the interface depth between the Mediterranean and Atlantic layers suggests a submaximal regime in the Strait that is reflected by the unlocked phase fluctuation of inflow and outflow. The main contribution to the inflow seasonal signal comes from the barotropic signal, Q_0, which follows the E-P seasonal cycle and leads to a maximum inflow in late summer. A second baroclinic mechanism is the seasonal change of the reduced gravity, g', due to the changes of the surface layer density produced by the seasonal cycle of heat fluxes, that peaks in summer, this contributing to the inflow maximum. It enhances the inflow

summer maximum and fades out the expected summer signal of the outflow, which only exhibits a pronounced maximum in late winter/early spring.

Acknowledgments

This work has been carried out in the frame of the P07-RNM-02938 Junta de Andalucía Spanish-funded project. JSN acknowledges a postgraduate fellowship from Consejería de Innovación, Ciencia y Empresa, Junta de Andalucía, Spain. Partial support from CTM2006-02326/MAR (INGRES 2) and CTM2009-05810-E projects are also acknowledged.

CHAPTER 5

Recent thermohaline trends of the Atlantic waters inflowing to the Mediterranean Sea[1]

Abstract

A total of 5077 Argo float profiles in the period 01/2002-05/2010 have been used to analyze salinity and temperature trends in the Atlantic waters adjacent to the Strait of Gibraltar in order to identify the source of recent changes observed in the inflow to the Mediterranean Sea. Positive salinity trends of 0.038±0.009 $year^{-1}$ and 0.013±0.003 $year^{-1}$ have been found for the Surface Atlantic Water and the Eastern North Atlantic Central Water, respectively. For temperature, no significant trend is observed in the surface layer while positive trend of 0.05±0.02 ºC/year is obtained for the thermocline waters. The Mediterranean Water layer does not show any significant trend for the entire period, but a switch from positive to negative trends is observed in year 2006. In contrast to previous findings, these thermohaline variations are driven by intrinsic water masses changes, instead of isopycnal vertical displacements, probably related to an enhancement of the net freshwater losses in the area.

[1]Javier Soto-Navarro, Francisco Criado-Aldeanueva, Jose Carlos Sánchez-Garrido and Jesús García-Lafuente (2012). Recent thermohaline trends of the Atlantic waters inflowing to the Mediterranean Sea. *Geophys. Res. Lett.*, 36, L01604, doi: 10.1029/2011GL049907

5.1 Introduction

The Mediterranean Sea is a semi-enclosed basin where the hydrologic budget, mainly dominated by the difference between evaporation (E) and precipitation (P), results in a water deficit that must be compensated by a net inflow of Atlantic Water (AW) through the Strait of Gibraltar, its only connection with the global ocean (Bethoux and Gentilli, 1999; Mariotti et al., 2002, Criado-Aldeanueva et al. 2012). Inflowing waters are mostly part of the Azores current, the southeastward flow component of the North Atlantic subtropical gyre, which flows eastward from the Atlantic ridge between 32° and 35° N (Klein and Siedler, 1989). However, local features as the Iberian current, flowing poleward (southward) during winter (summer) along the Iberian continental shelf, or the Canary current, flowing southward off Morocco also contribute to the inflow (Machin et al. 2006).

The inflow is composed by the near surface layers of the adjacent area that comprise Surface Atlantic Water (SAW) and Eastern North Atlantic Central Water (ENACW), the latter formed by isopycnal subduction of surface waters at northern latitudes (north to 43ºN). ENACW are the mode waters that constitute the permanent thermocline and are characterized by an almost linear T-S relationship. They stretch down to at least the level of minimum salinity around 35.5 (up to 36.0 at the northern and eastern Gulf of Cadiz) at about 600 m in most parts of the area (Pollard and Pu, 1985; Paillet and Mercier, 1997; van Aken, 2001; Machin et al. 2006). Below this level, Mediterranean Waters (MW) characterized by a salinity maximum around 36.5 (Ambar et al. 2002) and formed by the Mediterranean water leaving the strait after mixing with the ENACW in the Gulf of Cadiz can be found. MW has an important role in the deep water formation at the Norwegian Sea as source of salinity that enhances the deep convection process, hence affecting the Meridional Overturning Circulation and the global climate (Reid, 1979; van Aken and Beckaer, 1996; Sarafanov et al., 2008). Further down, North Atlantic Deep Water (NADW) is observed, mainly composed by Labrador Sea Water (LSW), formed by deep convection at the Labrador Sea, although fractions of Antarctic Intermediate Water (AAIW) can also be found in the lower latitudes (Machin et al., 2006; Machín and Pelegrí, 2008).

A recent study (Millot, 2007) has detected from experimental data collected at the Moroccan continental shelf in the period 2003-2007 a high salinity trend (~0.05 $year^{-1}$) of the AW that highly exceeds the estimations for the 1990s period in the Atlantic area adjacent to the strait (Boyer et al., 2005; Poliakov et al., 2005). However, analyses of the same area in more recent periods show salinity anomalies closer to this higher trend (Hosoda et al., 2009; Roemmich and Gilson, 2009) and this implies a salinity input to the Mediterranean Sea that may influence the intermediate and deep water formation processes and, consequently, the hydrological characteristics of the MW. Two main mechanisms may drive this salinity increase: changes in the intrinsic properties of the water masses or vertical displacement of the water column that makes saltier waters from the surface sink to deeper layers, or vice-versa (Bindoff and McDougall, 1994). Here we show that the high salinity trends recorded in the Strait of Gibraltar for the AW can also be found in the adjacent area of the North Atlantic and, in contrast to previous findings, are more likely related to changes in the water masses properties.

5.2 Data and methods

The area of study, covering from 28ºN to 42ºN in latitude and from 5ºW to 24ºW in longitude, has been divided into three zones (Fig. 5.1a) to separate out the influence of the different North Atlantic circulation features in the inflowing waters through the Strait of Gibraltar. The northernmost one (zone 1 hereinafter) catches the main pathways of the MW (Bower et al., 2002; Sarafanov et al., 2008) and the Iberian current. The central area (zone 2 hereinafter) covers the Azores Current and the southern zone (zone 3 hereinafter) covers the Canary Current (Pollard and Pu, 1985; Paillet and Mercier, 1997; van Aken, 2001, Machin et al., 2006). A total of 5997 Argo salinity and temperature profiles are available at the Argo data selection web site (http://www.argodatamgt.org/) for the area from 2002 to May 2010. 15% of the profiles have been neglected because they had less than ten values or were shallower than 500 m (the Argo floats cycle provides profiles from the surface to 2000 m approximately in the North Atlantic). All standard corrections detailed in the Argo Data User's Manual have

been applied. Moreover, data exceeding the mean profile more than three standard deviations have also been erased. Once the selection has been made, a total of 5077 profiles covering the area of study were separated by zones and monthly distributed (Fig. 5.1b). The profiles were then vertically interpolated in 22 pressure levels (0 10 20 30 50 100 150 200 300 400 500 600 700 800 900 1000 1100 1200 1400 1500 1750 and 2000 dbar) and monthly averaged.

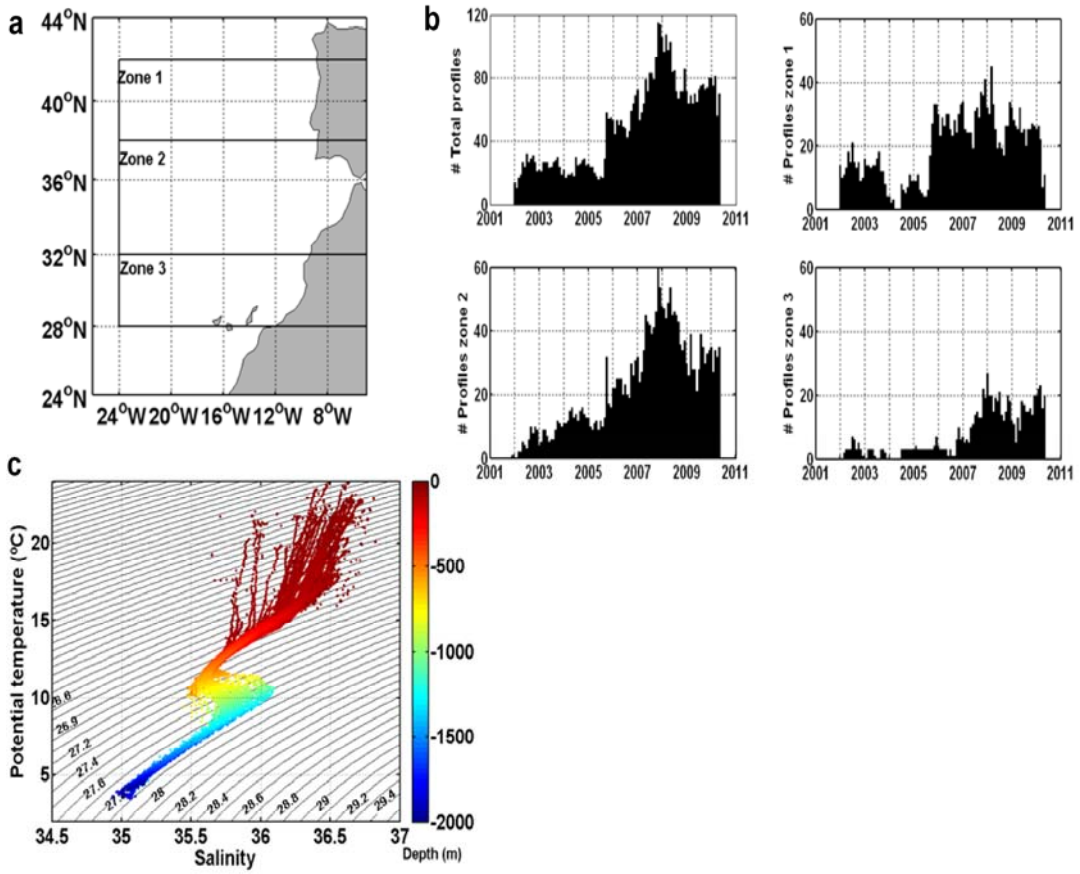

Figure 5.1 Area of study, Argo profile distribution and T-S diagram. a) Selected area of study and different subzones considered. b) Monthly distribution of the Argo profiles for the complete area (top left) and for the different zones (zone 1, top right, zone 2, bottom left, and zone 3, bottom right). c) T-S diagram of the monthly averaged profiles for the complete area. The colours represent the depth in which each T-S point is found.

In view of the monthly averaged T-S diagram of Fig. 5.1c, three main water masses will be properly analyzed: SAW in the first 100 m (although not strictly a proper water mass since its thermohaline properties have sources and sinks due to air-sea interactions, we will refer to it as representative of the surface layer (Criado-Aldeanueva

et al., 2006)), ENACW occupying the main thermocline from 100 to 600 m and MW extending from 600 to 1200 m. Although MW is found at shallower depths in the Gulf of Cadiz area, where it flows close to the continental shelf of the Iberian Peninsula between 400-600 m (Ambar et al., 2002), this area is very poorly sampled by the Argo floats and does not reflect in the T-S diagram. The deepest 800 m correspond to the upper layer of the NADW, which is not completely sampled and will not be analyzed in this work. Vertically averaged time series of salinity and temperature for the first three layers were constructed and least-square fitted to compute their linear trends. 95% confidence intervals of this computation were estimated with a t-student test.

For comparison purposes, two additional datasets were used: i) a total of 108 CTD profiles from the French Laboratory d'Océanographie de Villefranche Dyfamed project (www.obs-vlfr.fr/sodyf/), collected at (43.25ºN, 7.52ºE) and covering the period 2001-2009 were analyzed in a similar procedure than for the Argo data, although in this case the trend was calculated only for the surface layer (0-150, Rixen et al., 2005), which corresponds to the Atlantic Water (AW) spreading through the Mediterranean Sea; ii) MW salinity and temperature were analyzed from the time series collected at Espartel sill, western Strait of Gibraltar (35º51.70'N, 5º58.60'W), in the frame of the INGRES projects, at a mean depth of 356 m from October 2004 to February 2010.

The nature of the water properties changes at a given depth can be associated with two main different mechanisms. On one hand, modifications in the intrinsic properties of the water mass along isopycnal surfaces occupying that depth caused by mixing or horizontal advection. On the other hand, vertical displacements of the water column that make water masses of different densities reach deeper or shallower depths without changing their intrinsic properties; this is known as isopycnal heave. It is possible to separate out the influence of these two mechanisms applying a simple decomposition equation (Bindoff and McDougall, 1994).

$$\left.\frac{d\xi}{dt}\right|_p = \left.\frac{d\xi}{dt}\right|_n - \left.\frac{dp}{dt}\right|_n \left(\frac{\partial \xi}{\partial p}\right) \qquad (5.1)$$

The left hand side term of Eq. 5.1 represents the time variation at isobaric surfaces of a scalar property, in our case potential temperature and salinity. The first

term of the right hand side represents the time variation of the property along isopycnal surfaces, due to either intrinsic changes in the water mass properties or horizontal advection. The second term of the right hand side accounts for changes at a particular pressure level produced by the vertical displacement of the isopycnal surfaces.

5.3 Results and discussion

Estimated thermohaline trends

The time series for the different zones and layers are represented in Fig. 5.2 and the fitting results are summarized in Table 5.1. Whereas no significant temperature trends are observed in the surface layer, clear positive salinity trends are estimated in the complete area, 0.038±0.009 year^{-1}, and also for zones 1 and 2, of 0.010±0.005 year^{-1} and 0.04±0.01 year^{-1} respectively. These values are higher than those obtained for the 90s (Boyer et al., 2005; Poliakov et al., 2005), where positive but smaller anomalies were found. However, recent studies show an increase in the salinity and temperature anomalies of the SAW in the last decade closer to our findings (Hosoda et al., 2009, Roemmich and Gilson., 2009) and measurements in the AW reaching the Mediterranean (Millot, 2007) provide a salinity trend of 0.05 year^{-1} for the period 2003-2007, a value very close to our result for the complete area of study and even more to that of zone 2, which corresponds to the path of the Azores Current.

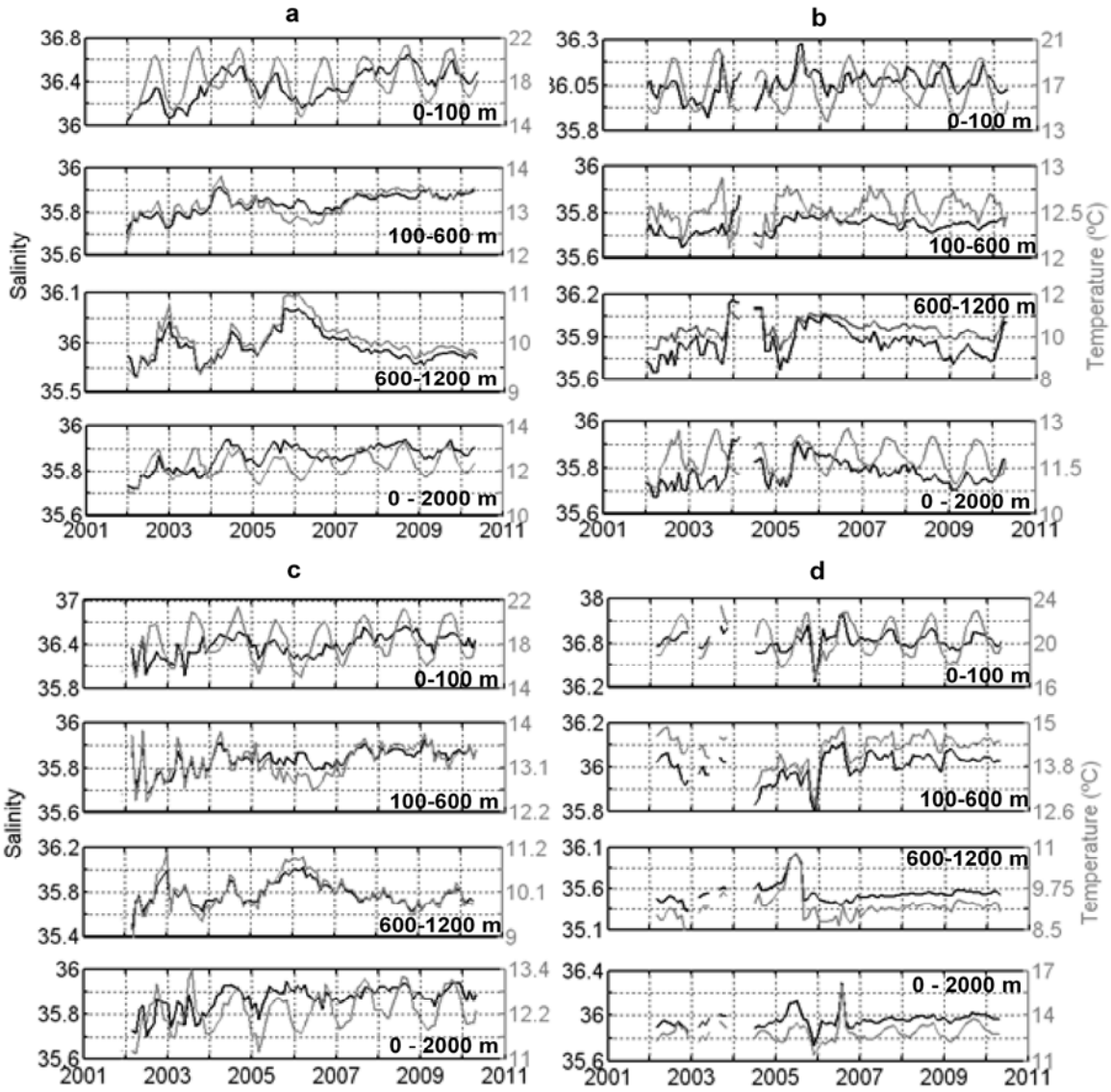

Figure 5.2 Time series of the monthly averaged salinity (black) and temperature (grey). a) Complete area, b) Zone 1, c) Zone 2, d) zone 3. For each zone the layers corresponding to the main water masses considered are shown: SAW (0-100 m) in the top graph of the panel, ENACW layer (100-600 m) in the second graph of the panel, MW layer (600-1200 m) in the third graph of the panel and the entire profile in the fourth graph of the panel.

In the ENACW layer, positive trends are observed both for salinity (with values ranging 0.005-0.013 year^{-1}) and temperature, about 0.05 ºC/year (Table 5.1). These results are also higher than those historically observed in this layer (Boyer et al., 2005; Poliakov et al., 2005), but are in good agreement with more recent estimations (Leadbetter et al., 2007; Benitez-Barrios et al., 2008). Numerical studies also predict a high intensification of the salinity anomalies for the upper 500 m of the North Atlantic in the first half of 21st century (Stott et al., 2008). For the MW, even though the

computed trends for the entire period are not significant, their values are of the same order than those estimated from time series at the monitoring station of Espartel sill, the last gateway of Mediterranean waters towards the Atlantic. A positive trend of 0.0017±0.0003 ºC/year is observed for temperature and a negative trend of -0.0022±0.0003 $year^{-1}$ for salinity in the period October 2004 – February 2010 at this location (Fig. 5.3a). However, it is worth to mention two different periods for this layer in the whole area and zones 1 and 2: first significant positive trends from 2002 to 2006, with common values of 0.06±0.02 $year^{-1}$ and 0.2±0.1 ºC/year for salinity and temperature respectively, and a switch to negative trends from then onwards, with values around -0.05±0.02 $year^{-1}$ for salinity and -0.2±0.04 ºC/year for temperature. The positive trend continues that of the previous period 1992-2002 in the intermediate waters of the subpolar North Atlantic, where values of 0.0088±0.0026 $year^{-1}$ for salinity and 0.049±0.01 ºC/year for temperature at 53ºN were found and attributed to a combination of MW salinification and a low North Atlantic Oscillation (NAO) phase (Sarafanov et al., 2008).

To further investigate the influence of these results in the evolution of the thermohaline properties of the first 150 m along the Mediterranean basin, salinity and temperature time series from the Dyfamed station corresponding to the AW layer (the first 150 m) are represented in Fig. 5.3b, where a positive trend of 0.016±0.008 $year^{-1}$ can be observed for salinity (no significant trend is found for temperature). Even though this trend is smaller than our estimation for the inflowing waters, it must be taken into account that the cyclonic circulation of the Mediterranean Sea makes the AW reaching the Ligurian Sea differ from the AW entering the Mediterranean (Millot, 1999). However, this result is one order of magnitude higher than the previous estimation for the last decade of the 20^{th} century from the MEDAR-MEDATLAS dataset (Rixen et al., 2005; Vargas-Yáñez et al., 2010).

	Complete area		Zone 1		Zone 2		Zone 3	
	S trend ($year^{-1}$)	T trend (ºC/year)	S trend ($year^{-1}$)	T trend (ºC/year)	S trend ($year^{-1}$)	T trend (ºC/year)	S trend ($year^{-1}$)	T trend (ºC/year)
0 - 100 m	0.038 ± 0.009	n.s.	0.010 ± 0.005	n.s.	0.04 ± 0.01	n.s.	n.s.	n.s.
100 - 600 m	0.013 ± 0.003	0.05 ± 0.02	0.005 ± 0.003	0.02 ± 0.01	0.013 ± 0.004	0.06 ± 0.03	0.010 ± 0.005	n.s.
600 – 1200 m	n.s.	n.s.	n.s.	n.s.	n.s.	n.s.	n.s.	n.s.
0 – Bottom	0.014 ± 0.003	0.05 ± 0.04	n.s,	n.s.	0.015 ± 0.004	0.07 ± 0.04	0.007 ± 0.006	n.s.

Table 5.1 Estimated linear trends for the complete area and for the zones considered. Each row corresponds to the different water masses analyzed: SAW layer (0-100 m), ENACW layer (100-600 m), MW layer (600-1200 m) and the entire profile. The 95% confidence intervals have been computed by a *t*-student test where *n.s.* means that the fitting is not significant.

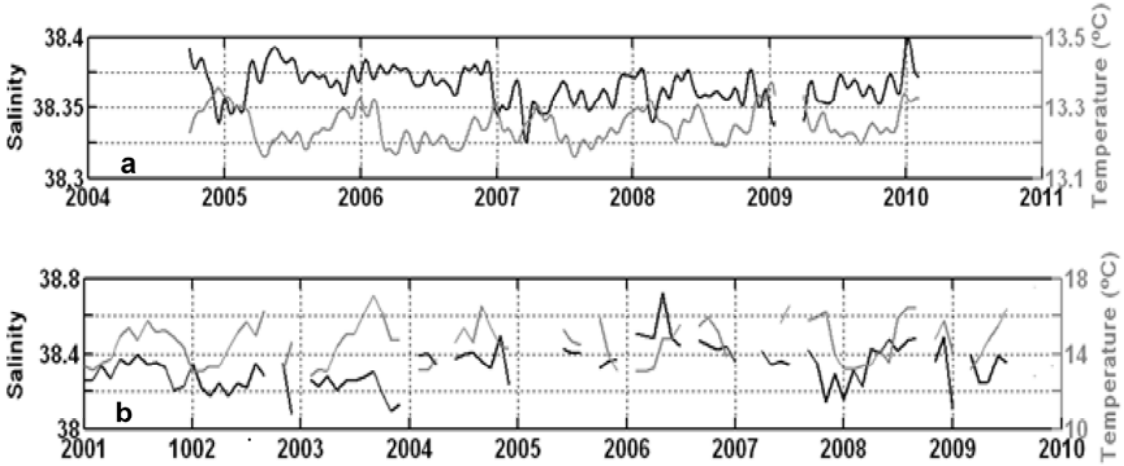

Figure 5.3.Time series of salinity and temperature from the permanent station of Espartel sill (a) and from the Dyfamed station (b).

Mechanisms controlling changes

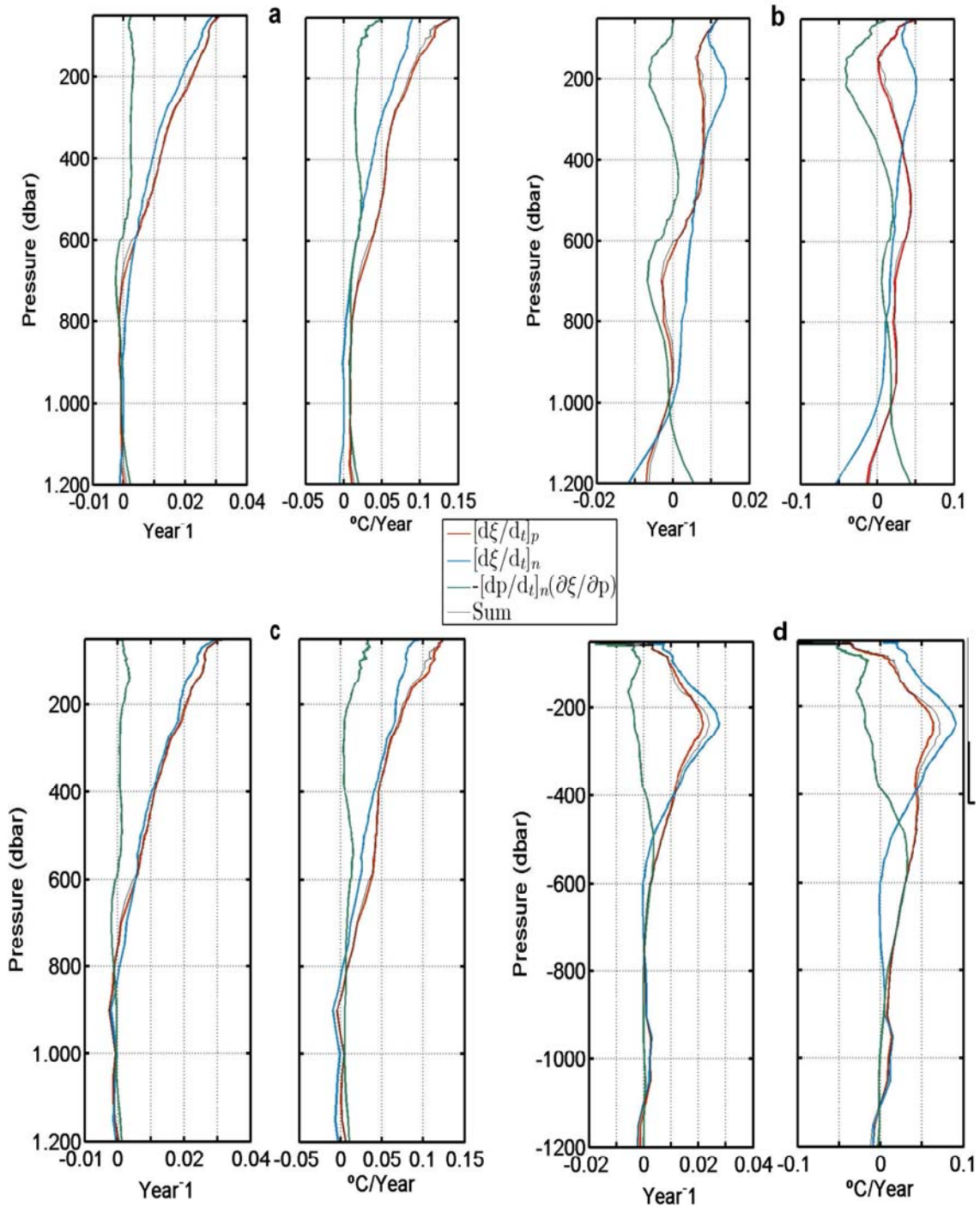

Figure 5.4 Results of the Eq. (5.1) decomposition for salinity and temperature. a) Complete area, b) zone 1, c) zone 2 and d) zone 3. On each panel the red line represents the trend along isobaric surfaces, the blue line the contribution of changes along isopycnal surfaces and the green line the contribution of the vertical displacements. The grey line is the sum of these two latter contributions. The left graph of each panel represents salinity trends and the right graph temperature trends.

The decomposition results of Eq. (5.1), displayed in Fig. 5.4, reveal that the observed trends are strongly related to changes along isopycnal surfaces (blue), while the vertical displacements (green) have a secondary role. For the complete area and zone 2 (Fig. 5.4a, c), which exhibit similar patterns, the influence of the former mechanism is clearer, with a monotonic decrease from 0.03 $year^{-1}$ for salinity and 0.12 ºC/year for temperature at 50 m to almost zero at 800 m (the shallower 50 m are not considered because Eq. (5.1) does not apply in the strong near-surface gradients, Arbic and Owens, 2001). In a previous study from CTD data collected at the 36ºN section, lower temperature trends were obtained for the period 1981-2005 (Leadbetter et al. 2007). But the main contrast with the present work is the mechanism responsible of the trend, which in that case was the isopycnal displacement. Even taking into account the differences between the sampled areas, the authors estimated a negative sign (opposite to our results) for the isopycnal changes term in the first 800 m, which means an important change in the thermocline water characteristics of this area in the last years.

For zone 1 (Fig. 5.4b) the isopycnal heave is more important; in the first 400 m it has negative sign that, for temperature, compensates the positive intrinsic changes making the total trend zero at 200 m. For salinity, the weakening of the isopycnal changes term below 600 m makes the heave responsible for the negative sign of the trend in the MW layer. In zone 3 (Fig. 5.4d) the highest trend is not found at the surface but at about 250 m, and is again caused by changes in the neutral surfaces, with negative contribution of the isopycnal displacements in the shallower 400 m, more important for temperature. From this depth, the heaving term becomes positive while the intrinsic changes term tends to zero, this leading to a small positive trend in the deeper layer for temperature. As for zone 2, studies referred to earlier periods found lower trends in this area (Vargas-Yáñez et al., 2004; Cunningham and Alderson, 2007; Benitez- Barrios et al., 2008) with the isopycnal displacement mechanism controlling the process, especially in the ENACW layer.

The results described above emphasize that the observed trends in the SAW and in the ENACW filling the permanent thermocline, the main components of the Atlantic inflow to the Mediterranean, are the result of an intrinsic warming and salinification process. The existence of a salinity minimum in the bottom of the thermocline (Fig. 5.1c) discards the mixing with the Mediterranean water as the source of salinity for the

upper layers. The most likely hypothesis for the salinity increase is an enhancement of the freshwater evaporative losses in the surface layer that increases the salinity in both SAW and ENACW by subduction processes. For the complete area, the necessary trend in the net evaporation (E-P) to match the obtained salinity trend is about 10 cm/year, a value similar to previous estimations for the 90s, which can be a consequence of an intensification of the trade winds related to a high NAO index state (Curry et al., 2003).

5.4 Conclusions

We have found that the historically observed salinity (and, in a lesser extent, temperature) trends of the Atlantic inflow in the Strait of Gibraltar correspond to a similar salinification/warming in the first 600 m of the surrounding Atlantic waters. The highest salinity trends are found in the surface layer of the Azores current area (0.04 $year^{-1}$), although positive values are also found northward and southward. Lower but positive values are computed in the main thermocline (around 0.01 $years^{-1}$), which in all cases exceed previous estimations. But the main novelty presented here is that, in contrast to other studies for earlier periods, trends are mainly related to intrinsic changes in the water masses instead of isopycnal displacements. The changes in the water masses properties are probably linked to a recent increase in the net evaporation that may affect salinity in the surface layer and also in the main thermocline by subduction and advection processes.

Acknowledgments

This work has been carried out in the frame of the P07-RNM-02938 Junta de Andalucía Spanish-funded project. Partial support from CTM2006-02326/MAR (INGRES 2) and CTM2009-05810-E projects are also acknowledged. We also thank to DYFAMED (CNRS-INSU) Observatoire Océanologique de Villefranche-sur-mer for the data used in this work. The comments and suggestions of two anonymous reviewers helped to improve the manuscript.

CHAPTER 6

Validation of regional circulation models for the Mediterranean Sea at the Strait of Gibraltar: volume transport and thermohaline properties of the outflow

6.1. Introduction

The characterization of the exchange through the Strait of Gibraltar is crucial to understand the functioning of the Mediterranean Sea due to its important role in the closure of the water and heat budgets (Bethoux and Gentilli, 1999; Mariotti et al., 2002). The evaporative losses of the basin generate a water deficit that must be compensated by a net inflow of warm a fresh Atlantic waters, which are progressively transformed along the basin, becoming saltier and eventually sinking to intermediate and deep layers in convection processes triggered by winter cooling. Finally, the colder and saltier Mediterranean waters leave the basin through the strait. The close relationship between the circulation of the basin and the exchange through Gibraltar makes the modeling of the volume transport and the water mass properties of the exchanged flows a key factor in the development of regional circulation models for the Mediterranean Sea.

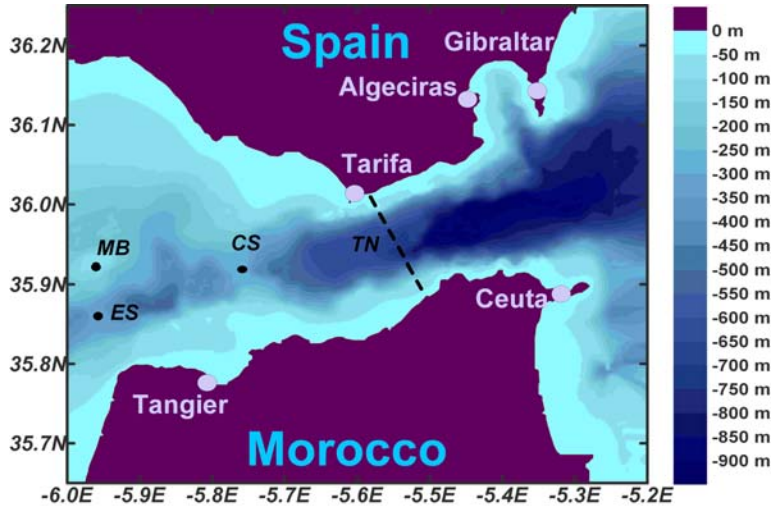

Figure 6.1 Bathymetric map of the Strait of Gibraltar showing the main topographic features. CS and ES indicate the location of the sills of Camarinal and Espartel, respectively. MB is the submarine ridge of Majuan bank and TN the Tarifa Narrows.

The volume transport variability depends on the hydraulic characteristics of the strait, and can be described by two variables: the interface depth between the Mediterranean and Atlantic layers, h, and the flow velocity, u. In an ideal two-layer model of the strait, hydraulically controlled at Camarinal sill (CS in fig. 6.1), the velocity of the flows is proportional to $g'^{1/2}$, g' being the reduced gravity defined as $g' = g\,(\rho_2 - \rho_1)\,/\rho_0 = g\,\Delta\rho\,/\rho_0$, where ρ is the density and subscripts 1 and 2 refer to the Atlantic and Mediterranean layers respectively (Farmer and Armi, 1986; Bormans et al., 1986; Bryden et al., 1994; García-Lafuente et al., 2002a). In a real stratified model, the relationship between u and $\Delta\rho$ remains and, thus, the seasonality of the transport depends on the seasonality of h and $\Delta\rho$.

The Mediterranean outflow is composed of Levantine Intermediate Water (LIW) and, to a lesser extent, of Western Mediterranean Deep Water (WMDW). The properties and fractions of these waters at Espartel sill (ES in fig 6.1), together with some traces of NACW present in the Mediterranean vein through mixing with the upper layer, determine the thermohaline characteristics of the waters leaving the strait. The proportion of WMDW in the outflow depends on the capacity of the flow to aspirate deep water from the Alboran Sea by Venturi-Bernouilli effect, a mechanism that can uplift waters from 600-700 m depth and incorporate them to the outflow (Stommel et

al., 1973; Kinder and Bryden, 1990). This is favoured when the winter deep convection in the Gulf of Lions reaches the bottom, filling it with newly formed WMDW and uplifting the ancient that is now available to be suctioned out through Gibraltar more easily. Other factors, like the circulation pattern in the Alboran Sea and the meteorological forcing also contribute to the process, varying the amount of deep water available (García-Lafuente et al., 2009, Naranjo et al., 2012).

The final properties of the Mediterranean waters leaving the strait are the result of a complex mixing process along the strait driven by tides, internal waves and the topographical constrains (García-Lafuente et al., 2011). It is not clear yet wether climate-scale regional ocean models can or not resolve or parameterize these complex processes. The aim of this work is to validate several simulations of the NEMOMED8, NEMOMED12 and NEMOMED36 ocean circulation models for the Mediterranean Sea using the observations collected in the Espartel station. Due to the characteristics of the data the comparison will be focused in the volume transport and the thermohaline properties of the Mediterranean outflow.

6.2 Observations

The observational data have been collected by a monitoring station in the Espartel sill (ES in fig. 6.1). The station was first deployed in September 2004 at the southern and main channel of the sill (35º51.7' N, 5º58.6'W), at 356 m depth and is still acquiring information. It was equipped with an up-looking 75 kHz Acoustic Doppler Current Profiler (ADCP) 20 m above the seafloor that provides 3-D velocity in 8-m thick bins every 30 minutes up to a depth above the Mediterranean-Atlantic interface layer, whose mean depth in Espartel is around 190 m (Sánchez-Román et al., 2009). Bellow the ADCP, at 10 m above the seafloor a Conductivity Temperature (CT) probe samples the conductivity and temperature of the Mediterranean water. The station is completed by a point wise current meter settled between the CT and the ADCP to measure the velocity in the shadow area of the ADCP allowing the full sampling of the Mediterranean vein velocity.

The Mediterranean outflow is computed from the velocity according to

$$Q_2(t) = \int_b^{h(t)} \langle u(z,t) \rangle W(z) dz \qquad (6.1)$$

where $\langle u(z,t) \rangle$ is the along-strait velocity, previously filtered to remove tidal and subinertial variability (periods lower than 21 days); *W(z)* is the channel width at depth *z* and *h(t)* is the time-dependent depth of the surface of zero low-passed velocity (interface). More details about this procedure can be found in García-Lafuente et al. (2002a) and Sánchez-Román et al. (2009).

6.3. Models and Simulations

6.3.1 NEMOMED8

General features

The NEMOMED8 model (Sevault et al., 2009; Beuvier et al., 2010) is a Mediterranean configuration of the NEMO ocean model (Madec, 2008), following the previous works done with OPAMED8 (Somot et al., 2006; Somot and Colin, 2008; Tsimplis et al., 2008, 2009), which is a regional configuration of the OPA ocean model (Madec et al., 1998).

The model grid covers the whole Mediterranean plus a buffer zone including a part of the Atlantic Ocean. The horizontal resolution is 1/8º x 1/8º cos(φ), with φ the latitude, equivalent to a range of 9 to 12 km from the north to the south of the Mediterranean domain. The NEMOMED8 grid is tilted and stretched at the Strait of Gibraltar in order to match the SW-NE axis of the real strait and to increase to 6 km the local resolution (two grid points in the narrowest section; Béranger et al., 2005; Drillet

et al., 2005). A time step of 20 minutes is applied. NEMOMED8 has 43 vertical Z levels, with an inhomogeneous distribution (from ΔZ=6 m at the surface to ΔZ=200 m at the bottom with 25 levels in the first 1000 m). The bathymetry is based on ETOPO 5'x5' database (Smith and Sandwell, 1997). A local cell parameterization is used, i.e., the local deepest level in the model has variable depth in order to fit the real bathymetry. The evolution of the sea surface is parameterized by a filtered free surface (Roullet and Madec, 2000). The horizontal eddy diffusivity is fixed to 125 m^2s^{-1} for the tracers (temperature, salinity) using a Laplacian operator and the horizontal viscosity coefficient is fixed to $-1.0 \cdot 10^{10}$ m^4s^{-2} for the dynamics (velocity) using bi-harmonic operator. A 1.5 turbulent closure scheme is used for the vertical eddy diffusivity (Blanke and Delecluse, 1993) with an enhancement of the vertical diffusivity coefficient up to 50 m^2s^{-1} in case of unstable stratification. A no-slip lateral boundary condition is used and the bottom friction is quadratic. The Total Variance Dissipation (TVD) scheme (Barnier at al., 2006) is used for the tracer advection. The solar radiation can penetrate into the ocean surface layer (Bozec et al., 2008).

Atmospheric forcing

ARPERA high resolution atmospheric data are used in the forced simulations for the air-sea fluxes. ARPERA is obtained by performing a dynamical downscaling of the ERA40 reanalysis (resolution 125 km) from the European Centre for Medium range Weather Forecast (ECMWF, Simmons and Gibson, 2000) up to 2001 and of the ECMWF analysis downgraded to the ERA40 resolution from 2002. It means that a break is possible in 2001 even if the RCM (Regional Circulation Model) ARPEGE is the same for the whole period. The downscaling method is described in Guldberg et al. (2005). The principle is to use a high resolution atmospheric model, here ARPEGE-Climate (resolution 50 km, Déqué and Piedelievre, 1995), in which small scales can develop freely and large scales are driven by the ECWMF reanalysis. The synoptic chronology then follows that of ECMWF while the high-resolution structures of the atmospheric flow are created by the model. All details can be found in Herrmann and Somot (2008), Tsimplis et al. (2009) and Beuvier et al. (2010).

Three of the NEMOMED8 simulations used in this study are forced by ARPERA daily mean fields of momentum, fresh water flux (evaporation minus precipitation) and net heat flux (mean sea level pressure is not used to force NEMOMED8). The latter is applied with relaxation term using the ERA-40 Sea Surface Temperature (SST). This term plays actually the role of a first order coupling between SST of the ocean model and the atmospheric heat flux, ensuring the consistency between those terms (Barnier et al., 1995). Following the CLIPPER Project Team (1999) the relaxation coefficient is -40 $Wm^{-2}K^{-1}$, equivalent to 8 days restoring time scale.

The last NEMOMED8 simulation is a coupled one. The ALADIN-Climate ARCM provides the net heat flux, wind stress, and water flux (evaporation minus precipitation), and receives the SST of NEMOMED8. The ARCM (Atmospheric Regional Circulation Model) grid has a 50 km resolution, and covers the whole catchment basin of the Mediterranean Sea and the Black Sea. A spectral nudging technique is used to follow the ECMWF ERAInterim reanalysis on the 1990-2008 period. The ALADIN-Climate (Aire Limitée Adaptation Dynamique INitialisation) ARCM version 5, the spectral nudging technique and the coupled model are described in Herrmann et al., 2011. The OASIS (Ocean Atmosphere Sea Ice Soil) coupler version 3 (Valcke, 2006) is used at a daily frequency.

River runoff and Black Sea inputs

No salinity damping is used at the surface and a freshwater flux due to rivers runoff is explicitly added to complete the water budget. In the three forced NEMOMED8 simulations, a monthly runoff is added at the main 33 river mouths of the Mediterranean, computed as a combination of the RivDis Database climatology (Vörösmarty et al, 1996) and the interannual variations coming from Ludwig et al. (2009).

The Black Sea, not included in NEMOMED8, is one of the major freshwater sources of the Mediterranean Sea. The exchanges between the Black Sea and the

Aegean subbasin consist in a two-layer flow across the Marmara Sea and the Turkish strait (Oguz and Sur, 1989). This exchange is replaced by a net freshwater flux diluting the salinity of the mouth grid point. Thus, the Black Sea is considered as a river for the Aegean. In the three forced simulations, monthly values are derived from Stanev et al. (2000) and Stanev and Peneva (2002). The rivers and Black Sea runoffs are the same as in Beuvier et al. (2010).

In the coupled system, the rivers and Black Sea runoffs are interactive. Except for the Nile which is kept as a climatological input, the ARCM sends the river runoffs of the Mediterranean and Black Sea basins to the TRIP model (Total Runoff Integration Pathways, Oki and Sud, 1998) in its 0.5° version (Decharme et al., 2010). Then the daily TRIP runoffs of all the river mouths of the Mediterranean are sent to the NEMOMED8 model. As for the Black Sea, the evaporation minus precipitation budget of the ARCM is added to the river runoffs of the catchment basin coming from the TRIP model, to form the runoff-equivalent input of fresh water at the Dardanelles mouth in the NEMOMED8 model.

Atlantic forcing

The exchange with the Atlantic Ocean is performed through a buffer zone. From 11ºW to 7.5ºW, 3D temperature and salinity of the model are relaxed towards T-S climatological fields. This relaxation is a Newtonian damping term in the tracer equation, equal to $-(X_{model} - X_{climatology})/\tau$. The restoring term is weak west of Cádiz and Gibraltar area (τ = 100 days at 7.5ºW) and stronger moving westward (τ = 3 days at 11ºW). The climatologies used in the buffer zone for the different simulations are summarized in table 1. When using anomalies, the monthly anomalies of the data computed on the data mean (1960-2006 for Daget et al. 2009, 1960-2008 for the NEMOVAR-COMBINE reanalysis, Balmaseda et al. 2010) are added to the Reynaud climatology (Reynaud et al. 1998). The reason why we use two different types of anomalies, which are not so different, is that the COMBINE reanalysis is a more recent and a longer one. In the coupled simulation, the COMBINE values are used.

Simulations

Four different simulations based in NEMOMED8 have been studied in this work. The first one (NM8-Long hereinafter) covers the period 1961-2010. In this simulation, as in the two other forced ones, the surface fresh water budget is balanced adding a monthly correction term designed as in Beuvier at al. (2010). To assure the model volume conservation, the net evaporation on the Mediterranean is added as precipitation in the Atlantic zone at each time step. The second simulation (NM8-Glorys hereinafter) uses the same forcing in the Atlantic, whereas the model volume is conserved through a damping of the Sea Surface Heigh (SSH) between 11ºW and 7.5ºW towards the monthly mean SSH of NM8-Long plus monthly anomalies. On the covered period, 2002 to 2008, the anomalies are taken from GLORYS-V1 (Ferry et al., 2010), a reanalysis of the global ocean circulation at 1/4º horizontal resolution available for this period. The third simulation (NM8-Combine hereinafter) uses anomalies coming from the COMBINE reanalysis in the Atlantic buffer zone both for the temperature and salinity damping, and the SSH relaxation. Apart from conserving the model volume, the SSH relaxation in the Atlantic buffer zone allows the model to represent correctly the SSH on the Mediterranean. It is very close in the two simulations with relaxation, even if the data used are a bit different. Indeed the GLORYS1V1 reanalysis uses the AVISO Sea Level Anomaly as an assimilated data, which is not the case for the COMBINE one.

THE NM8-long simulation begins in August 1960 after 15 years of spin-up, and the NM8-Glorys and NM8-Combine ones begin in August 2002 with the restart of NM8-long of the same date. In the coupled simulation the COMBINE values are used in the Atlantic conditions (no more in anomalies), and no SSH relaxation is performed. The simulation begins in Augusts 1989 after 25 years of spin-up.

6.3.2 NEMOMED12

General features

The development of NEMOMED12 (Lebeaupin Brossier et al. 2011, 2012; Beuvier et al. 2012) is the evolution of NEMOMED8. The horizontal grid is based on the ORCA grid of NEMO at 1/12º resolution. This corresponds in the Mediterranean area to a grid cell size between 6 and 8 km, from 46ºN to 30ºN. It has 50 vertical stretched levels (from ΔZ=1 m at the surface to ΔZ=450 m at the bottom with 35 levels in the first 1000 m). The bathymetry comes from the 10th MERCATOR-LEGOS bathymetry at resolution 30"x30", composed of merging between the GEBCO-0.8 database, the MEDIMAP bathymetry (Medimap Group, 2005) and the Ifremer bathymetry of the Gulf of Lions (Berné et al., 2004).

A time step of 12 minutes is used. The horizontal eddy diffusivity coefficient is set to 60 m^2s^{-1} for the tracers (temperature, salinity) using a Laplacian operator (the diffusion is applied along iso-neutral surfaces for the tracers) and the horizontal viscosity coefficient is set to -1.25×10^{10} m^4s^{-2} for the dynamics (velocity) using a biharmonic operator. TDV scheme is used for the tracer advection and the EEN (Energy and ENstrophy conservative) scheme is used for the momentum advection (Arakawa and Lamb, 1981; Barnier et al., 2006). A 1.5 turbulent closure scheme is used for the vertical eddy diffusivity (Blanke and Delecluse, 1993) with an enhancement of the vertical diffusivity coefficient up to 10 m^2s^{-1} in case of unstable stratification. The solar radiation can penetrate into the ocean surface layers (Bozec et al., 2008). A no-slip lateral boundary condition is used. The bottom friction is quadratic. The evolution of the sea surface is parameterized by a filtered free-surface (Roullet and Madec, 2000).

Atmospheric forcing, river runoff and Black Sea inputs

The atmospheric forcing, the river runoff and Black Sea inputs used in NEMOMED12 are almost the same than those used for NEMOMED8 and are described in sections 6.3.1. The only difference comes from the input of a coastal runoff to reach the surface freshwater budget given by the work of Ludwig et al. (2009).

Atlantic forcing

The exchanges with the Atlantic Ocean are performed through a buffer zone, as for NEMOMED8. In this case, 3D temperature and salinity of NEMOMED12 are relaxed towards the T-S climatological fields of Levitus et al. (2005). The restoring term is weak west of Cadiz and Gibraltar area (τ = 90 days at 7.5ºW) and increases westwards (τ = 2 days at 11ºW).

Simulation

In the simulation used in the study, NM12 hereinafter, the SSH dumping in the Atlantic buffer zone described in section 6.3.1 have been also included. The reference SSH has been built by adding the 2002-2008 mean SSH of reference simulation with monthly sea level anomalies. For the period 2002-2008, the anomalies are taken from GLORYS-1 (Ferry et al., 2010), a reanalysis of the global ocean circulation at a 1/4º horizontal resolution available for this period.

A difference between the NM8 and NM12 simulations is the initial state in the Mediterranean part of the domain: it is provided from the monthly potential temperature and salinity fields from the MEDATLAS-II climatology (MEDAR/MEDATLAS Group, 2002) corresponding to October. These fields are ponderated by a low pass filtering with a time-window of three years using the MEDATLAS data covering the

period 1997-1999. The NM12 simulation then starts with initial conditions close the Mediterranean Sea state of October 1998 and an ocean at rest.

Another particularity of NM12 is the use a different bottom friction scheme with respect to NEMOMED8. In this case the mean tidal energy have been included, computed from a tidal model (Lyard et al., 2006). The mean tidal energy is the highest in the Strait of Gibraltar (maximum value over 10000 cm^2s^{-2}) and has significant values mainly in the Channel of Sicily, in the Gulf of Gabes and in the northern Adriatic Sea.

6.3.3 NEMOMED36

General features

NEMOMED36 is the last product of the NEMOMED8 models hierarchy. The horizontal grid is based on the ORCA grid of NEMO at 1/36° resolution. This corresponds in the Mediterranean area to a grid cell size between 2 and 3 km, from North to South. The NM36 configuration used here has the same 50 vertical levels and the same bathymetry as NEMOMED12.

A time step of 4 minutes is used. The horizontal eddy diffusivity coefficient is set to 30 m^2s^{-1} for the tracers (temperature, salinity) using a Laplacian operator (the diffusion is applied along iso-neutral surfaces for the tracers) and the horizontal viscosity coefficient is set to $-1. \times 10^9$ m^4s^{-2} for the dynamics (velocity) using of a biharmonic operator. The other choices of schemes and parameterizations are the same as for NEMOMED12.

Atmospheric forcing, river runoff and Black Sea inputs

ECMWF analyses force NEMOMED36 in this simulation, from the 1st August 2003 to the 31st October 2007. The CLIO bulk formulation (Goosse et al. 2001) is used to compute the heat and water fluxes from the atmospheric variables of the ECMWF analyses. In addition, a Sea Surface Salinity (SSS) restoring is applied with a damping coefficient of -16.7 mm/day, towards the MEDATLAS-II monthly SSS climatology.

The river runoff and Black Sea inputs are the climatological values (with mean monthly cycles) of the values used for the NEMOMED12 simulation, i.e. including the coastal freshwater inputs.

Atlantic forcing

The exchanges with the Atlantic Ocean are performed through a buffer zone, as for NEMOMED12, with 3D temperature and salinity relaxations towards the climatological fields of Levitus et al. (2005). The restoring term is weak west of Cadiz and Gibraltar area (τ = 90 days at 7.5ºW) and increases westwards (τ = 2 days at 11ºW). In this simulation, we do not use a SSH damping in the Atlantic buffer zone. In order to keep constant the water volume of the whole model (Mediterranean Sea + Atlantic buffer zone), at each time-step, the water volume corresponding to the net evaporation averaged over the Mediterranean Sea was redistributed in the Atlantic area, between 11°W and 7.5°W, as an input of precipitation (as done in Tonani et al. 2008 or Beuvier et al. 2010).

Simulation

The NEMOMED36 simulation started on the 1st August 2003, with an ocean at rest and from the averaged August 2003 θ and S fields of a 1998-2008 companion NEMOMED12 simulation, also forced in bulk mode by the ECMWF analyses.

The characteristics of the different models and simulations are summarized in table 6.1.

	Resolution	Atmospheric forcing	T, S relaxation in the Atlantic buffer zone	ssh relaxation in the Atlantic buffer zone	Time period
NM8-long	1/8ºx1/8º grid tilted and stretched in Gibraltar (10 km and 6km around the Gib Strait)	ARPERA-V2	Climatology + anomalies of Daget	-	1961-2010
NM8-Glorys	-	ARPERA-V2	Climatology + anomalies of Daget	GLORYS1V1	2002-2008
NM8-Combine	-	ARPERA-V2	Climatology + anomalies of Combine Reanalysis	COMBINE anomalies	2002-2008
NM8-coupled	-	Coupled with ALADIN	Combine Reanalysis	-	1990-2008
NM12	1/12ºx1/12º (6-8km)	ARPERA-V2	Climatology from Levitus	GLORYS1V1	2002-2008
NM36	1/36ºx1/36º (2.5-2km)	ECMWF	Climatology from Levitus	GLORYS1V1	08/2003-10/2007

Table 6.1. Characteristics of the different simulations used in the study.

6.4. Validation

The validation process has been focused on two topics: the seasonality of the volume transport and the thermohaline characteristics of the outflowing waters. For the first one we have analyzed the inflow, outflow and net flow seasonal cycles, focusing on the outflow, for which direct measurements are available. The inflow and net flow have been compared with the indirect estimations of Soto-Navarro et al. (2010, SN10 hereinafter), based on a combination of reanalysis model and observed data. The transport has been computed across different sections for the model and for the observations, Tarifa and Espartel sections respectively (fig. 6.1). At seasonal time scale, the differences between these two sections due to entrainment are not higher than 3% (García-Lafuente et al., 2011), in any case smaller than the standard deviation of the monthly time series used in the comparison.

The validation of the θ-S characteristics have been performed analysing the model outputs at the model grid points closest to the Espartel station (Table 6.2). We have analysed both the water thermohaline properties and the fraction of LIW, WMDW and NACW composing the flow

	Longitude	**Latitude**	**Depth (m)**
ES	5º 58.6’ W	35º 57.1’ N	345
NM8	5º 56.22’ W	35º 51.1’ N	292
NM12	5º 56.04’ W	35º 54’ N	266
NM36	5º 59.58’ W	35º, 50’ N	318

Table 6. 2 Positions and depth of ES and the model grid points used in the validation.

6.4.1 Volume transport

The monthly mean time series of the outflow for the observations and simulations in their common periods (table 6.1) are represented in figure 6.2a. NM8 simulations show better agreement with the observations, particularly NM8-Long in the last two years 2008 and 2009. Table 6.3 also reflects this fact, with higher correlation for NM8 and lower for NM12 and NM36. In terms of mean values, NM8 and the observations almost coincide for the outflow and inflow (table 6.4) while in NM12 and NM36 both flows are underestimated. The mean net flow is very similar for all the simulations and close to SN10, as expected considering that most of the run are forced by ARPERA and the same river data.

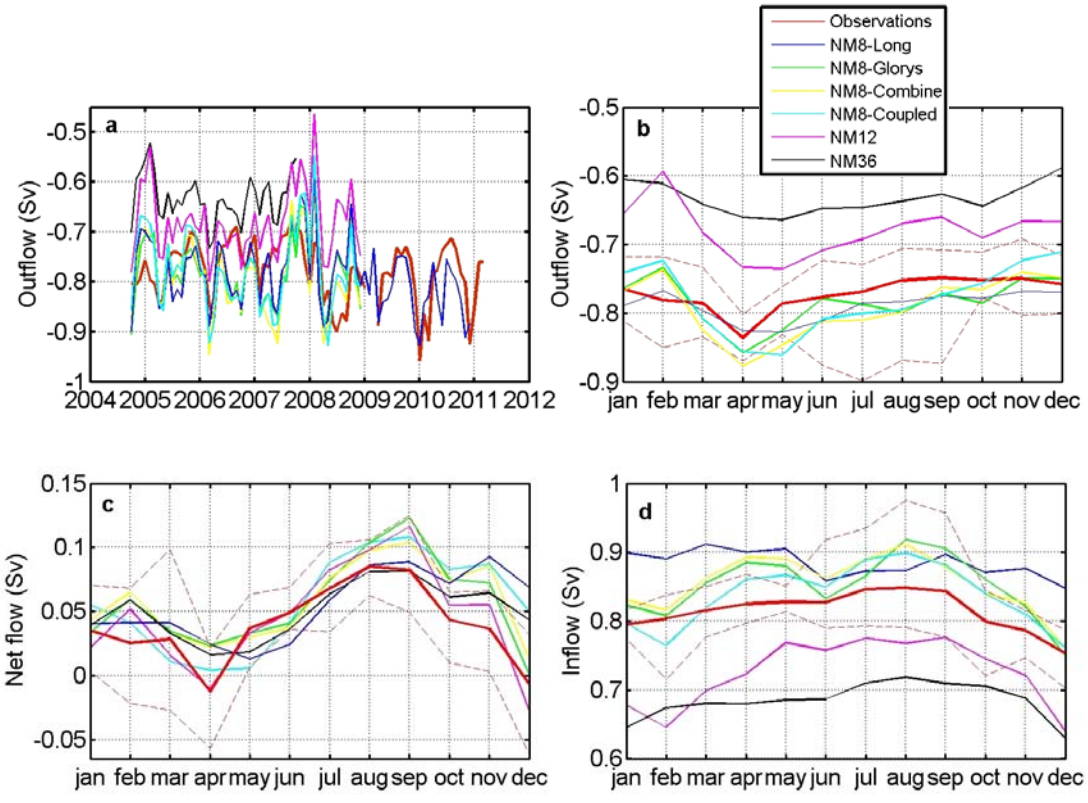

Figure 6.2 Monthly mean time series of the outflow for the observations and the different simulations. **b)** Monthly mean seasonal cycle of the outflow for the observations and the different simulations. **c)** Monthly mean seasonal cycle of the inflow for the observations and the different simulations. **d)** Monthly mean seasonal cycle of the net flow for the observations and the different simulations. In all figures solid lines represent: Observations (red), NM8-Long (blue), NM8-Glorys (green), NM8-Combine (yellow), NM8- Coupled (ligh blue), NM12 (magenta) and NM36 (black). The dashed lines correspond to the maximum and minimum values of every month for the observations. The observed inflow and net flow are those indirectly estimated by Soto-Navarro et al., (2010).

NM8-Long	NM8-Glorys	NM8-Combine	NM8-Coupled	NM12	NM36
0.40	0.34	0.43	0.41	0.28	0.32

Table 6.3 Correlation between the Mediterranean outflow observations and the different simulations in their common periods.

The outflow seasonal cycle is also better represented by NM8, especially by the simulations including SSH relaxation in the Atlantic buffer zone (Table 6.1, fig. 6.2b). All the NM8 simulations are included in the variability range of the observations and the different climatologies used to force the Atlantic buffer zone have little impact on the transport. The maximum in April, which is likely linked with the winter WMDW production in the Gulf of Lions (Sánchez-Román et al., 2009; Soto-Navarro et al., 2010), is very well captured by NM8-Glorys and NM8-Combine. On the other hand, all simulations overestimate the transport in spring and summer. For NM12 and NM36, apart from the biased mean value, the seasonality is quite similar to NM8-Long, with the spring maximum delayed one month with respect to the observed one.

	Obs.	NM8 Long	NM8 Glorys	NM8 Combine	NM8 Coupled	NM12	NM36
Outflow (Sv)	**-078±0.06**	-0.79±0.07	-0.78±0.07	-0.79±0.08	-0.78±0.08	-0.69±0.07	-0.63±0.04
Inflow (Sv)	0.81±0.05*	0.85±0.09	0.8±0.2	0.8±0.2	0.83±0.08	0.73±0.09	0.68±0.07
Net flow (Sv)	0.04±0.04*	0.05±0.02	0.06±0.09	0.06±0.09	0.05±0.04	0.05±0.06	0.05±0.06

Table 6.4 Mean inflow, outflow and net flow at Gibraltar for the observations and the different simulations. The values of the observed inflow and net flow, marked with an asterisk (*), are those indirectly obtained by Soto-Navarro et al. (2010).

The net flow seasonality reflects the net surface water flux (E-P-R-B) seasonal cycle (that is equal to the net flow for NM8-Long, blue line in fig. 6.2c), although some differences are achieved when the SSH variability in the Atlantic is considered (fig. 6.2c). In the simulations that include SSH relaxation in the Atlantic, the net flow is driven by its difference between the Atlantic and the Alboran Sea, while in those that do not include SSH, the net flow is the result of the artificial incorporation of the net evaporation over the Mediterranean basin as precipitation in the Atlantic. The first and

more realistic mechanism produces better results, with a more pronounced decrease in late autumn that agrees better with SN10. For instance, in the cycle of NM8-Combine (yellow line in figure 6.2c) the maximum in late summer and the minimum in April coincide with the results of SN10, while for NM8-Long (blue line in figure 6.2c) the maximum occurs in November and the minimum is shifted to May.

The maximum of the inflow cycle in the simulations and the SN10 estimation is strongly influenced by the net flow, and thus driven by the net surface flux (fig. 6.2d). For the simulations the summer maximum coincides in the cycle of both net flow and inflow, but in NM8, the inflow shows a secondary maximum in spring that is not appreciated in SN10 and may be a consequence of a velocity increase due to the outflow maximum in this season. Simulations including SSH variability show better agreement with the SN10 estimation while NM8-Long cycle is completely different. As for the outflow, the different forcing in the Atlantic buffer zone in NM8 does not have a noticeable effect in the inflow seasonality. In NM36 the cycle fits quite accurately the SN10 estimation while in NM12 the shape of the cycle is not so well reproduced.

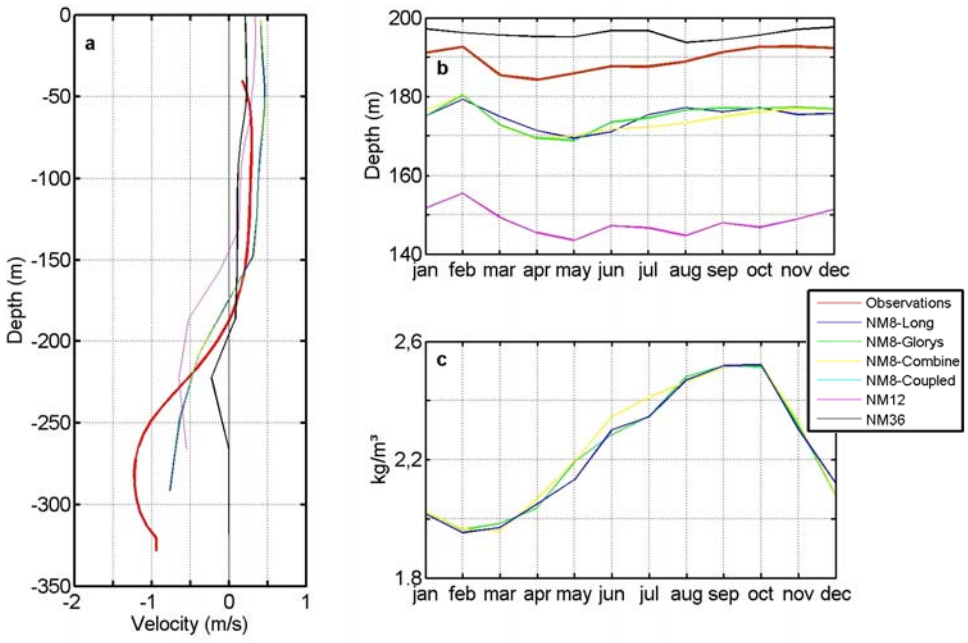

Figure 6.3 a) Mean velocity profile at ES for the observations and the different simulations. **b)** Mean seasonal cycle of the interface depth at ES for the observations and the different simulations. **c)** Mean seasonal cycle of the density difference between the Mediterranean and Atlantic layers for NM8-Long, NM8-Glorys and NM8-Combine. In all figures solid lines represent: Observations (red), NM8-Long (blue), NM8-Glorys (green), NM8-Combine (yellow), NM8- Coupled (ligh blue), NM12 (magenta) and NM36 (black).

The better results achieved by NM8 with respect to NM12 and NM36 can be the consequence of a better representation of the strait topography or of the physical processes controlling the exchange. These processes seem to be better resolved by the models with higher resolution, as we will show in the next sections, so the different geometry of the strait is thought to be responsible. The main difference between the grids of NM8 and NM12/36 in the Gibraltar area is that the former is tilted to follow the along strait axis. Other difference is the bathymetry: the cross section of NM8 at Tarifa, where the transport is computed, is 5% larger than the real one, while NM12 and NM36 deviations are 30% and 24% respectively. These two geometrical factors may play an important role in the simulation of the exchange, improving the results of NM8. On the other hand, the velocity profiles are more realistic for NM12 and NM36. As shown in figure 6.3a, the mean profile of NM8 at Espartel reaches its maximum at the bottom, this meaning that the bottom friction is not affecting the flow. Yet, in NM12 and NM36 the velocity is maximum at the center of the Mediterranean layer, and the profiles show the same shape than the observed one. In any case, all the simulations underestimate the velocity of the outflow.

As previously mentioned, the volume transport variability depends on two variables: the interface depth, h, and the flow velocity, u (eq. 6.1). The cycle of the interface depth is closely related to the net flow seasonality (compare figures 6.2c and 6.3b), and is well reproduced by NM8 and NM12 simulations, although the mean value is underestimated. This is probably due to the bathymetry of the models, whose lower levels at Espartel are 292 m and 266 m respectively, while the real depth of the sill is 356 m. Another factor affecting the interface variability is the volume of WMDW present in the adjacent basin, the Alboran Sea, which could contribute to the minimum depth in spring by raising the interface between the LIW and WMDW after the winter convection process in the Gulf of Lions, and then also raising the Mediterranean-Atlantic interface. The one month shift of the minimum in the model may be consequence of an underestimation of the deep water volume formed (Herrmann et al., 2011; Beuvier et al., 2012) that leads to a slower rising of the interface in the Alboran Sea.

Since the Mediterranean layer has a rather steady density, the seasonal cycle of $\Delta\rho$ follows the changes in the density of the Atlantic layer, which is mirrored by the sea

level seasonal cycle whose origin is the thermal expansion of the water column (steric effect). Figure 6.3c shows $\Delta\rho$ seasonal cycle for NM8 simulations at the Tarifa section, computed as the difference between the integrated density for the layers of negative and positive velocities. The maximum values in late summer coincide with the temperature seasonality (Cazenave et al., 2002; Criado-Aldeanueva et al., 2008) and give rise to a maximum in the inflow (fig. 6.2d). It is worth to mention that there are not important differences between simulations, even when different climatologies are used to force the Atlantic area.

6.4.2 Thermohaline characteristics of the outflow

In the θ-S diagram of figure 6.4a, the ES observations and the different simulations in their common period are represented. The NM8-Long, Glorys and Combine show similar values, with abnormally warm waters. One explanation to the bias could lie in the abnormally high temperature and salinity of the intermediate layer in the western basin that make LIW be warmer and saltier than in the observations (Beuvier et al., 2010). If we compare with NM8-Coupled simulation (light blue dots), where the warm anomaly in the intermediate layer is weaker, the properties of the outflow are closer to the observations. On the other hand, the similar properties of NM8-Glorys and Combine imply that the different θ-S characteristics of the AW in the buffer zone do not affect the outflow characteristics. In contrast, the outflow properties in NM36 and, particularly, in NM12 fit well the observations, this meaning that both the properties of the different water masses in the Mediterranean basin and their eventual proportion in the outflow composition are better represented.

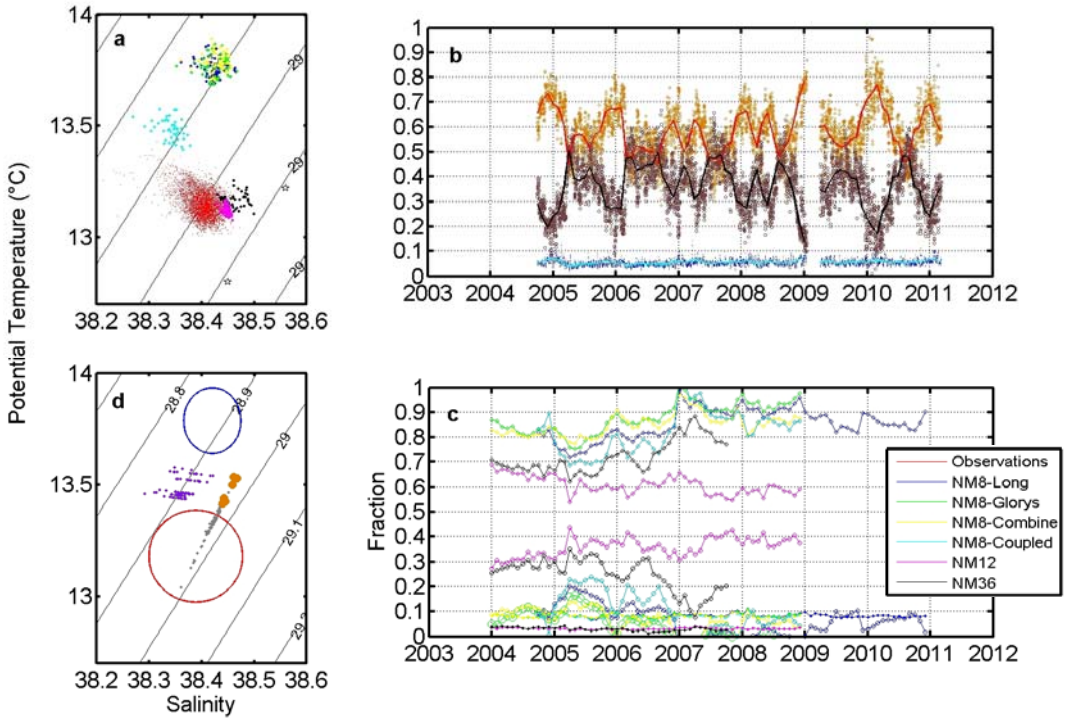

Figure 6.4 a) θ-S diagram of the outflowing waters for the observations and the different simulations. Colors correspond to: Observations (red), NM8-Long (blue), NM8-Glorys (green), NM8-Combine (yellow), NM8-Coupled (light blue), NM12 (magenta) and NM36 (black). Black stars are the reference points for the LIW and WMDW used in the decomposition and specified in table 6.5. The NACW point is out of the diagram. **b)** Fraction of LIW (orange diamonds), WMDW (brown circles) and NACW (blue points), present in the Mediterranean outflow measured at ES. Thick lines are the monthly means. **c)** Fraction of LIW (diamonds), WMDW (circles) and NACW (points) in the Mediterranean outflow for the different simulations. The colors represent the same as in a). **d)** Results of the water mass fraction tests for NM8-Long. Grey points are the θ-S values when the fraction of NACW is forced to be 0.05, purple points are the values when the WMDW fraction is forced to be 0.35 and orange points result when both conditions are imposed at the same time. The red circle indicates the position of the ES data and the blue one the original position of the NM8-Long points.

The other factor controlling the thermohaline characteristics of the outflow is the fraction of the different water masses that comprise it. Figures 6.4b,c show these fractions for observations and simulations respectively. The characteristics of the LIW and WMDW in the Alboran Sea, and those of the NACW in the Gulf of Cádiz, have been used as a reference for the estimations. For the observations, NM12 and NM36 the reference θ-S values have been retrieved from previous works based on oceanographic surveys (Parrilla et al., 1986; MEDAR Group, 2002), and are summarized in table 6.5 (the points for the reference values of the LIW and WMDW are represented by black stars in the θ-S diagram of fig. 6.4a). For the NM8 simulations, the θ-S pairs have been computed every year, using the corresponding to the maximum salinity of the spatially averaged vertical profile in the Alboran Sea for the LIW and to the minimum

temperature for the WMDW. For the NACW the mean values at 150 m depth in the Gulf of Cádiz have been used. This procedure aims to take into account the interannual to long-term variability of the salinity and temperature in NM8 for the intermediate and deep layers (Beuvier et al., 2010), redefining the water masses characteristics according to those of the simulations. Of course this should be considered as an approximation. The hydrological properties of the water masses are variable in time and space over the Strait area. This decomposition has been performed in order to compare the outflow composition of the models and the observations, and not to describe it with accuracy.

	Salinity	**Temperature (ºC)**
LIW	38.56	13.22
WMDW	38.45	12.8
NACW	36.2	15.0

Table 6.5 Thermohaline characteristics of the LIW, WMDW and NACW used as reference for the estimation of their respective fraction in the composition of the outflow.

The results show that the fraction of the WMDW is clearly underestimated in NM8, this making the outflow be almost completely composed by LIW and, thus, warmer, even when there is no temperature bias in the intermediate layer (simulation NM8-Coupled, light blue lines in fig. 6.4c). It is also important to notice that the fraction of NACW in these simulations is around 0.09, slightly higher than the 0.05 of the observations. Even though these values are close, the great difference between the properties of NACW and Mediterranean waters makes this discrepancy have an important effect in the θ-S characteristics of the resulting mixed waters that leave the Strait. For NM12 the outflow composition is very close to the observations and for NM36 there is a good agreement in the first two years but not from 2006 onwards.

The main driving force for the ventilation of WMDW is tides (Kinder and Bryden, 1990). Since they are not included in the models, the low fraction of WMDW, and hence the overestimation of the amount of LIW, is not unexpected, but there is a clear difference among the three models. In NM8 the proportion of the water masses is highly biased, although the recent years of large deep water formation, for instance

2005, 2006, 2009 and 2010 (López-Jurado et al., 2005; Schroeder et al., 2008; Loic Houpert, CEFREM, pers. comm.), are reflected in all simulations with an increase in the proportion WMDW (a mean value of 0.15 in 2005 in contrast with 0 in 2007 and 2009). For NM12 and NM36 the composition of the flow is much closer to the observations. The main reason for this difference is the depth at which the WMDW is found in the Alboran Sea for the different models. In fig. 6.5 the cross sections of temperature at 4ºW for the three models are represented. For NM8 the coldest waters are found deeper than 1000 m (fig. 6.5a), a depth that make them inaccessible to be suctioned over the sill. In contrast, for NM12 and NM36 (fig. 6.5b,c) the coldest waters can be found up to 600-700 m, from where they can be easier aspirated and incorporated to the outflow. Moreover, the higher resolution of NM12 and NM36 leads to a better representation of the mesoscale features in the adjacent basin that may affect the ventilation process. Naranjo et al. (2012) argue that the Western Alboran Gyre (WAG) helps to accumulate dense water in the eastern approach of the strait, which makes it available for its subsequent aspiration. Therefore, the ability of the higher resolution models to realistically resolve the WAG may have improved their capacity to reproduce the WMDW aspiration and hence its proportion in the outflow. However, this potentially interesting link is a hypothesis that requires further study to be proved.

To further investigate the influence of the fraction of each different water mass in the final θ-S properties of the outflow, three tests were performed for NM8-Long, imposing different conditions to the outflow composition while the characteristics of the water masses were kept constant (with the same values used in the decomposition)(fig. 6.4d). Grey points in fig. 6.4d are the resulting θ-S values when the fraction of NACW is forced to be 0.05, purple points are the values obtained when WMDW fraction is set to 0.35 and orange points result when both previous conditions are imposed at the same time (these values have been chosen following the results of the observations at ES, Fig. 6.4b). The red and blue circles represent the positions of the ES data and the original NM8-Long points, respectively. All tests imply significant changes, with the resulting mixed waters closer to the observations, although a good parameterization of the mixing with the NACW seems to be more important. Indeed, the great difference between the characteristics of the Atlantic and Mediterranean waters makes a small variation in their mixing ratio have a larger impact in the outflow properties.

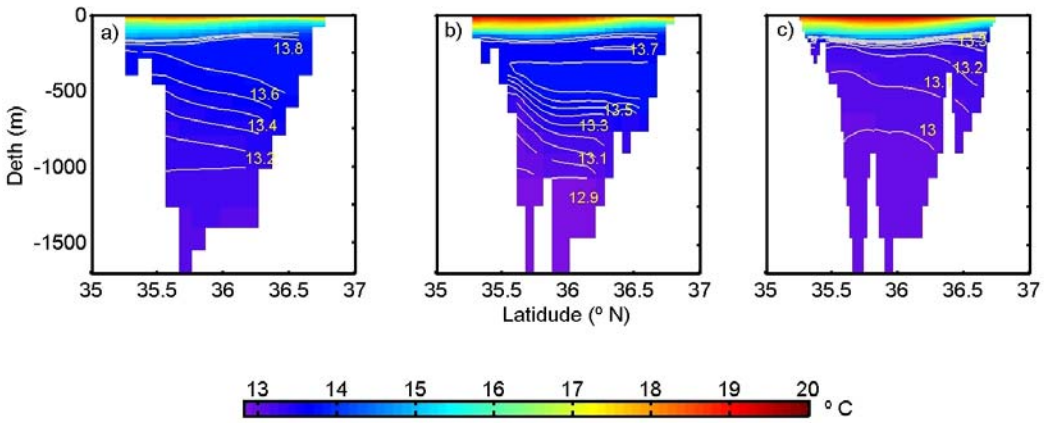

Figure 6.5 Temperature cross section at the Alboran Sea (4ºW) for NM8 (a), NM12 (b) and NM36 (c). Grey lines indicate isotherms

6.5. Interannual variability and trends

In order to study the interannual variability and the climatic trends of the exchange, annual mean time series from the 50 years long term simulation NM8-Long have been analysed (fig. 6.6). Inflow and outflow show slightly negative trends (in absolute value) of $(-0.7\pm0.5)\cdot10^{-3}$ Sv·year^{-1} and $(-0.8\pm0.6)\cdot10^{-3}$ Sv·year^{-1} respectively, and no significant trend is found for the net flow (table 6.6). In the recent-most years, where observations are available, the interannual evolution of the flows in the simulations fits reasonably well the observations and the SN10 estimation (figs. 6.6a-c). The main bias is for the net flow, although the year-to-year evolution is well represented. It should be noted that only the outflow is computed from direct measurements while inflow and net flow are reanalysis based estimations.

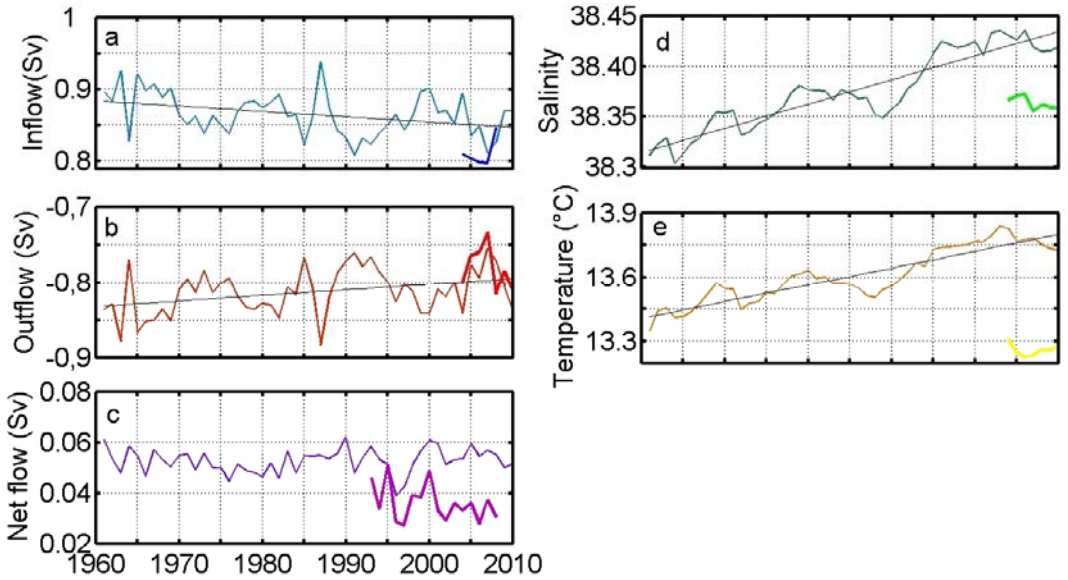

Figure 6.6. Annual mean time series of the variables characterizing the outflow in NM8-Long. **a)** Inflow (thick line correspond to the results of SN10), **b)** Outflow (thick line are the ES observations), **c)** Net flow (thick line are the results of SN10), **d)** Salinity at Espartel (thick line are the observations at ES), **e)** Potential temperature at Espartel (thick line are the observations at ES). Black lines are the least square fitted linear trends, which have only been represented when the fitting is statistically significant.

Figures 6.6d and 6.6e show that model salinity and temperature at the deeper level of Espartel (292 m) are higher than the observations in their common period, probably as a result of the intermediate layer bias in the simulations (Beuvier et al., 2010). They show trends of $(2.4\pm0.3)\cdot10^{-3}$ year^{-1} and $(8\pm1)\cdot10^{-3}$ ºC·year^{-1} respectively (table 6.6), which indicate a warming and salinification of the Western Mediterranean and/or Atlantic surface layer. The intermediate and deep layers of the western Mediterranean show positive trends around $4\cdot10^{-3}$ ºC· year^{-1} for temperature and $1.4\cdot10^{-3}$ year^{-1} for salinity, while in the Atlantic surface layer higher values of $(11\pm6)\cdot10^{-3}$ ºC· year^{-1} and $(20\pm1)\cdot10^{-3}$ year^{-1} are found. The trends found in the simulation at Espartel for the outflowing waters result from the combination of those found for the Mediterranean and the Atlantic. In spite of these results, no significant trends are found for the densities of the Mediterranean and Atlantic layers.

Inflow		$(-0.7\pm0.5)\cdot10^{-3}$ Sv·year^{-1}
Outflow		$(-0.8\pm0.6)\cdot10^{-3}$ Sv·year^{-1}
Net flow		n.s
T $_{Espartel}$		$(8\pm1)\cdot10^{-3}$ ºC·year^{-1}
S $_{Espartel}$		$(2.4\pm0.3)\cdot10^{-3}$ year^{-1}
T $_{W\ Mediterranean}$	0-150 m	$(9\pm4)\cdot10^{-3}$ ºC·year^{-1}
	150-600 m	$(4\pm1)\cdot10^{-3}$ ºC·year^{-1}
	600 m-bottom	$(4.3\pm0.2)\cdot10^{-3}$ ºC·year^{-1}
S $_{W\ Mediterranean}$	0-150 m	$(1.7\pm0.4)\cdot10^{-3}$ year^{-1}
	150-600 m	$(1.5\pm0.2)\cdot10^{-3}$ year^{-1}
	600 m-bottom	$(1.30\pm0.03)\cdot10^{-3}$ year^{-1}
T$_{Atlantic}$		$(20\pm1)\cdot10^{-3}$ ºC·year^{-1}
S$_{Atlantic}$		$(11\pm6)\cdot10^{-3}$ year^{-1}

Table 6.6 Least square fitted linear trends for the outflow parameters and for the salinity and temperature in different layers in the Western Mediterranean and in the suface layer of the Atlantic buffer zone. Letters n.s. means that the fitting is not significant. The 95% confidence intervals have been estimated with a *t*-student test.

6.6 Summary and conclusions

A set of simulations from NEMOMED8, NEMOMED12 and NEMOMED36 regional circulation models of the Mediterranean Sea have been compared with observations collected at the Espartel station in order to validate their representation of the exchange through the Strait of Gibraltar in terms of volume transport and thermohaline properties of the Mediterranean outflow.

NM8 show better results for the volume transport, with mean values very close to the observations for all the simulations and seasonal cycles varying within the range of the observed ones. Simulations including SSH relaxation in the Atlantic buffer zone show an improvement in the seasonality of the net flow, also reflected in the inflow. On

the other hand, the different climatologies used in the forcing of the Atlantic buffer zone do not have any relevant effect in the variability of the volume transport. NM12 and NM36 underestimate the inflow and outflow, although the seasonal cycles of the different flows are quite similar to NM8. The difference between the results of the three models is likely due to their different geometries in the strait, particularly in the values of the cross section where the transport is estimated. Other factors like the different forcing may also contribute.

The Mediterranean outflow waters are warmer and slightly saltier in NM8 due to three main causes: the first one is a too warm LIW, a bias that is not present in the coupled simulation. The second is the small fraction of WMDW in the flow due to the too deep pooling of this water mass in the Alboran Sea. Finally, a high percentage of NACW in the flow, which is almost double than in the observations and have a strong impact in the properties of the outflow due the large difference between the Atlantic and Mediterranean waters. In contrast, in NM12 and NM36 the outflow properties and its composition fits quite well the observations, which could be a consequence of their capacity to better resolve the processes involved in the exchange.

The analysis of the interannual variability of the exchanged flows for the long term simulation NM8-Long shows a good agreement with the observations and the estimations of SN10 in their common period. Salinity and temperature at ES show higher values than the observation and positive trend that are likely the effects of those found in the Mediterranean intermediate and deep layers and in the Atlantic waters comprising the outflow.

CONCLUSIONES

Conclusiones

1. Variabilidad estacional e interanual de los flujos de calor y agua dulce a través de la superficie en el mar Mediterráneo: balances e intercambio a través del estrecho de Gibraltar

El ciclo estacional del flujo de calor total es positivo (hacia el océano) entre marzo y septiembre, con su máximo en enero, y negativo el resto del año. Para la cuenca completa, en promedio anual, se ha obtenido un balance neto prácticamente neutro de 0.7 Wm^{-2}. El balance es positivo para la cuenca occidental (~12 Wm^{-2}) y negativo para la oriental (-6.4 wm^{-2}), debido a las grandes pérdidas de calor latente de este área (hasta 100 Wm^{-2}). La evaporación neta (E-P) tiene un ciclo estacional con un rango de variabilidad de 600 $mm \cdot año^{-1}$, alcanza su máximo en agosto-septiembre y su mínimo en mayo. El valor promedio para todo el periodo y para la cuenca completa del déficit de agua dulce es de 680±70 $mm \cdot año^{-1}$, aunque estas pérdidas son casi un 70% mayores en la cuenca oriental. Se ha encontrado una tendencia positiva para E-P en el periodo analizado (1948-2009) de 1.6±0.9 $mm \cdot y^{-2}$, consecuencia de un descenso de la precipitación.

A partir los valores climatológicos de la descarga de ríos y del intercambio neto con el mar Negro, se ha obtenido un valor del flujo neto a través del estrecho de Gibraltar de

G=0.035±0.005 Sv. Combinando este valor con el flujo medio de salida G_{out}=0.78±0.05 Sv obtenido a partir del registro de velocidades del ADCP instalado en la estación de Espartel, resulta un flujo medio de entrada de ($G_{in} = G + G_{out}$) 0.82 ± 0.05 Sv. Este resultado es un valor intermedio entre los pocos calculados previamente por otros autores, que al estar basado en una combinación de medidas experimentales de probada precisión y de una climatología que involucra a toda la cuenca, se considera bastante realista. En lugar de usar las ecuaciones de conservación de sal para la estimación del flujo de entrada, que introducen mucha incertidumbre en el cálculo, se ha empleado la estimación realizada para determinar el cociente entre las salinidades del flujo de entrada y de salida, S_{in}/S_{out} = 0.956, que puede emplearse para futuros cálculos de las componentes del intercambio cuando únicamente se disponga de uno de los flujos, ya sea mediante estimaciones climatológicas o medidas in situ.

Considerando el flujo de entrada obtenido, se calcula una advección de calor hacia el Mediterráneo a través del estrecho de Q_a = 3.2 ± 1.5 Wm^{-2}, un valor menor que los históricamente documentados pero que es probablemente más realista ya que las discrepancias son fruto de sobreestimaciones previas del flujo de entrada. Este valor de la advección, junto con la estimación del valor intercambiado con la atmósfera, implicaría un incremento del contenido neto de calor en el Mediterráneo durante las últimas décadas.

2. Influencia del forzamiento atmosférico a gran escala en los balances de calor y agua dulce del Mediterráneo: índices climáticos

Se han correlacionado series interanuales e interdecadales de precipitación, evaporación, déficit de agua dulce (E-P) y flujo neto de calor con los índices climáticos MO y NAO para investigar la influencia de estos patrones atmosféricos en los balances de calor y agua dulce del Mediterráneo. Ambos índices exhiben una importante variabilidad interanual e interdecadal, con periodos comunes de fases tanto positivas como negativas. Aunque el descenso en la precipitación promedio de la cuenca entre

mediados de los 60 y mediados de los 80 se corresponde claramente con un incremento en ambos índices, la variabilidad de E-P no muestra una correlación tan clara, debido a la diferente sensibilidad de E y P, que se traduce en correlaciones de signo opuesto en las cuencas occidental y oriental.

La efectividad de los índices NAO y MO es muy parecida para P y E-P, pero en el caso de los flujos de calor y la evaporación el índice MO parece ser un mejor indicador de la variabilidad interdecadal ya que desde mediados de los 70 a principios de los 90 ambos índices difieren significativamente. Debido a la persistencia y estabilidad del MO durante todo el año los valores anuales del índice son los que presentan en general una mejor correlación. En el caso del NAO, son los promedios invernales los que presentan la mejor correlación para todas las variables dada la mayor proximidad de su centro meridional al Mediterráneo en esta estación.

Puesto que la similitud de ambos índices se limita a los meses de otoño e invierno, es plausible considerar que el MO representa un patrón específico de circulación regional más que una extensión regional de la NAO, por lo que constituye un índice adecuado para la monitorización en el Mediterráneo de la variabilidad a largo término de los balances hídrico y, especialmente, de calor.

3. Estimación del flujo atlántico de entrada a través del estrecho de Gibraltar mediante datos climatológicos y experimentales

Se ha caracterizado la variabilidad estacional del flujo atlántico de entrada a través del estrecho de Gibraltar mediante la combinación de una estimación indirecta del flujo neto basada en el balance hidrológico del Mediterráneo, descrito mediante datos de reanálisis, satélite y modelos, con datos experimentales del flujo de salida medidos en la estación de Espartel en el periodo de octubre de 2004 a enero de 2009. La señal estacional del flujo neto, Q_0, depende del ciclo de E-P, que tiene un rango de 582±21

mm·año^{-1} y alcanza su máximo en agosto, y de la señal de la componente másica del nivel del mar, con un ciclo de amplitud 4.2 ±1.2 cm y máximo en noviembre. La descarga de ríos y el intercambio neto con el mar Negro se han incluido en el balance hídrico aunque su contribución es menor del 20%. Se obtiene un valor medio del flujo neto de 0.038±0.007 Sv, y un ciclo estacional con una amplitud anual de 0.042±0.018 Sv y máximo en septiembre.

A partir de los más de cuatro años de medidas experimentales se ha obtenido un valor promedio del flujo Mediterráneo de salida de -0.78±0.05 Sv, con una amplitud del ciclo anual de 0.027±0.015 Sv y semianual de 0.017±0.009 Sv y máximos en abril y septiembre respectivamente. Al sumar la serie de flujo neto, resulta un flujo atlántico promedio de 0.81±0.06 Sv, amplitud anual de 0.034±0.011 Sv con máximo en agosto y semianual de 0.022±0.014 con máximo en abril. La serie temporal, la más larga obtenida hasta el momento, presenta una alta variabilidad interanual, con una anomalía especialmente alta en el flujo de salida del año 2008 que puede haber sesgado parcialmente el cálculo del ciclo estacional. Se requerirán series temporales de mayor longitud para confirmar los resultados obtenidos.

La evolución temporal tanto de los flujos intercambiados como de la superficie interfacial de separación entre las capas atlántica y mediterránea sugieren un régimen de intercambio submáximo en el estrecho, reflejado en la fluctuación desfasada de las dos componentes de los flujos de entrada y salida. El forzamiento principal del flujo de entrada es la señal barotrópica del flujo neto, Q_0, que sigue el ciclo de E-P dando lugar al máximo a finales de verano. Un segundo mecanismo de forzamiento baroclino es la variación estacional de la gravedad reducida, $g' = g\,(\rho_2 - \rho_1)\,/\rho_0$, debida a los cambios en la densidad de la capa superficial que produce el ciclo estacional de intercambio de calor, cuyo máximo en septiembre contribuye al máximo del flujo atlántico.

4. Tendencias termohalinas recientes en las aguas atlánticas que fluyen hacia el interior del Mediterráneo

Mediante el análisis de 5077 perfiles Argo durante el periodo 01/2001-05/ 2010 se ha demostrado que las tendencias de salinidad (y en menor medida de temperatura) documentadas en el flujo atlántico de entrada a través del estrecho de Gibraltar se corresponden con una similar salinificación (calentamiento) en los primeros 600 m de las aguas atlánticas adyacentes al estrecho. La mayor tendencia en la salinidad se da en la capa superficial del área de la corriente de las Azores (0.04 año^{-1}), aunque también se han encontrado valores positivos al norte y al sur de esta área. Valores menores, también positivos, se encuentran en la capa correspondiente a la termoclina permanente (sobre 0.01 año^{-1}), que en cualquier caso exceden las estimaciones previas. Pero la mayor novedad de estos resultados es que, en contraste con otros estudios realizados en periodos anteriores, las tendencias calculadas son ahora consecuencia de cambios intrínsecos de las masas de agua, en lugar de ser el efecto de desplazamientos verticales de las isopicnas. Estos cambios en las propiedades de las masas de agua están probablemente ligados a un reciente incremento de la evaporación neta que afecta a la salinidad de las aguas superficiales y de la termoclina mediante procesos de advección y subducción.

5. Validación del transporte de volumen y las propiedades termohalinas del intercambio en el estrecho de Gibraltar en modelos regionales de circulación en el Mediterráneo

Se ha comparado un conjunto de simulaciones de los modelos regionales de circulación del Mediterráneo NEMOMED8, NEMOMED12 y NEMOMED36 con observaciones recogidas en la estación de Espartel con objeto de validar la representación que dichos modelos hacen del intercambio en el estrecho de Gibraltar en términos de transporte de volumen y de propiedades termohalinas del flujo Mediterráneo.

NEMOMED8 muestra mejores resultados para el transporte de volumen, con valores medios muy próximos a los experimentales para todas las simulaciones y ciclos estacionales comprendidos en el rango de los observados. Las simulaciones que incluyen un término de relajación de la altura del nivel del mar en la zona atlántica del dominio muestran mejores resultados en la representación de los ciclos estacionales del flujo neto y de entrada. Por otro lado, el uso de diferentes climatologías en el forzamiento de esta zona no tiene ningún efecto relevante en la variabilidad del transporte. NEMOMED12 y NEMOMED36 subestiman los flujos de entrada y salida, aunque los ciclos estacionales son similares a los obtenidos por NEMOMED8. La diferencia de resultados entre los tres modelos probablemente se deba a su diferente geometría en el estrecho, particularmente a los valores de la sección transversal donde se calcula el transporte, aunque otros factores como sus distintos forzamientos también pueden contribuir.

Las aguas del flujo mediterráneo de salida son más cálidas y ligeramente más salinas que las observadas en NEMOMED8 debido a tres causas principales: la primera es un LIW excesivamente cálida, una desviación que no se da en la simulación acoplada con el modelo atmosférico ALADIN. La segunda es el bajo porcentaje de WMDW presente en el flujo debido a que esta masa de agua se encuentra a profundidades demasiado grandes en el mar de Alborán como para ser incorporada al flujo. Finalmente, el alto porcentaje de NACW, que es casi el doble del observado, lo que tiene un fuerte impacto en las propiedades del flujo debido a la gran diferencia entre las aguas atlánticas y mediterráneas. En el caso de NEMOMED12 y NEMOMED36 tanto las propiedades termohalinas del flujo mediterráneo como su composición se ajustan bastante bien a las observaciones, lo que podría ser consecuencia de una mayor capacidad para resolver los procesos que influyen en el intercambio.

El análisis de la variabilidad interanual de los flujos intercambiados en la simulación de largo término NM8-Long (1961-2010) muestra un buen acuerdo entre ésta y las observaciones y estimaciones en su periodo común. Sin embargo, los valores de salinidad y temperatura en ES son mayores que los observados y presentan tendencias

positivas que probablemente son consecuencias de las encontradas en las capas intermedia y profunda del Mediterráneo así como en la superficial de la zona atlántica.

ANEXO

ANEXO:

Resumen de datos y metodología

A.1 Reanálisis

La mayoría de los datos climáticos empleados en el presente trabajo, especialmente en los capítulos 2 y 3, son datos de reanálisis del National Center for Enviromental Prediction/National Center for Atmospheric Research (NCEP/NCAR). Éstos se obtienen mediante la combinación de simulaciones numéricas con la asimilación de datos experimentales, y la base de datos resultante se extiende desde 1948 hasta la actualidad (Kalnay et al., 1996). Los datos asimilados provienen de distintas fuentes globales, integradas en la red GTS (Global Telecomunication System). El modelo atmosférico empleado en la asimilación tiene una resolución espectral T62 (equivalente a una resolución horizontal de aproximadamente 210 km), con 28 niveles verticales, cinco de ellos en la capa límite atmosférica. Tras la aplicación de diversos controles de calidad, los datos se analizan mediante un esquema de análisis variacional (3D-Var), y las distintas variables o productos obtenidos por este procedimiento se clasifican en función de la influencia que sobre ellos tienen los datos experimentales.

De esta extensa base de datos se han utilizado valores medios mensuales de diferentes variables: las componentes del flujo de calor en el Mediterráneo (onda corta,

onda larga, calor latente y calor sensible), la precipitación, la evaporación y el campo de presión a nivel del mar. Los datos se han tratado estadísticamente para calcular ciclos estacionales, variabilidad interanual y tendencias, tanto promedios para toda la cuenca como distribuciones espaciales. También se han utilizado para la estimación del flujo neto a través del estrecho de Gibraltar (capítulo 5).

Además de los datos de reanálisis, se han empleado datos de precipitación de la base de datos del CMAP (Climate Prediction Centre Merged Analysis of Precipitation), que proporciona una estimación de la precipitación media mensual, con una resolución espacial de 2.5º x 2.5º entre 1979 y 2009, basada en datos de estaciones de medida sobre tierra y en estimaciones por satélite sobre el mar.

En el estudio sobre índices climáticos desarrollado en el capítulo 3 se hace uso de series temporales de los índices NAO y MO. Para el primero se han utilizado los valores mensuales calculados por la National Oceanic and Atmospheric Administration (NOAA), basados en un análisis de las componentes principales rotadas de la presión atmosférica normalizada a 500 mb en el área del Atlántico Norte comprendida entre 20ºN y 90º N. En el caso del índice MO, se han tomado los coeficientes temporales del primer modo de la descomposición en componentes principales de la presión atmosférica normalizada a nivel del mar para el área comprendida entre los 30ºW-40ºE en longitud y los 30ºN-60ºN en latitud. Los valores de presión atmosférica empleados han sido los datos de reanálisis de NCEP/NCAR descritos previamente.

A.2 Datos de satélite

Los datos de nivel del mar provienen del Archiving Validation and Interpretation of Satelite Oceanographic Data (AVISO), y son un compendio de datos de altimetría de diversas misiones (TOPEX/POSEIDON, ERS-1/2, GFO, ENVISAT y JASON 1), que los hace muy fiables. Consisten en anomalías de nivel del mar en el periodo entre octubre de 1992 y febrero de 2009, con una resolución espacial de 1/8ºx1/8º y resolución temporal semanal. Los datos están corregidos teniendo en cuenta todas las fuentes de error geofísicas y ambientales, resumidas en AVISO (1996). Entre éstas está

la de barómetro invertido, que corrige el efecto de la presión atmosférica sobre el nivel del mar. La validez de esta corrección en cuencas semicerradas es discutible, ya que la respuesta del nivel del mar está fuertemente influenciada por las restricciones topográficas del flujo en los estrechos; no obstante, esta influencia es importante en periodos menores de 200-300 días (Le Traon and Gauzelin, 1997) por lo que el barómetro invertido es aplicable en este estudio, que se centra en variabilidad interanual y tendencia sobre periodos mayores.

Además de la anomalía total del nivel del mar, se ha realizado una estimación de la componente estérica, mediante la ecuación:

$$\xi_S = -\frac{1}{\rho_0}\int_{-H}^{0} \left.\frac{\partial\rho(S,T,P)}{\partial T}\right|_{T,P=cte} \cdot T'(z)dz + \frac{1}{\rho_0}\int_{-H}^{0} \left.\frac{\partial\rho(S,T,P)}{\partial S}\right|_{S,P=cte} \cdot S'(z)dz \quad \text{(A.1)}$$

donde *T'(z)* y *S'(z)* son las anomalías de temperatura y salinidad referidas a su valor medio climatológico, ρ_0 es la densidad de referencia y *H* la profundidad. Se han utilizado perfiles de salinidad y temperatura del modelo ECCO (Estimating the Circulation and Climate of the Ocean) del Jet Propulsion Laboratory (JPL) de la NASA para esta estimación. En este caso se han utilizado los datos de simulación, sin reanálisis, para no introducir información a priori sobre lo que se desea obtener. Son datos con una resolución espacial de 1ºx1º, con 46 niveles de profundidad en intervalos de 10 metros en los primeros 150, que luego van aumentando, y una resolución temporal de diez días. El modelo usa como forzamiento los datos de reanálisis de NCEP/COADS (Comprehensive Ocean-Atmosphere Datasets).

También se han empleado datos de SST, concretamente imágenes infrarrojas de alta resolución (4km x 4km) del Advanced Very High Resolution Radiometer (AVHRR) de la misión pathfinder v5 de la NASA tomadas por diversos satélites. Se han analizado valores medios mensuales entre 1985 y 2007.

A.3 Perfiladores Argo

En el capítulo 5 se hace uso de perfiles de salinidad y temperatura de la red Argo en una pequeña parcela del Atlántico nororiental. Este sistema de observación consiste en un conjunto de boyas perfiladoras sumergibles repartidas por todo el océano. Cada uno de estos perfiladores deriva a una profundidad de 1000 m. Cada diez días desciende hasta los 2000 m de profundidad para, a continuación, iniciar el ascenso a la superficie, midiendo en su camino de subida los campos que permiten determinar el estado físico del océano, principalmente temperatura, salinidad y presión. Los datos son enviados por satélite desde la superficie, disponiéndose en tiempo real de las estructuras de temperatura y salinidad de las capas superiores e intermedias de los océanos que permiten obtener una imagen del estado del océano cada diez días (fig. A.1).

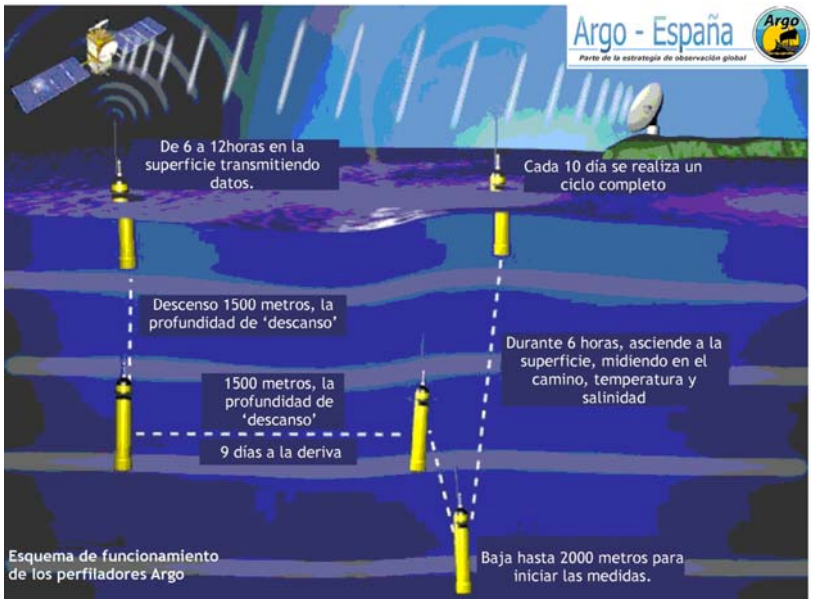

Figura A.1 Esquema del ciclo de funcionamiento de los perfiladores Argo (tomada de www.oceanografia.es/argo)

Los datos de los perfiladores son posteriormente sometidos a diversos controles de calidad para garantizar en la medida de lo posible su precisión. Considerando que un perfilador autónomo que deriva libremente por el océano puede ser objeto de múltiples

percances que afecten a su funcionamiento, es muy importante llevar a cabo un exhaustivo procesado de los datos para evitar errores derivados de un mal funcionamiento de los instrumentos. Una primera etapa de este procesado se realiza automáticamente cuando los datos son transferidos por el perfilador a los distintos servidores que conforman la red, dando lugar a los denominados "real-time data" (datos en tiempo real). Simultáneamente, los datos son enviados a grupos de investigación donde se les aplican controles más profundos, dando lugar a los denominados "delayed mode data" o datos en modo retrasado, ya que éstos son reenviados a los servidores entre seis y doce meses después de ser medidos.

En función de los resultados de los distintos controles a los que han sido sometidos, los datos son marcados con diferentes "banderas" que indican la calidad de los mismos, así como los diferentes controles realizados (un resumen actualizado puede consultarse en el Argo Users Manual, 2012, disponible en www.argodatamgt.org). Los datos utilizados en este trabajo han sido seleccionados de entre los considerados de "buena calidad" en la base de datos en tiempo real. Posteriormente, han sido reprocesados, interpolados e integrados verticalmente para poder construir las series temporales que se analizan en el capítulo 5.

A.4 Observaciones en el estrecho de Gibraltar

Muchos de los resultados del presente trabajo se apoyan en las medidas experimentales del flujo de salida mediterráneo de la estación permanente de Espartel. Ésta fue fondeada en septiembre de 2004, en el canal meridional del umbral de Espartel (35º51.7'N, 5º58.6' W), a 356 m de profundidad, en el marco de los proyectos INGRES (Intercambios en el Estrecho de Gibraltar y su respuesta a forzamientos meteorológicos y climáticos), y desde entonces ha estado midiendo las características del flujo mediterráneo.

En la figura A.2 puede verse un esquema con las características de la línea que conforma la estación. Su elemento principal es un perfilador acústico por efecto Doppler (ADCP) de 75 kHz, que mide las tres componentes de la velocidad a lo largo

de la columna de agua. Está instalado en una boya a 20 m del fondo, mirando hacia arriba, y mide la velocidad cada 30 minutos en celdas de 8 m de espesor, hasta una profundidad por encima de la interfase entre las capas atlántica y mediterránea, que en Espartel es de unos 190 m (Sánchez-Román et al., 2009), lo que permite registrar la velocidad de la vena mediterránea de salida. Por debajo del ADCP, a unos 10 m sobre el fondo, hay colocada una sonda de conductividad y temperatura (CT), que permite muestrear las características termohalinas del agua mediterránea. La línea se completa con un correntímetro puntual que permite medir la velocidad del flujo de salida en la zona de sombra del ADCP, es decir, entre la boya y el fondo.

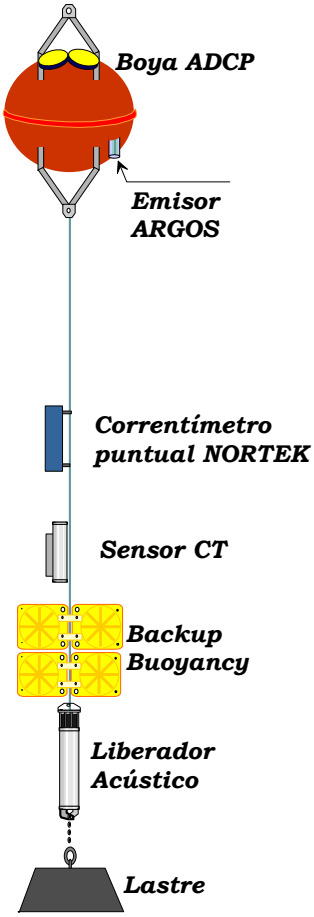

Figura A.2 Esquema de la estación de medida de Espartel

A partir del registro del ADCP el flujo de agua mediterránea que abandona el estrecho es calculado integrando el producto de la velocidad por la sección como:

$$Q_2(t) = \int_b^{h(t)} \langle u(z,t) \rangle W(z) dz \qquad \text{(A.2)}$$

donde $\langle u(z,t) \rangle$ es la componente de la velocidad a lo largo del eje del estrecho, *W(z)* la sección transversal del canal y *h(t)* la profundidad de la interfase entre las capas atlántica y mediterránea, calculada por interpolación como la superficie de velocidad cero. Dos son los principales inconvenientes de este procedimiento: por un lado, considerar una medida puntual de la velocidad en el centro del canal como representativa de toda la sección da lugar a una sobreestimación del transporte, ya que no se tienen en cuenta las pérdidas de velocidad por fricción en las paredes del mismo. Por otro lado, el transporte se calcula para el canal principal, es decir, el meridional, y no se considera la parte de la vena mediterránea que fluye por la zona septentrional, al norte del Banco de Majuán (MB en la fig. 1.5). Sánchez-Román et al. (2009) llevaron a cabo un estudio complementario usando una versión mejorada del modelo numérico CEPOM, desarrollado por la Unidad de Modelado Oceánico del ENEA (Agenzia Nazionale per le nuove tecnologie, l'energia e lo sviluppo economico sostenibile, Italia) y concluyeron que el flujo se sobreestima en un 22% al despreciar la fricción con las paredes del canal, mientras que se subestima en un 18% al despreciarse la aportación del canal norte. Ambas correcciones son aplicadas en la estimación del flujo de la ecuación (A.2).

Como se indicó en el capítulo 1, existen varias escalas de variabilidad temporal en el flujo, consecuencia de los distintos forzamientos de éste. Como puede observarse en la fig. A.3a, la mayor variabilidad temporal en el registro de velocidad se da en el rango mareal. Si se pretende estudiar fenómenos cuya escala temporal es de baja frecuencia, como es el caso de la variabilidad estacional o interanual, la serie de velocidad ha de filtrarse para eliminar las frecuencias mayores. En la fig. A.3b se representa la velocidad a baja frecuencia, obtenida aplicando un filtro de paso-baja para eliminar variabilidad con periodos menores de 21 días, correspondiente a las componentes mareal y subinercial del flujo. En ella se aprecia muy claramente la estructura bicapa del intercambio, y la interfase entre la capa atlántica y la mediterránea. Esta serie es la que posteriormente se ha empleado, promediada mensualmente, para la estimación del flujo atlántico de entrada descrita en el capítulo 5.

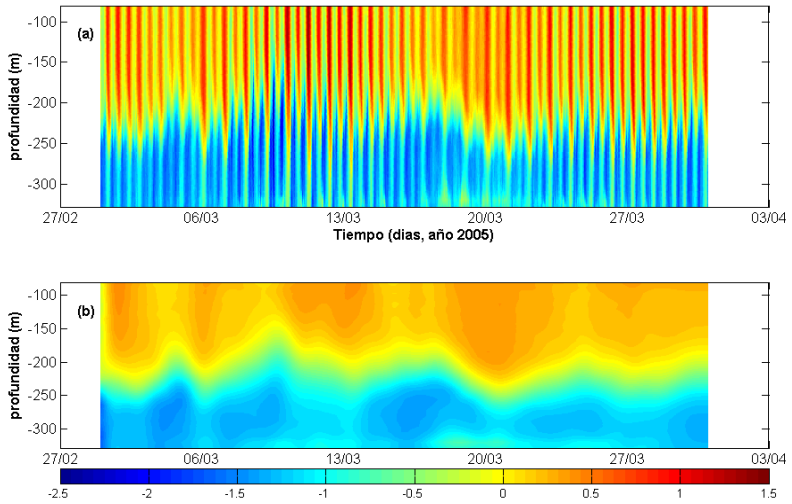

Figura A.3 Ejemplo de las series temporales del registro de velocidad del ADCP en la estación de Espartel. La escala de color tiene unidades de m/s **a)** Serie original. **b)** Serie de baja frecuencia, obtenida mediante la aplicación de un filtro paso-baja con frecuencia de corte de $5.5 \cdot 10^{-7}$ ciclos/s (periodos menores de 21 días)

Como complemento al registro de velocidades, las medidas de salinidad y temperatura del sensor CT de la estación proporcionan una información muy valiosa, ya que permiten caracterizar las aguas mediterráneas que abandonan el estrecho. Estas características dependen de las propiedades de las distintas masas de agua que componen el flujo, que a su vez, dependen de la circulación y el forzamiento sobre toda la cuenca. Las observaciones de la estación permiten, además de conocer las propiedades termohalinas de las aguas que abandonan el estrecho, como se ejemplifica en el diagrama T-S de la fig. A.4a, hacer una estimación de las fracciones de las distintas masas de agua que componen el flujo mediterráneo de salida (fig. A.4b). Como se explicó en el capítulo 1, el flujo mediterráneo está compuesto principalmente por LIW, en menor medida por WMDW y posee algunas trazas de NACW que se incorpora a éste por difusión. Ahora bien, la proporción de cada una de estas masas de agua no es constante, sino que varía respondiendo a los distintos forzamientos del intercambio. A escala estacional e interanual esta variabilidad depende principalmente del forzamiento

climático de la cuenca, lo que pone de manifiesto la interrelación entre la evolución del Mediterráneo y la del intercambio en Gibraltar (García-Lafuente et al., 2007, 2009).

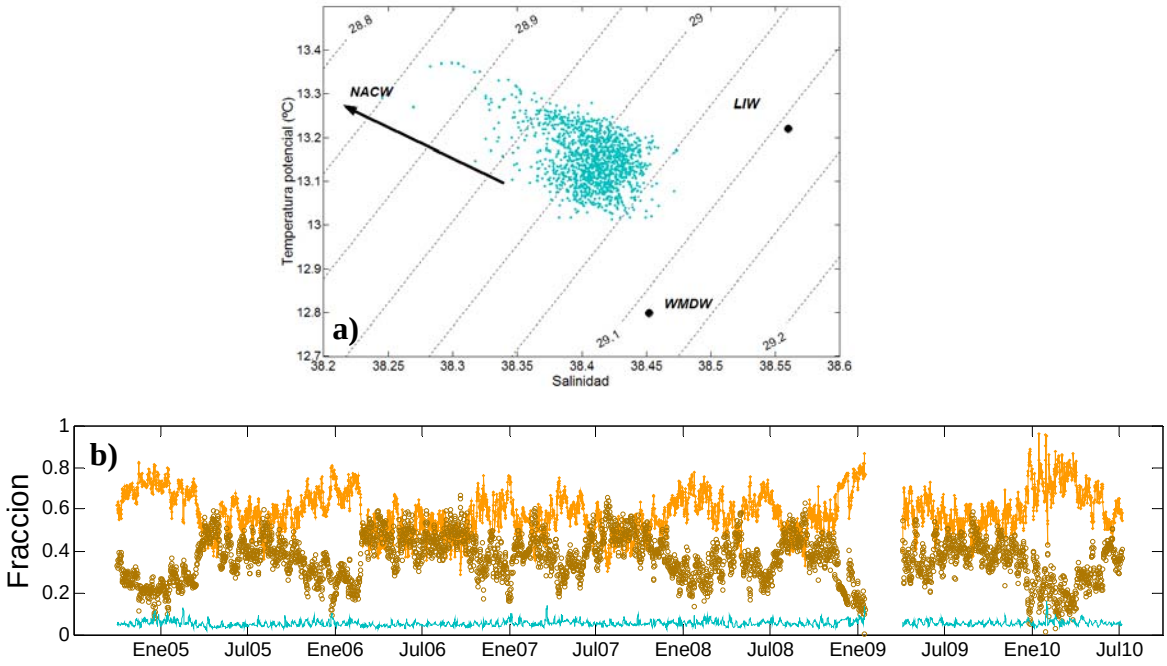

Figura A.4 a) Diagrama T-S de las observaciones de la estación de Espartel entre septiembre de 2004 y julio de 2010. **b)** Estimación de las fracciones de LIW (naranja), WMDW (marrón) y NACW (azul) presentes en el flujo de salida mediterráneo. Las propiedades (T,S) de las masas de agua tomadas como referencia para la estimación, y marcadas con puntos negros en el diagrama T-S son: LIW (13.22 ºC, 38.56), WMDW (12.8 ºC, 38.45) y NACW (15 ºC, 36.2).

A.5 Modelos numéricos

En el capítulo 6 se lleva a cabo un análisis de validación de varias simulaciones numéricas realizadas con los modelos NEMOMED8, NEMOMED12 y NEMOMED36, desarrollados por el Grupo de Modelización de Gran Escala y Clima (GMGEC), del Centro Nacional de Investigaciones Meteorológicas (CNRM, Meteo-France) en Toulouse (Francia). Todos están basados en el modelo de circulación oceánica NEMO, implementado en el Mediterráneo y están ideados para la simulación a escala climática. La mayoría de las simulaciones analizadas cubre el periodo 2002-2008, que coincide con las series de tiempo utilizadas para su validación: las medidas de la estación de

Espartel. También se ha estudiado la variabilidad interanual y las tendencias de una simulación de largo periodo, de 1961 a 2010, para el NEMOMED8.

La diferencia fundamental entre los tres modelos es la resolución: 1/8ºx1/8º para NEMOMED8, 1/12ºx1/2º para NEMOMED12y 1/36ºx1/36º para NEMOMED36. También difieren en las características de sus mallas, en el forzamiento que utilizan y algunas parametrizaciones. Además, se ha hecho un análisis de sensibilidad a las condiciones impuestas en la zona atlántica del dominio para NEMOMED8, con tres simulaciones que utilizan diferentes climatologías en esta área. Una descripción pormenorizada de los modelos y las simulaciones puede consultarse en el capítulo 6.

En el cuadro A.1 se resume de forma esquemática la información de este anexo.

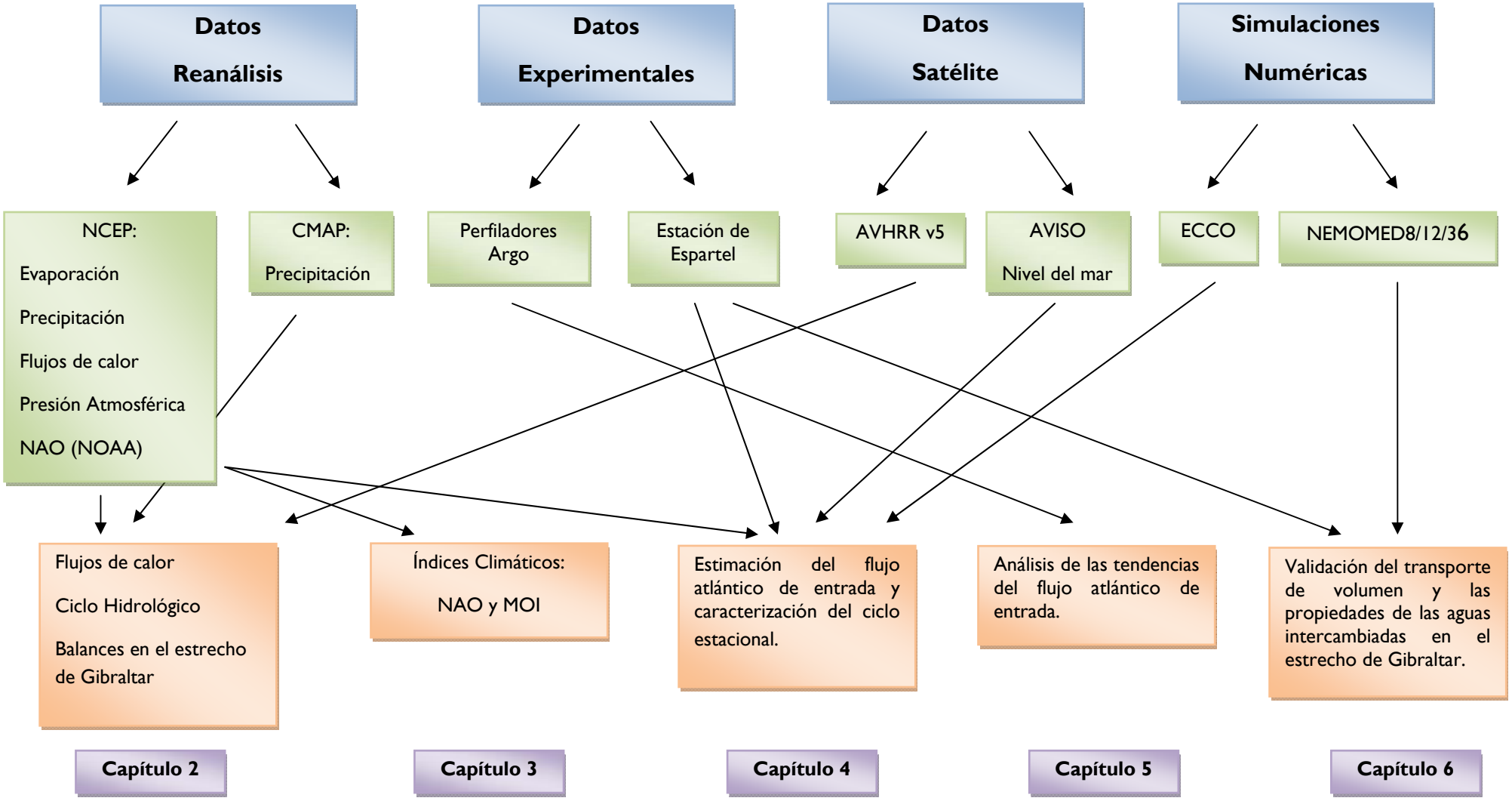

Cuadro A.1. Esquema resumen de los datos empleados en los diferentes capítulos.

REFERENCIAS

Referencias

Ambar, I., Serra, N., Brogueira, M. J., Cabeçadas, G., Abrantes, F., Freotas, P., Gonçalves, C. and Gonzalez, N. (2002). Physical, chemical and sedimentological aspects of the Mediterranean outflow off Iberia. *Deep Sea Res. Part II*. 49, 4163-4177.

Angelucci, M. G., N. Pinardi, and S. Castellari, (1998). Air–sea fluxes from operational analyses fields: Intercomparison between ECMWF and NCEP analyses over the Mediterranean area. *Phys. Chem. Earth*, 23, 569–574.

Arakawa, A., and V. R. Lamb (1981), A Potential Energy and Enstrophy Conserving Scheme for the Shallow Water Equations, *Mon. Weather Rev.*, 109, 18–36.

Arbic, B. K., and Owens, W. B. (2001), Climatic warming of the Atlantic intermediate waters. *J. Climate.* 14, 4091-4108.

Armi, L. and Farmer, D. M. (1986), Maximal two layer exchange through a contraction with barotropic flow, *J. Fluid. Mech.*, 164, 27-51.

Astraldi, M., Balopoulos, S., Candela, J., Font, J., Gacic, M., Gasparini, G. P., Manca, B., Theocharis, A. and Tintore, J. (1999). The role of straits and channels in understanding the characteristics of Mediterranean circulation. *Prog. Oceanog.,* 44(1-3), *65*-108.

Astraldi M., F. Conversano, G. Civitarese, G. P. Gasparini, M. Ribera D'Alcalà, and A. Vetrano., (2002). Water mass properties and chemical signature in the central Mediterranean region. *J. Marine Syst.*, 33-34: 155-177.

AVISO, (1996). AVISO user handbook: merged TOPEX/POSEIDON products. 201 pp. Available at www.aviso.oceanobs.com/donnees/tools/hdbk._gdrm.pdf.

Balmaseda A. M., K. Mogensen, F. Molteni and A. Weaver, (2010). The NEMOVAR-COMBINE ocean re-analysis. COMBINE Technical Report No. 1. http://www.combine-project.eu/Technical-Reports.1668.0.html

Barnier, B., L. Siefridt, and P. Marchesiello (1995), Thermal forcing for a global ocean circulation model using a three-year climatology of ECMWF analyses. *J. Marine Syst.*, 6, 363–380.

Barnier, B., et al. (2006), Impact of partial steps and momentum advection schemes in a global ocean circulation model at eddy-permitting resolution. *Ocean Dyn.*, 56, 543–567.

Barnston, A.G. and Livezey, R.E., (1987). Classification, seasonality and persistence of low-frequency atmospheric circulation patterns. *Mon. Weather Rev*. 115, 1083-1126.

Baschek, B., Send, U., Lafuente, J.G., and Candela, J., (2001). Transport estimates in the Strait of Gibraltar with a tidal inverse model. *J. Geophys. Res.* 106 (C12), 31033-31044.

Benitez-Barrios, V.M., Hernández-Guerra, A., Vélez-Belchí, P., Machín, F. & Fraile-Nuez, E. (2008), Recent changes in the subsurface temperature and salinity in the Canary region. *Geophys. Res. Lett.* 35, L07603.

Béranger, K., L. Mortier, and M. Crépon (2005), Seasonal variability of water transport through the Straits of Gibraltar, Sicily and Corsica, derived from a high-resolution model of the Mediterranean circulation, *Prog. Oceanogr.*, 66, 341–364.

Berné, S., D. Carré, B. Loubrieu, J.-P. Mazé, L. Morvan, and A. Normand (2004), Le golfe du Lion - Carte morpho-bathymtrique, Ifremer/Conseil Rgional du Languedoc-Roussillon Edition.

Besiktepe, S. T., Sur, H. I., Ozsoy, E., Latif, M.A., Oguz, T. and Unluata, U., (1994). The circulation and hydrography of the Marmara Sea. *Prog. Oceanogr*, 34 (4), 285-334.

Bethoux, J. P., (1979). Budgets of the Mediteranean Sea: Their dependence on the Global Climate and on the characteristics of the Atlantic Waters. *Oceanol acta*, (2), 105-119.

Bethoux, J. P. and Gentilli, B. (1996). The Mediterranean Sea, coastal and deep-sea signatures of climatic and environmental changes. *J. Mar. Sys.,* 1, 383-394.

Bethoux, J.P. and Gentilli B., (1999), Functioning of the Mediterranean Sea: Past and Present Changes relaled to freshwater input and climatic changes. *J. Mar. Syst.* 20, 33-47.

Bethoux, J. P., Gentilli, B., and Tailliez, D. (1998). Warming and freshwater budget change in the Mediterranean since the 1940s, their possible relation to the greenhouse effect. *Geophys. Res. Let.,* 25, 1023-1026.

Bethoux, J. P., Gentilli, B., Morin, P., Nicolas, E., Pierre, C. & Ruiz-Pino, D. (1999), The Mediterranean Sea: a miniature ocean for climatic and environmental studies and a key for the climatic functioning of the North Atlantic. *Prog. Oceanogr*. 44, 131-146.

Beuvier, J., F. Sevault, M. Herrmann, H. Kontoyiannis, W. Ludwig, M. Rixen, E. Stanev, K. Béranger, and S. Somot (2010), Modeling the Mediterranean Sea interannual variability during 1961-2000: Focus on the Eastern Mediterranean Transient. *J. Geophys. Res.*, 115 (C08017), doi:10.1029/2009JC005950.

Beuvier J., Béranger K., Lebeaupin-Brossier C., Somot S., Sevault F., Drillet Y., Bourdallé-Badie R., Ferry N. and Lyard F. (2012) Spreading of the Western Mediterranean Deep Water after winter 2005: time scales and deep cyclone transport. *J. Geophys. Res.-Oceans.* doi:10.1029/2011JC007679

Bignami, F., Marullo, S., Santoleri, R. and Schiano, M. E. (1995). Longwave radiation budget in the Mediterranean Sea. *J. Geophys. Res.*, 100(C2), 2501-2504.

Bindoff, N. L. and McDougall, T. J. (1994), Diagnosing climate change and ocean ventilation using hydrographic data, *J. Phys. Oceanogr.*, 24, 1137–1152.

Blanke, B., and P. Delecluse (1993), Low frequency variability of the tropical Atlantic Ocean simulated by a general circulation model with mixed layer physics, *J. Phys. Oceanogr.*, 23, 1363–1388.

Bormans, M., C. Garrett, and K. R. Thompson (1986), Seasonal variability of the surface inflow through the Strait of Gibraltar, *Oceanol. Acta*, 9, 403–414.

Boscolo, R. and Bryden, H. L. (2001). Causes of long-term changes in Aegean Sea deep water. *Oceanol. Acta,* 24, 519-527.

Boukthir, M., and B. Barnier, (2000). Seasonal and inter-annual variations in the surface freshwater flux in the Mediterranean Sea from the ECMWF re-analysis project. *J. Mar. Syst.*, (24), 343–354.

Bower, A. S., Serra, N. and Ambar, I. (2002), Structure of the Mediterranean Undercurrent and Mediterranean Water spreading around the southwestern Iberian Peninsula. *J. Geophys. Res.* 107, C103161.

Boyer, T.P., Levitus, S., Antonov, J.I., Locarnini, R. A. and Garcia, H.E. (2005), Linear trends in salinity in the World Ocean, 1955-1998. *Geophys. Res. Lett.*, 32, L01604.

Bozec, A., P. Bouret-Aubertot, D. Iudicone, and M. Crépon (2008), Impact of penetrative solar radiation on the diagnosis of water mass transformation in the Mediterranean Sea, *J. Geophys. Res.*, 113, C06012, doi:10.1029/2007JC004606.

Brandt, P., Rubino, A., Sein, D. V., Baschek, B., Izquierdo, A., and Backhaus, J. O. (2004). Sea level variations in the Western Mediterranean studied by a numerical tidal model of the Strait of Gibraltar. *J. Phys. Oceanogr.*, 34 (4), 433-443.

Brankart, J. M., and Pinardi, N. (2001). Abrupt cooling of the Mediterranean Levantine intermediate water at the beginning of the 1980s: observational evidence and model simulation. *J . Phys. Oceanogr.*, 31(8), 2307-2320.

Bruce, J. G., and Charnock, H. (1965). Studies in winter sinking of cold water in the Aegean Sea. *Rapport Comm. Int. Mer. Medit.*, 18, 773-778.

Bruno, M., Mañanes, R., Alonso, J.J., Izquierdo, A., Tejedor, L. and Kagan, B. (1999). Vertical structure of the semidiurnal tidal currents at Camarinal Sill, the Strait of Gibraltar. *Oceanol. Acta*, 23 15 – 24.

Bryden, H.L. and Stommel, H.M., (1982). Origin of the Mediterranean outflow. *J. Mar. Res* 40, 55–71.

Bryden, H. L., and T. H. Kinder, (1991a). Recent progress in strait dynamics. *Rev. Geophys.* (Suppl.), 617–631.

Bryden, H. L., and T. H. Kinder, (1991b). Steady two-layer exchange through the Strait of Gibraltar. *Deep-Sea Res.* 38S, 445–463.

Bryden, H. L., J. Candela, and T. H. Kinder, (1994). Exchange through the Strait of Gibraltar, *Prog. Oceanogr.* 33, 201–248.

Bunker, A.F., Charnock, H. and Goldsmith, R.A., (1982). A note on the heat balance of the Mediterranean and Red Seas. *J. Mar. Res.* 40, 73-84, Suppl.

Buongiorno-Nardelli, B. and Salusti, E. (2000). On dense water formation criteria and their application to the Mediterranean Sea. *Deep Sea Res. I,* 47 (Suppl 1), 193-221.

Candela, J., C.D. Winant and H.L. Bryden (1989), Meteorologically forced subinertial flows through the Strait of Gibraltar. *J. Geophys. Res.*, 94, 12667-12679.

Candela, J., Winant, C. and Ruiz, A. (1990). Tides in the Strait of Gibraltar. *Prog. Oceanogr.* 33, 7313 – 7335.

Candela, J., (2001). Mediterranean water and global circulation, in Ocean Circulation and Climate, edited by G. Siedler, J. Church, and J. Gould, pp. 419–429, Academic Press, San Diego, Ca.

Castellari, S., Pinardi, N. and Leaman K., (1998). A model study of air-sea interactions in the Mediterranean Sea. *J. Mar. Sys.* 18, 89-114.

Cazenave, A., Bonnefond, P., Mercier, F., Dominh, K. and Toumazou, V., (2002). Sea level variations in the Mediterranean Sea and Black Sea from satellite altimetry and tide gauges. *Glob. Planet. Change* 34, 59–86.

Church J. A., Gregory, J. M., Huybrechts, P., Kuhn, M., Lambeck, K., Nhuan, M. T., Qin, D. and Woodworth, P. L. (2001). Chapter 11 Changes in sea level. Intergovernmental Panel on Climate Change Third Assessment Report, Cambridge University Press.

CLIPPER Project Team (1999), Modélisation à haute résolution de la circulation dans l'océan Atlantique forcée et couplée océan-atmosphére, *Sci. Tech. Rep.* CLIPPER-R3-99, Ifremer, Brest, France.

Conte, M., Giuffrida, A. and Tedesco, S., (1989). The Mediterranean Oscillation, impact on precipitation and hydrology in Italy. Conference on Climate Water. Pub. of the Academy of Finland, Helsinki, 121-137.

Criado-Aldeanueva, F., García-Lafuente, J., Vargas, J.M., Del Río, J., Vázquez, A., Reul, A. and Sánchez, A. (2006). Distribution and circulation of water masses in the Gulf of Cádiz from in situ observations. . *Deep Sea Res. Part II* 53, 1144-1160.

Criado-Aldeanueva F., Del Río Vera J. and García-Lafuente J., (2008). Steric and mass induced Mediterranean sea level trends from 14 years of altimetry data. *Glob. Planet. Change* 60, 563-575.

Criado-Aldeanueva, F., Soto-Navarro, J. and García-Lafuente, J., (2012). Seasonal and interannual variability of surface heat and freshwater fluxes in the Mediterranean Sea: budgets and exchange through the Strait of Gibraltar. *Int. J. Climatol.* 32, 286–302. doi: 10.1002/joc.2268.

Cunningham, S. A. and Alderson, S. (2007), Transatlantic temperature and salinity changes at 24.5ºN from 1957 to 2004. *Geophys. Res. Lett.* 34, L14606.

Curry, R., Dickson B. and Yashayaev I. (2003), A change in the freshwater balance of the Atlantic Ocean over the past four decades. *Nature*. 426, 826-829.

Daget, N., A. T. Weaver, and M. A. Balmaseda (2009), Ensemble estimation of background-error variances in a three-dimensional variational data assimilation system for the global ocean. *Q. J. R. Meteorol. Soc.*, 135, 1071–1094

Dai, A., Fung, I.Y. and del Genio, A.D., (1997). Surface observed global land precipitation variations during 1900-88. *J. Clim* 10, 2943-2962.

Decharme, B., R. Alkama, H. Douville, M. Becker, A. Cazenave, 2010: Global Evaluation of the ISBA-TRIP Continental Hydrological System. Part II: Uncertainties in River Routing Simulation Related to Flow Velocity and Groundwater Storage. *J. Hydrometeor*, **11**, 601–617. doi: http://dx.doi.org/10.1175/2010JHM1212.1

Del Río-Vera, J., Criado-Aldeanueva, F., García-Lafuente, J. and Soto-Navarro, J., (2009). A new insight on the decreasing sea level trend over the Ionian basin in the last decades. *Glob. Planet. Change*, 68, 232-235.

Demirov, E. and Pinardi, N. (2002). Simulation of the Mediterranean Sea circulation from 1979 to 1993: Part I. The interannual variability. *J. Mar. Syst.*, 33-34, 23-50.

Déqué, M., and J. Piedelievre (1995), High resolution climate simulation over Europe, *Clim. Dyn.* 11, 321–339.

Drillet, Y., R. Bourdallé-Badie, L. Siefridt, and C. Le Provost (2005), Meddies in the Mercator North Atlantic and Mediterranean Sea eddy-resolving model, *J. Geophys. Res.* 110, C03016, doi:10.1029/2003JC002170.

Farmer D. and Armi L., (1986). The internal hydraulics of the Strait of Gibraltar and asociated sills and narrows. *Oceanol. Acta.* (8), 37-46.

Fenoglio-Marc, L., (2002). Long-term sea level change in the Mediterranean Sea from multi-satellite altimetry and tide gauges. *Phys. Chem. Earth* 27, 1419–1431.

Fenoglio-Marc, L., Kusche J. and Becker M., (2006). Mass variations in the Mediterranean Sea from GRACE and its validation by altimetry, steric and hydrologic fields. *Geophys. Res. Lett.*, 33, L19606, doi:10.1029/2006GL026851.

Ferry, N., L. Parent, G. Garric, B. Barnier, N. C. Jourdain, and the Mercator Ocean team (2010), Mercator Global Eddy Permitting Ocean Reanalysis GLORYS1V1: Description and Results, Mercator Ocean Quarterly Newsletter, #36 - January 2010, pp 15–28.

Font, J., P. Puig, J. Salat, A. Palanques, M. Emelianov, (2007). Sequence of hydrographic changes in NW Mediterranean deep water due to the exceptional winter of 2005. *Sci. Mar.* 71(2), 339-346.

Franco, P., Jeftic, L., Malanotte-Rizzoli, P., Michelato, A. and Orlic, M. (1982). Descriptive model of the Northern Adriatic. *Oceanol. Acta*, 5, 379-389.

Fuda, J. L., Millot, C , Taupier-Letage, I., Send, U. and Bocognano, J. M. (2000). XBT monitoring of a meridian section across the Western Mediterranean Sea. *Deep Sea Res.,* 41, 2191-2218.

García, D., B. F. Chao, J. Del Río, I. Vigo, and J. García Lafuente (2006). On the steric and mass-induced contributions to the annual sea level variations in the Mediterranean Sea, *J. Geophys. Res.* 111, C09030, doi:10.1029/2005JC002956.

García-Lafuente, J. (1986). Variabilidad del nivel del mar en el Estrecho de Gibraltar: mareas y oscilaciones residuals. PhD Thesis, Universidad de Málaga.

García-Lafuente, J., J.M. Vargas, F. Plaza, T. Sarhan, J. Candela and B. Basheck (2000). Tide at the eastern section of the Strait of Gibraltar. *J. Geophys. Res.*, 105, 14197-14213.

García-Lafuente, J., J. Delgado, J. M. Vargas, M. Vargas, F. Plaza, and T. Sarhan, (2002a). Low-frequency variability of the exchanged flows through the Strait of Gibraltar during CANIGO, *Deep Sea Res. II*, 49, 4051– 4067.

García-Lafuente, J., E. Alvarez Fanjul, J. M. Vargas, and A. W. Ratsimandresy, (2002b). Subinertial variability in the flow through the Strait of Gibraltar, *J. Geophys. Res.*, 107 (C10), 3168, doi:10.1029/ 2001JC001104.

García-Lafuente, J and J.M. Vargas (2003). Recent observations of the exchanged flows through the Strait of Gibraltar and their fluctuations at difference time scales. In Recent.

Res. Devel. In Geophysics, pp 73-84. Research Signpost, 37/661 (2) Fort P. O. Trivandum- 605 023, Kerala, India.

García-Lafuente, J., Sánchez-Román, A., Díaz del Río, G., Sannino, G. and Sánchez-Garrido, J.C., (2007). Recent observations of seasonal variability of the Mediterranean outflow in the Strait of Gibraltar. *J. Geophys. Res.* 112 C10, doi: 10.1029/2006JC003992.

García-Lafuente, J., Delgado, J., Sánchez-Román, A., Soto, J., Carracedo, L. and Díaz del Río, G., (2009). Interannual variability of the Mediterranean outflow observed in Espartel sill, western Strait of Gibraltar. *J. Geophys. Res.* 114 C10, doi: 10.1029/2009JC005496.

García-Lafuente, J., Sánchez-Román, A., Naranjo, C. and Sánchez-Garrido, J.C., (2011). The very first transformation of the Mediterranean outflow in the Strait of Gibraltar. *J. Geophys. Res.* 116, C07010, doi: 10.1029/2011JC006967.

Garrett, C., (1996). The role of the strait of Gibraltar in the evolution of Mediterranean water, properties and circulation. Bull. Inst. Oceanogr. Mónaco 17, 1-19.

Garrett, C. J. R., J. Akerley and K. R. Thompson, (1989). Low-frecuency fluctuations in the Strait of Gibraltar from Medalpex sea level data. *J.Phys. Oceanogr.*, 19, 1682-1696.

Garrett, C., Outerbridge, R. and Thompson, K., (1993). Interannual variability in Mediterranean heat and buoyancy fluxes. *J. Climate* 6, 900-910.

Georgopoulos, D., Theocharis, A., and Zodiatis, G. (1989). Intermediate water formation in the Cretan Sea (S. Aegean Sea). *Oceanol. Acta*, 12(4), 353-359.

Gilman, C. and Garrett, C., (1994). Heat flux parameterization for the Mediterranean Sea: the role of atmospheric aerosols and constraints from the water budget. *J. Geophys. Res.* 99 (C3), 5119-5134.

Gomis, D., Tsimplis, M.N., Martín-Míguez, B., Ratsimandresy, A.W., García-Lafuente, J. and Josey, S.A., (2006). Mediterranean sea level and barotropic flow through the Strait

of Gibraltar for the period 1958-2001 and reconstructed since 1659. *J. Geophys. Res.* 111, C11005 doi: 10.1029/2005JC003186.

Goosse, H., Selten, F.M., Haarsma, R.J. and Opsteegh, J.D., (2001). Decadal variability in high northern latitudes as simulated by an intermediate-complexity climate model *Annals of Glaciology*, 33, pp. 525-532.

Guldberg, A., E. Kaas, M. Déqué, S. Yang, and S. Vester Thorsen (2005), Reduction of systematic errors by empirical model correction: Impact on seasonal prediction skill, *Tellus, Ser. A*, 57, 575–588.

Harzallah, A., D. L. Cadet, and M. Crepon, (1993). Possible forcing effects of net evaporation, atmospheric pressure and transients on water transports in the Mediterranean Sea. *J. Geophys. Res.*, 98 (C7), 12 341–12 350.

Herbaut, C, Martel, P., and Grepon, M. (1997). A sensitivity study of the general circulation of the Western Mediterranean Sea. 2. The response to atmospheric forcing. *J. Phys. Oceanogr.*, 27(10), 2126-2145.

Herrmann, M. J., and S. Somot (2008), Relevance of ERA40 dynamical downscaling for modeling deep convection in the Mediterranean Sea, *Geophys. Res. Lett.*, 35, L04607, doi:10.1029/2007GL032442.

Herrmann M., Somot S., Calmanti S., Dubois C. and Sevault F. (2011). Representation of daily wind speed spatial and temporal variability and intense wind events over the Mediterranean Sea using dynamical downscaling : impact of the regional climate model configuration. *Nat. Hazards Earth Syst. Sci.*, 11, 1983-2001, doi:10.5194/nhess-11-1983-2011

Hosoda, S., Suga, T., Shikima, N. and Mizuno K. (2009), Global surface layer salinity change detected by Argo and its implication for hydrological cycle intensification. *J. Oceanogr.* 65, 579-586.

Hurrell, J.W., (1995). Decadal trends in the North Atlantic Oscillation – regional temperatures and precipitation. *Science* 269 (5224), 676-679.

Hurrell, J.W. and van Loon, H., (1997). Decadal variations in climate associated with the North Atlantic Oscillation. *Clim. Change* 36, 301-326.

Hurrell, J.W., Kushnir, Y., Ottersen, G. and Visbeck, M., (2003). The North Atlantic Oscillation: climate significance and environmental impact. *Geophys. Monogr.* Ser 134, 279.

Hurrell, J.W. and Deser, C., (2010). North Atlantic climate variability: the role of the North Atlantic Oscillation. *J. Mar. Sys.* 79, 231-244.

Jaeger, L., (1976). Monatskarten des Niederschlags fur die ganze Erde. Ber. Dtsch. Wetterdienstes, 18, 1–38.

Jones, P.D., Jonsson, T. and Wheeler, D., (1997). Extension to the North Atlantic Oscillation using early instrument pressure observations from Gibraltar and south-west Iceland. *Int. J. Climatol*. 17, 1433-1450.

Jones, P.D., Osborn, T.J. and Briffa, K.R., (2003). Pressure-based measures of the North Atlantic Oscillation (NAO), a comparison and assessment of changes in the strength of the NAO and its influence on surface climate parameters. In: Hurrell, J.W., Kushnir, Y., Ottersen, G. and Visbeck, M (eds), The North Atlantic Oscillation, climatic significance and environmental impact. *AGU Geophys. Monogr.*, vol. 134, pp 51-62.

Josey, S. A., Kent, E. G., & Taylor, P. K. (1999). New insights into the ocean heat budget closure problem from analysis of the SOG air-sea flux climatology. *J. Climate*, 12, 2880.

Josey, S. A. (2003). Changes in the heat and freshwater forcing of the Eastern Mediterranean and their influence on deep water formation. *J. Geophys. Res.*, 108(C7), 3237, doi:10.1029/2003JG001778.

Kalnay, E and co-authors (1996). The NCEP/NCAR 40-year reanalysis project. *Bull. Amer. Meteor. Soc.*, 77:437-471.

Kanarska Y. and Maderich V., (2008). Modelling of seasonal Exchange flows through the Dardanelles Strait. *Estuar. Coast. Shelf Sci.* 79, 449-458.

Kinder, T.H. and H.L. Bryden (1987). The 1985-86 Gibraltar Experiment: data collection and preliminary results. EOS, 68, 786-787, 280-281.

Kinder, T.H. and H.L. Bryden (1988). Gibraltar Experiment: summary of the field program and initial results of the Gibraltar Experiment. Whoi-88-30, Woods Hole Oceanographic Institution Technical Report.

Kinder, T. H., and H. L. Bryden (1990), Aspiration of deep waters through straits, in The Physical Oceanography of Sea Straits, edited by L. J. Pratt, pp. 295– 319, Kluver Academic, Norwell, Mass.

Klein, B. and Siedler, G. (1989). On the origin of the Azores Current. *J. Geophys. Res.* 94, 6159-6168.

Klein, B., Roether,W., Manca, B., Bregant, D., Beitzel, V., Kovacevic, V. and Luchetta, A., (1999). The large deep water transient in the Eastern Mediterranean. *Deep Sea Res. I*, 46, 371–414.

Knudsen M. (1899). De hydrografiske forhold i de danske farvande indenfor Skagen i 1894−98. Komm For Vidensk Unders I de danske farvande 2(2):19–79.

Kutiel, H., Maheras, P. and Guika, S., (1996). Circulation indices over the Mediterranean and Europe and their relationship with rainfall conditions across the Mediterranean. *Theor. Appl. Climatol.* 54, 125-138.

Lacombe, H., and P. Tchernia, (1972). Caracteres hydrologiques et circulation des eaux en Mediterranee. The Mediterranean Sea: A Natural Sedimentation Laboratory, D. J. Stanley, Ed., Dowden, Hutchinson and Ross, 25–36.

Lacombe H. and Richez C., (1982). The regime of the Strait of Gibraltar. In Hydrodynamics of Semi-Enclosed Seas. Ed. J.C.J. Nihoul. Amsterdam. 13-74.

Lascaratos, A. (1993). Estimation of deep and intermediate water mass formation rates in the Mediterranean Sea. *Deep Sea Res. II*, 40, 1327-1332.

Lascaratos, A., Williams, R., & Tragou, E. (1993). A mixed layer study of the formation of Levantine intermediate water. *J. Geophys. Res.* 98, 739-749.

Lascaratos, A., and Nittis, K. (1998). A high resolution 3-D numerical study of intermediate water formation in the Levantine Sea. *J. Geophys. Res.* 103, 18497-18511.

Le Traon, P.Y. and Gauzelin, P., (1997). Response of the Mediterranean sea level to atmospheric pressure forcing. *J. Geophy. Res.*, 102, 973–984.

Leadbetter, S. J., Williams, R. G., McDonagh, E. L. & King, B. A. (2007), A twenty year of reversal in the water mass trends in the subtropical North Atlantic. *Geophys. Res. Lett.* 34, L12608.

Lebeaupin Brossier, C., K. Béranger, C. Deltel, and P. Drobinski (2011), The Mediterranean response to different space-time resolution atmospheric forcings using perpetual mode sensitivity simulations, *Ocean Model.*, 36, 1–25, doi:10.1016/j.ocemod.2010.10.008.

Lebeaupin Brossier, C., K. Béranger and P. Drobinski (2012). Sensitivity of the northwestern Mediterranean Sea coastal and thermohaline circulations simulated by the 1/12°-resolution ocean model NEMO-MED12 to the spatial and temporal resolution of atmospheric forcing. *Ocean Model.*, 43-44, 94-107, doi:10.1016/j.ocemod.2011.12.007.

Lee, T. and Fukumori, I., (2003). Interannual-to-decadal variations of tropical–subtropical exchange in the Pacific Ocean: boundary versus interior pycnocline transports. *J. Climate,* 16, 4022–4042.

Legates, D. R., and C. J. Wilmot, (1990). Mean seasonal and spatial variability in gauge-corrected, global precipitation. *Int. J. Climatol.*, 10, 111–127.

Levitus, S., J. Antonov, and T. Boyer (2005), Warming of the world ocean, 1955-2003, *Geophys. Res. Lett.*, 32 (L02604).

List, R.J., 1951. Smithsonian Meteorological Tables, 6th rev. ed. Smithsonian Institute Press, 527 pp.

Liu K.K. et al. (Eds.), (2009). Carbon and nutrients fluxes in continental margins, Global Change-The IGBP series. Doi:10.1007/978-3-540-92735-2_7. © Springer-Verlag Berlin Heidelberg.

López-Jurado, J.L., González-Pola, C. and Vélez-Belchí, P. (2005). Observation of an abrupt disruption of the long-term warming trend at the Balearic Sea, Western Mediterranean Sea, in summer 2005, *Geophys. Res. Lett.* 32, L24606, doi:10.1029/2005GL024430.

Ludwig, W., E. Dumont, M. Meybeck, and S. Heussner (2009), River discharges of water and nutrients to the Mediterranean and Black Sea: Major drivers for ecosystem changes during past and future decades?, *Prog. Oceanogr.* 80, 199–217.

Lyard, F., F. Lefevre, T. Letellier, and O. Francis (2006), Modelling the global ocean tides: modern insights from FES2004, *Ocean Dyn.* 56 (5-6), doi:10.1007/s10236- 006-0086-x.

MacDonald, A.M., Candela, J. and Bryden H.L, (1994). An estimate of the net heat transport through the Strait of Gibraltar, in Seasonal and Interannual variability of the Western Mediterranean Sea, Coastal Estuarine Stud., vol. 46, edited by P.E. LaViolette, pp. 12-32, AGU, Washington, D.C.

Machín, F. and Pelegrí, J. L. (2008), Northward penetration of Antarctic Intermediate Water off Northwest Africa. *J. Phys. Oceanogr.* 39, 512-534.

Machín, F., Pelegrí, J.L., Marrero-Díaz, A., Laiz, I. and Ratsimandresy, A.W. (2006). Near-surface circulation in the southern Gulf of Cadiz. *Deep Sea Res. Part II* 53, 1161-1181.

Madec, G. (2008), NEMO ocean engine, Note Pôle Model. 27, Inst. Pierre-Simon Laplace des Sci. de l'Environ., Paris, France.

Madec, G., M. Delecluse, M. Imbard, and C. Levy (1998), OPA 8.1 Ocean General Circulation Model reference manual, Note Pôle Model. 11, 91 pp., Inst. Pierre-Simon Laplace des Sci. de l'Environ., Paris, France.

Maheras, P., Xoplaki, E. and Kutiel, H., (1999). Wet and dry monthly anomalies across the Mediterranean basin and their relationship with circulation 1860-1990. *Theor. Appl. Climatol* 64, 189-199.

Malanotte-Rizzoli, P. (1991). The Northern Adriatic Sea as a prototype of convection and water mass formation on the continental shelf. In: P. C. Chu, & J. C. Gascard (Eds), Deep Convection and Deep Water Formation in the Oceans. *Elsevier Oceanogr. Ser.* 57, 229-239.

Malanotte-Rizzoli, P., and Hecht, A. (1988). Large-scale properties of the eastern Mediterranean: a review. *Oceanol. Acta* 11, 323-335.

Malanotte-Rizzoli, P., Manca, B. B., Ribera Dacala, M., Theocharis, A., Bergamasco, A., Bregant, D., Budillon, G., Civitarese, G., Georgopoulos, D., Michelato, A., Sansone, E., Scarazzato, P., and Souverrmezoglou, E. (1997). A synthesis of the Ionian hydrography, circulation and water mass pathways during POEM-Phase I. *Prog. Oceanogr.,* 39**,** 153-204.

Manca, B.M. (2000). Recent changes in dynamics of the Eastern Mediterranean affecting the water characteristics of adjacent basins. *CIESM Workshop Series 2000*, 27-31.

Manca, B. B., Kovacevic, V., Gacic, M. and ViezzoH, D. (2002). Dense water formation in the Southern Adriatic Sea and spreading into the Ionian Sea in the period 1997-1999. *J. Mar. Syst*, 33-34, 133-154.

Manca, B. B., Budillon, G., Scarazzato, P., and Ursella, L. (2003). Evolution of dynamics in the Eastern Mediterranean affecting water mass structures and properties in the Ionian and Adriatic Seas. *J. Geophys. Res.*, 108(C9).

Margat, J., (1992). L'Eau dans le Bassin Mediterraneen: Situation et Perspective. Les Fascicules du Plan Bleu, No. 6, Economica, Paris, France, 196 pp.

Mariotti, A., (2010). Recent changes in the Mediterranean water cycle: a pathway toward long-term regional hydroclimatic change? *J. Climate* 23, 1513-1525.

Mariotti, A., Struglia, M.V., Zeng, N. and Lau, K.-M., (2002). The hydrological cycle in the Mediterranean region and implications for the water budget of the Mediterranean Sea. *J. Climate* 15, 1674–1690.

Mariotti, A. and Arkin, P., (2007). The North Atlantic Oscillation and oceanic precipitation variability. *Clim. Dyn* 28, 35-51.

Mariotti, A., Zeng, N., Yoon, J. H., Artale, V., Navarra, A., Alpert, P. and Li, L.Z.X, (2008). Mediterranean water cycle changes: transition to drier 21st century conditions in observations and CMIP3 simulations. *Environ. Res. Lett.* 3 (4), 044001, doi: 10.1088/1748-9326/3/4/044001.

Marshall, J. and Schott, F. (1999). Open-ocean convection: Observations, theory, and models, *Rev. of Geophys.*, 37 (1), 1–64.

Marsigli, L. F. (1681). Osservazioni Intomo al Bosforo Tracio o vero Canale di ConstantinopH rappresentate in lettera alia Sacra Real Maesta di Cristina Regina di Svezia Nicolb Angelo Tinassi, Rome. Reprinted in: Bollettino di pesca, di piscicoltura e di idrobiologia. Anno XI, Fast. 5, Settembre-Ottobre 1935, 734-758.

Marullo, S., Santoleri, R., Malanotte-Rizzoli, P. and Bergamasco, A., (1999). The sea surface temperature field in the eastern Mediterranean from advanced very high resolution radiometer (AVHRR) data. Part II: interannual variability. *J. Mar. Syst.* 20, 83–112.

Matsoukas, C., Banks, A. C., Hatzianastassiou, N., Pavlakis, K. G., Hatzidimitriou, D., Drakakis, E., Stackhouse, P. W.and Vardavas, I., (2005). Seasonal heat budget of the Mediterranean Sea. *J. Geophys. Res.* 110, C12008, doi:10.1029/2004JC002566.

May, P.W., (1986). A brief explanation of Mediterranean heat and momentum flux calculations. NORDA code 322, NSTL, MS 39529.

MEDAR-MEDATLAS Group (2002), MEDAR/MEDATLAS 2002 database, Cruise inventory, observed and analysed data of temperature and bio-chemical parameters [CD-ROM], Ifremer, Brest, France.

Medimap Group (2005), Morpho-bathymetry of the Mediterranean Sea, CIESM/Ifremer Edition, 2 maps at 1/2000000.

MEDOC Group (1970), Observation of formation of deep water in the Mediterranean Sea, (1969). *Nature*, 227, 1037–1040.

Mertens, C. and Schott, F. (1998). Interannual variability of deep water formation in the northwestern Mediterranean Sea. *J . Phys. Oceanogr.* 28, 1410-1424.

Miller, L. and Douglas, B. C. (2004). Mass and volume contributions to twentieth century global sea level rise. *Nature* 428, 406-409.

Millot, C. (1987). Circulation in the Western Mediterranean Sea. *Oceanol. Acta,* 10 (2), 143-149.

Millot, C. (1999), Circulation in the Western Mediterranean Sea. *J. Mar. Syst.* 20, 423-442.

Millot C. (2007), Interannual salinification of the Mediterranean inflow. *Geophys. Res. Lett.* 34, L21609.

Millot, C. and Taupier-Letage, I. (2005). Circulation in the Mediterranean Sea. *Hdb Env Chem Vol.* 5, Part K, 29–66. DOI 10.1007/b107143.

Millot, C, Benzohra, M., and Taupier Letage, I. (1997). Circulation off Algeria inferred from the Mediprod-5 current meters. *Deep Sea Res. I* 44(9-10), 1467-1481.

Millot, C., Candela, J., Fuda, J.-L., Tber, Y., (2006). Large warming and salinification of the Mediterranean outflow due to changes in its composition. *Deep Sea Res. I* 53/4, 656-666. doi:10.1016/j.dsr.2005.12.017.

Morcos, S. A. (1972). Sources of Mediterranean intermediate water in the Levantine Sea. In: A. L. Gordon (Ed), Studies in Physical Oceanography, Vol. 2. Gordon and Breach, New York, pp. 185-206.

Moron, V., (2003). L'évolution séculaire des températures de surface de la mer Méditerranée (1856–2000). Comptes Rendus Geoscience (335), 721–727 (in French with abridged English version).

Naranjo, C., García-Lafuente, J., Sánchez-Garrido, J,C., Sánchez-Román, A. and Delgado-Cabello, J. (2012).The western alboran gyre helps ventilate the western mediterranean deep water through Gibraltar. *Deep Sea Res. I* 63, 157-163.

Nielsen, J. N. (1912). Hydrography of the Mediterranean and adjacent seas. Danish Oceanographic Expeditions 1908-10. Report I, pp. 72-191.

Nittis, K., and Lascaratos, A. (1988). Diagnostic and prognostic numerical studies of LIW formation. *J. Mar. Syst.* 18, 179-195.

Oguz, T., and Sur, H. I., (1989), A two-layer model of water exchange through the Dardanelles Strait, *Oceanol. Acta,* 12, 23–31.

Oki, T. and Sud, Y. C. (1998), Design of Total Runoff Integrating Pathways (TRIP) - A global river channel network. *Earth Interact.* 2.

Orlic, M., and Pasaric, M. (2000). Sea-level changes and crustal movements recorded along the east Adriatic coast. *II Nuovo Cimento*, 23, 351-364.

Ovchinnikov, I.M., (1974). On the water balance of the Mediterranean Sea. *Oceanology*, 14, pp. 198-202.

Ovchinnikov, I. M. (1984). Formation of intermediate waters in the Mediterranean Sea. *Oceanology*, 24, 217-255.

Ovchinnikov, I. M. and Plakhin, Ye. A. (1984). Formation of the intermediate waters of the Mediterranean Sea in the Rhodes Cyclonic Gyre. *Oceanology*, 24, 317-319.

Ovchinnikov, I. M., Zets, V. I., Kroshaye, V. G., Menirovsk, M. S. and Udodov, A. I. (1987). Winter convection in the Adriatic and formation of deep Eastern Mediterranean water. *Oceanol. Acta*, 5B, 89-92.

Ozturgut, E. (1976). The source and spreading of the Levantine intermediate water in the Eastern Mediterranean. Saclant antisubmarine warfare Res. Cen. Memor. SM-92, La Spezia, Italy, pp. 45.

Paillet, J. and Mercier, H. (1997), An inverse model of the eastern North Atlantic general circulation and thermocline ventilation. *Deep Sea Res. Part I.* 44, 1293-1328.

Painter, S. C. and Tsimplis, M. N. (2003). Temperature and salinity trends in the upper waters of the Mediterranean Sea as determined from the MED ATLAS dataset. *Cont. Shelf Res.* 23, 1507-1522.

Parrilla, G., T. H. Kinder, and R. H. Preller (1986), Deep and intermediate Mediterranean water in the western Alborn Sea. *Deep Sea Res. I*, 33, 55– 88.

Peixoto, J. P., M. De Almeida, R. D. Rosen, and D. A. Salstein, (1982). Atmospheric moisture transport and the water balance of the Mediterranean Sea. *Water Resour. Res.*, 18, 83–90.

Poliakov, I.V., Bhatt, U.S., Simmons, H.L., Ealsh, D., Waldh, J.E. and Zhang X. (2005), Multidecadal Variability of North Atlantic Temperature and Salinity during the Twentieth Century. *J. Climate*, 18, 4562-4581.

Pollard, R. T. and Pu, S. (1985), Structure and circulation of the upper Atlantic Ocean northeast of the Azores. *Prog. Oceanogr.* 14, 443-462.

Raicich, F. (1996). On the fresh water balance of the Adriatic Sea. *J. Mar. Sys.*, 9, 305-319.

Reid, J. L. (1979), On the contribution of the Mediterranean outflow to the Norwegian-Greenland Sea. *Deep Sea Res.* 26, 1199-1223.

Reynaud, T., P. Legrand, H. Mercier, and B. Barnier (1998), A new analysis of hydrographic data in the Atlantic and its application to an inverse modeling study, Int. WOCE Newsl., 32, 29–31.

Rhein, M. (1995). Deep water formation in the Western Mediterranean. *J. Geophys. Res.*, 100, 6943-6959

Rixen, M., Bechers, J.M., Levitus, S., Antonov, J., Boyer, T., Maillard, C., Fichaut, M., Balopoulos, M., Iona, S., Dooly, S., García, M.J., Manca, B., Giorgetti, A., Manzella,

G., Mikhailov, N., Pinardi, N. and Zavatereli, M. (2005), The western Mediterranean deep water: A proxy for climate change. *Geophys. Res. Lett.* 32, LI2608.

Roemmich, D. and Gilson, J. (2009), The 2004-2008 mean and annual cycle of temperature, salinity, and steric height in the global ocean from the Argo program . *Prog. Oceanogr.*, 82, 81-100.

Roether, W., Manca, B. B., Klein, B., Bregant, D., Georgopoulos, D., Beitzel, V., Kovacevic, V., and Luchetta, A. (1996). Recent changes in Eastern Mediterranean deep waters. *Science,* 111**,** 333-335.

Rogers, J.C. and van Loon, H., (1979). The see-saw of winter temperatures between Greenland and northern Europe. Part II: some oceanic and atmospheric effects in middle and high latitudes. *Mon. Weather Rev* 107, 509-519.

Rogers, J.C., (1984). The association between the North Atlantic Oscillation and the Southern Oscillation in the northern hemisphere. *Mon. Weather Rev*. 112 1999-2015.

Rohling, E.J. and Bryden, H.L., (1992). Man-induced salinity and temperature increases in western Mediterranean deep water. *J. Geophys. Res.* 97 (C7), 11191–11198.

Ross, T., Garrett, C. and Le Traon, P.-Y. (2000). Western Mediterranean sea-level rise: changing exchange flow through the Strait of Gibraltar. *Geophys. Res. Let.* 11, 2949-2952.

Roullet, G., and G. Madec (2000), Salt conservation, free surface, and varying levels: A new formulation for ocean general circulation models, *J. Geophys. Res.* 105, 23,927–23,942.

Ruiz S., Gomis D., Sotillo M. G. and Josey S. A., (2008). Characterization of surface heat fluxes in the Mediterranean Sea from a 44-year high-resolution atmospheric data set. *Glob. Planet. Change*, 63, 256-274.

Ruti, P. M., Marullo, S., D'Ortenzio, F. and Tremant, M., (2008) Comparison of analyzed and measured wind speeds in the perspective of oceanic simulations over the Mediterranean basin: Analyses, QuikSCAT and buoy data. *J. Mar. Syst.* 70, 33-48.

Sánchez-Román, A. (2008), Intercambios a través del estrecho de Gibraltar y su respuesta a forzamientos de distintas escalas temporales. PhD Thesis. University of Málaga, Spain.

Sanchez-Román A., Sannino G., García-Lafuente J., Carillo A. and Criado-Aldeanueva F., (2009). Transport stimates at the western section of the Strait of Gibraltar: A combined experimental an numerical modeling study. *J. Geophys. Res.* (114), C06002, doi:10.1029/2008JC005023.

Sannino, G., A. Bargagli, and V. Artale (2002), Numerical modelling of the mean exchange through the Strait of Gibraltar, *J. Geophys. Res.*, 107(C8), 3094, doi:10.1029/2001JC000929.

Sarafanov, A., Falina, A., Sokov, A. and Demidov, A. (2008), Intense warming and salinification of intermediate waters of southern origin in the eastern subpolar North Atlantic in the 1990s to mid-2000s., *J. Geophys. Res.* 113, C12022.

Schiano M.E., L. Santoleri, F. Bignami, R.M. Leonardo, Marullo S. and Bohm, (1993). Air-sea interactions measurements in the west Mediterranean Sea during the Thyrrhenian Eddy Multi-Platform Observations Experiments, *J. Geophys. Res.* 98(C2), 2461-2474.

Schroeder K., A. Ribotti, M. Borghini, R. Sorgente, A. Perilli and G.P. Gasparini, (2009). An extensive western Mediterranean deep water renewal between 2004 and 2006. *Geophys. Res. Lett.* 35(18), L18605.

Send, U., Font, J., Krahmann, G., Millot, C , Rhein, M., and Tintore, J. (1999). Recent advances in observing the physical oceanography of the Western Mediterranean Sea. *Prog. Oceanogr.* 44, 37-64.

Serreze, M.C., Carse, F., Barry, R.G. and Rogers, J.C., (1997). Icelandic low cyclone activity: climatological features, linkages with the NAO and relationships with recent changes in the northern hemisphere circulation. *J. Climate* 10(3), 453-464.

Sevault, F., S. Somot, and J. Beuvier (2009), A regional version of the NEMO ocean engine on the Mediterranean Sea: NEMOMED8 user's guide, Note Cent. 107, Groupe

de Meteorol. de Grande Echelle et Clim., Cent. Natl. de Rech. Meteorol., Toulouse, France.

Simmons, A., and J. Gibson (2000), The ERA40 project plan, ERA40 Proj. Rep. 1, Eur. Cent. for Medium-Range Weather Forecasts, Reading, U. K.

Schlitzer, R., Roether, W., Oster, H., Junghans, H., Hausmann, M., Johannsen, H., and Michelato, A. (1991). Chlorofluoromethane and oxygen in the Eastern Mediterranean. *Deep Sea Res.,* 38, 1531-1535.

Slonosky, V.C. and Yiou, P., (2001). Secular changes in the North Atlantic Oscillation and its influence on 20th century warming. *Geophys. Res. Lett.,* 28, 807-810.

Smith, W. H. F., and D. T. Sandwell (1997), Global sea floor topography from satellite altimetry and ship depth sounding, *Science* 277, 1956–1962.

Somot, S., F. Sevault, and M. Déqué (2006), Transient climate change scenario simulation of the Mediterranean Sea for the twenty-first century using a high-resolution ocean circulation model, *Clim. Dyn.* 27, 851–879.

Somot, S., and J. Colin (2008), First step towards a multi-decadal highresolution Mediterranean Sea reanalysis using dynamical downscaling of ERA40, Research activities in atmospheric and oceanic modelling, Rep. 38, World Meteorol. Organ., Geneva, Switzerland.

Soto-Navarro, J., F. Criado-Aldeanueva, J. García-Lafuente, and A. Sánchez-Román (2010), Estimation of the Atlantic inflow through the Strait of Gibraltar from climatological and in situ data, *J. Geophys. Res.* 115 (C10023), doi:10.1029/2010JC006302.

Stanev, E. V., P.-Y. Le Traon, and E. L. Peneva (2000), Sea level variations and their dependency on meteolorogical and hydrological forcing: Analysis of altimeter and surface data for the Black Sea, *J. Geophys. Res.* 105, 17,203–17,216.

Stanev, E. and Peneva, E. L. (2002). Regional sea level response to global climatic change: Black Sea examples. *Glob. Planet. Change.* 32, 33-47.

Stommel, H. (1972). Deep winter-time convection in the Western Mediterranean Sea. In: A. L. Gordon (Ed), Studies in Physical Oceanography, Vol. 2 (Gordon and Breach, New York, pp. 207-218).

Stommel, H., H. Bryden, and P. Mangelsdorf (1973), Does some of the Mediterranean outflow come from great depth?, *Pure Appl. Geophys.*, 105, 879–889.

Stott, P.A., Sutton, R.T. and Smith, D.M. (2008), Detection and attribution of Atlantic salinity changes. *Geophys. Res. Lett.* 35, L21702.

Struglia M.V., Mariotti A. and Filograsso, A., (2004). River discharge into the Mediterranean Sea: Climatology and aspect of the Observed Variability. *J. Climate.* 17, 4740-51.

Supic, N., Grbec, B., Vilibic, I. and Ivancic, I., (2004). Long-term changes in hydrograpic conditions in northern Adriatic and its relationship to hydrological and atmospheric processes. *Ann. Geophys.* 22, 733-745.

Suselj, K. and Bergant, K., (2006). Mediterranean Oscillation Index. *Geophys. Res. Abstr*. 8, 02145 European Geosciences Union.

Theocharis, A., Gacic, M. and Kontoyiannis, H. (1998). Physical and dynamical processes in the coastal and shelf areas of the Mediterranean. In: A. R. Robinson, & K. H. Brink (Eds), The Sea, Vol. 11. John Wiley and Sons, Inc., pp. 863-887.

Theocharis, A., Nittis, K., Kontoyiannis, H., Papageorgiou, E., and Balopoulos, E. (1999). Climatic changes in the Aegean Sea influence the Eastern Mediterranean thermohaline circulation. *Geophys. Res. Lett.* 26, 1617-1620.

Theocharis, A., Klein, B., Nittis, K. and Roether, W. (2002). Evolution and status of the Eastern Mediterranean transient (1997-1999). *J . Mar. Syst.* 33-34, 91-116.

Tixeront, J., (1970). Le bilan hydrologique de la Mer Noire et de la mer Mediterranee. *Cah. Oceanogr.* 3, 227–237.

Tolmazin, D., (1985). Changing coastal oceanography in the Black Sea. I: Northwestern Shelf. *Prog Oceanogr.* 15.217-276.

Tonani, M., N. Pinardi, S. Dobricic, I. Pujol, and C. Fratianni (2008), A high-resolution free-surface model of the Mediterranean Sea. *Ocean Science,* 4, 1–14.

Tragou, E., and Lascaratos, A (2003). The role of aerosols on the Mediterranean solar radiation. *J. Geophys. Res.*, 108(C2), doi: 10.1029/2001JC001258.

Trenberth, K.E., (1984). Signal versus noise in the Southern Oscillation. *Mon. Weather Rev.* 112, 326-332.

Trigo, I.F., Bigg, G.R. and Davies, T.D. (2002). Climatology of cyclogenesis mechanisms in the Mediterranean. *Mon. Weather Rev.* 130 (3), 549-569.

Tsimpis, M. N. and Spencer, N. E. (1997). Collection and analysis of monthly mean sea level data in the Mediterranean and Black Sea. *J. Coast. Res.* 13(2), 534-544.

Tsimpis, M. N. and Baker, T. F. (2000). Sea level drop in the Mediterranean Sea: an indicator of deep water salinity and temperature changes? *Geophys. Res. Lett.* 27(12), 1731-1734.

Tsimplis, M. N. and Bryden, H., (2000). Estimation of the transports through the Strait of Gibraltar. *Deep Sea Res. I*, 47(12), 2219-2242.

Tsimplis, M. N. and Josey, S. A. (2001). Forcing of the Mediterranean Sea by atmospheric oscilations over the North Atlantic. *Geophys. Res. Let.,* 28(5), 803-806.

Tsimplis, M. N. and Rixen, M. (2002). Sea level in the Mediterranean Sea: The contribution of temperature and salinity changes. *Geophys. Res. Lett.*, 29 (3).

Tsimplis, M. N., Josey, S. A., Rixen, M. and Stanev, E. V. (2004). On the forcing of sea level in the Black Sea. *J. Geophys. Res.,*109(C8)**,** C08015.

Tsimplis, M. N., Gomis, D., and Fenoglio-Marc, L. (2005). Mediterranean Sea level trends: Atmospheric pressure and wind contribution. *Geophys. Res. Lett.* 32 (20), L20602.

Tsimplis, M., M. Marcos, S. Somot, and B. Barnier (2008), Sea level forcing in the Mediterranean Sea between 1960 and 2000, *Global Planet. Change* 63, 325–332.

Tsimplis, M., M. Marcos, J. Colin, S. Somot, A. Pascual, and A. G. P. Shaw (2009), Sea level variability in the Mediterranean Sea during the 1990s on the basis of one 2D and one 3D model, *J. Mar. Syst.* 78, 109–123.

Tziperman, E., and Speer, K. (1994). A study of water mass transformation in the Mediterranean Sea - analysis of climatological data and a simple 3-box model. *Dyn. Atmos. Oceans*. 21(2-3), 53-82.

UNESCO, (1996). Global River discharges database. Vol. I: Africa, Vol. II: Asia, and Vol. III: Europe.

Unluata, U., Orguz, T., Latif, M.A. and Ozsoy, E., (1990). On the physical oceanography of the Turkish Straits. The physical oceanography of sea straits. Nato/Asi Series, pp. 25-60. Pratt, L.J. (Ed), Kluwer, Dordrecht.

Valcke, S. (2006). OASIS3 User Guide (prism_2-5). CERFACS Technical Report TR/CMGC/06/73, PRISM Report No 3, Toulouse, France. 60 pp

van Aken, H. M. and Beckaer, G. (1996), Hydrography and through-flow in the north-eastern North Atlantic: the NANSEN project. *Prog. Oceanogr.* 38, 297-346.

van Aken, H. M. (2001), The Hydrography of the mid-latitude Northeast Atlantic Ocean – Part III: the subducted thermocline water mass (2001), *Deep Sea Res. Part I*. 48(1), 237-267.

van Loon, H. and Rogers, J.C., (1978). The see-saw of winter temperatures between Greenland and northern Europe. Part I: general descriptions. *Mon. Weather Rev*. 106, 296-310.

Vargas, J.M. (2004) Fluctuaciones subinerciales y estado hidráulico del intercambio a través del Estrecho de Gibraltar. PhD Thesis. Universidad de Sevilla

Vargas, J.M., J. García Lafuente, J. Candela, and A.J. Sánchez, (2006), Fortnightly and monthly variability of the exchange through the Strait of Gibraltar, *Prog. Oceanogr.* 70 (2-4), 466-485.

Vargas-Yáñez, M., Parrilla, G., Lavín, A., Vélez-Belchí, P. and González-Pola C. (2004), Temperature and salinity increase in the eastern North Atlantic along the 24.5ºN in the last ten years. *Geophys. Res. Lett.* 31, L06210.

Vargas-Yáñez, M., Zunino, P., Belani, A., Delpy, M., Pastre, F., Moya, F., García-Martínez, M. C., and Tel, E. (2010), How much is the western Mediterranean really warming and salting? *J. Geophys. Res.*, 115, C04001.

Vigo, I., García, D. and Chao, B.F., (2005). Change of sea level trend in the Mediterranean and Black seas. *J. Mar. Res.*, 63, 1085–1100.

Vörösmarty, C., B. Fekete, and B. Tucker (1996), Global River Discharge Database, RivDis, http://www.rivdis.sr.unh.edu/, U. N. Educ. Sci. and Cult. Organ., Paris.

Waitz, J. S. (1755). v. Undersokning om orsaken, hvarfore vattnet i Atlantiska hafvet altid stromar in uti medelhafvet genom Sundet vid Gibraltar. Kungliga Svensk.a Vetenskupsakademiens Handlingar, 16, 27-50.

Walker, G.T. and Bliss, W.E., (1932). World Weather V. Memories of the Royal Meteorological Society 44, 53-84.

Woodworth, P. L. (2003). Some comments on the long sea level records from the Northern Mediterranean. *J. Coast. Res.* 19, N. 1.

Woolf, D., Shaw, A. and TsimpHs, M. N. (2003). The influence of the North Atlantic Oscillation on sea level variability in the North Atlantic region. *The Global Atmosphere and Ocean System,* 9(4), 145-167.

Wu, P. and Haines, K. (1996). Modeling the dispersal of Levantine Intermediate Water and its role in Mediterranean deep water formation. *J. Geophys. Res.* 101, 6591-6607.

Wüst, G. (1961). On the vertical circulation of the Mediterranean Sea. *J. Geophys. Res.* 66, 3261-3211.

Xie, P. and P. A. Arkin, (1996). Analysis of global monthly precipitation using gauge observations, satellite estimates, and numerical model predictions. *J. Climate* 9, 840-858.

Xie, P. and P. A. Arkin, (1997). Global precipitation: A 17-year monthly analysis based on gauge observations, satellite estimates, and numerical model outputs. *Bull. Amer. Meteor. Soc.* 78, 2539–2558.

Zavatarelli, M., Raicich, F., Bregant, D., Russo, A., and Artegiani, A. (1998). Climatological biogeochemical characteristics of the Adriatic Sea. *J. Mar. Sys.,* 18, 227-263.